Characterization of the 6D Phase Space of a Muon Beam for the Measurement of the Muon Electric Dipole Moment

A Thesis
submitted to

Department of Physics
Indian Institute of Science Education and Research, Pune
in partial fulfillment of the requirements for the BS-MS Dual Degree Programme

by

Harrsh Goyal

April 2025

Under the supervision of:

Dr. Philipp Schmidt-Wellenburg
Senior Scientist
Laboratory for Particle Physics
Paul Scherrer Institute, Switzerland

Certificate

This is to certify that this dissertation entitled **Characterization of the 6D Phase Space of a Muon Beam for the Measurement of the Muon Electric Dipole Moment** towards the partial fulfillment of the BS-MS dual degree programme at the Indian Institute of Science Education and Research, Pune represents work carried out by Harrsh Goyal at the Paul Scherrer Institute under the supervision of Dr. Philipp Schmidt-Wellenburg, Senior Scientist, Laboratory for Particle Physics, during the academic year 2024-2025.

Dr. Philipp Schmidt-Wellenburg

Prof. Sourabh Dube

Committee:

Dr. Philipp Schmidt-Wellenburg

Prof. Sourabh Dube

This thesis is dedicated to my parents, Shikha & Sanjay Goyal

Declaration

I hereby declare that the matter embodied in the report entitled **Characterization of the 6D Phase Space of a Muon Beam for the Measurement of the Muon Electric Dipole Moment** are the results of the work carried out by me at the Laboratory of Particle Physics, Paul Scherrer Institute under the supervision of Dr. Philipp Schmidt-Wellenburg, and that the same has not been submitted elsewhere for any other degree. Wherever others contribute, every effort is made to indicate this clearly, with due reference to the literature and acknowledgment of collaborative research and discussions.

Harrsh Goyal

20201006

Acknowledgments

I am deeply grateful to Prof. Klaus Kirch for putting me in touch with Dr. Philipp Schmidt-Wellenburg, thus facilitating this thesis. Philipp himself was always the model supervisor to me, and I greatly admire how he remains welcoming and approachable while also being direct in his communication. So, I would like to express my deep gratitude to him for guiding me throughout my thesis and beyond. Special thanks to Dr. Diego Alejandro Sanz Becerra for being ever present to help me whenever I was stuck, for being a great partner to brainstorm ideas with and indeed for being a great friend. Thank you to Timothy David Hume for providing invaluable feedback on the thesis, and for all his help throughout. I would also like to thank Dr. Chavdar Dutsov, David Hohl, Dr. Ritwika Chakraborty, Dr. Ljiljana Morvaj, Pranas Juknevicius and Dr. Giovanni Dal Maso for all their advice and support, and for being such a welcoming and fun group to work with and have the company of. Another word of thanks to Prof. Angela Papa for her support and encouragement, and to Dr. Massimo Giovannozzi for providing invaluable counsel. The whole muon group at PSI was great to be around and share experiences with, the memories of which I will not forget in a hurry. Thank you to Prof. Sourabh Dube for agreeing to be the expert on my thesis advisory committee, and indeed for all his support and advice.

I would like to raise a metaphorical glass to all my friends at IISER Pune who made the past 5 years some of the best I've lived thus far, and to the professors and instructors who introduced me to and helped guide me through the world of academia. I would have not accomplished even half as much as I have without all of their help and support.

I would like to thank the μEDM collaboration for sharing their knowledge, the PSI administration for their effort and IISER Pune for allowing this thesis to occur. Last but certainly not the least, I remain eternally indebted to my family for being exactly who they are.

Contents

List of Tables

List of Figures

Abstract

The Universe as we know it has an asymmetry between matter and antimatter (called 'baryon asymmetry'), a phenomenon which requires CP violation in the laws of physics. Although CP violation is established in the Standard Model, the amount is insufficient to explain the much larger observed asymmetry. As the electric dipole moments (EDMs) of fundamental particles are a source of CP violation any non-zero measurement of the EDMs above the values predicted by the Standard Model would indicate an excess of CP violation in the Universe which could help explain the observed baryon asymmetry. The μEDM experiment at the Paul Scherrer Institute (PSI) aims to measure the muon's EDM at a greater sensitivity than ever before. The ultimate sensitivity goal, corresponding to $|d_\mu| < 6 \times 10^{-23} e.cm$, would improve upon the current direct limit of $|d_\mu| < 1.8 \times 10^{-19} e.cm$ by almost four orders of magnitude, as well as the current indirect limit of $|d_\mu| < 2 \times 10^{-20} e.cm$ by nearly three orders of magnitude.

This thesis describes efforts to characterize the 6-dimensional phase space of the muon beam from the μE1 beamline at PSI, Switzerland for phase 2 of the μEDM experiment. Data was collected using a scintillating fibre array (SciFi) and a LaBr calorimeter, and the modelling of the results was performed using CERN's Transport simulation software, Python's XSuite library and G4Beamline software. These models will inform the design of phase 2 and are an important step towards an end-to-end experimental simulation which integrates the beamline and experimental apparatus. The results will also aid any experiments that may make use of the μE1 beamline at PSI in the future.

1 Introduction to μEDM

The Standard Model (SM) of Particle Physics has been widely successful to date in describing the laws that govern the Universe[1]. There are however a few anomalies that remain unexplained by this elegant theory, such as the lack of explanation for the dark sectors of the Universe (dark matter and dark energy[2]), the baryon asymmetry (also known as matter-antimatter asymmetry) of the Universe[3] and the recent muon g-2 anomaly at Fermilab[4] among others. The μEDM experiment at PSI[5] was proposed in order to get closer to bridging the knowledge gap for the baryon asymmetry in the Universe by measuring the muon's electric dipole moment (EDM) at a greater sensitivity than ever before.

The violation of charge-parity invariance (or CP violation) was discovered in 1964 in the decay of neutral kaons[6]. Since then, CP violation has been added into the Standard Model, and is today thought to be integral in order to explain the matter-antimatter asymmetry of the Universe[3]. However, the real degree of baryon asymmetry in the Universe is far greater than that predicted by the SM due to CP violation, and hence any evidence towards an excess of CP violation in the Universe could help us explain the gap between the theoretical SM prediction and the real observations. One such probe to test for excess CP violation are the EDMs of fundamental particles such as muons, since the existence of a non-zero value for the EDM of fundamental particles violates time-reversal symmetry (T), and assuming charge-parity-time (CPT) symmetry, for which there is yet no evidence of violation[7], these non-zero EDMs also violate CP symmetry (since T violation must therefore correspondingly violate CP to satisfy CPT symmetry). The CP violation present in the SM of particle physics predicts highly suppressed values for the EDMs of fundamental particles, much smaller than sensitivities in reach of current experiments. Any non-zero measurement of these EDMs at a value higher than the theoretical values would lend evidence to there being an excess of CP violation in the Universe above what is currently predicted, bringing us closer to explaining the baryon asymmetry.

The current most sensitive direct measurement of the muon's EDM put an experimental upper limit of $|d_\mu| < 1.8 \times 10^{-19} e.cm$. This measurement was made by the muon g-2 experiment at Fermilab[8], and sits about eight orders of magnitude higher than the Minimal Flavour Violation (MFV) muon EDM limit of $|d_\mu| < 2.3 \times 10^{-27} e.cm$ which was obtained by scaling the electron EDM prediction ($|d_e| \leq 1.1 \times 10^{-29} e.cm$[9]) by the ratio of masses of the muon to the electron (m_μ/m_e). The μEDM experiment at the Paul Scherrer Institute (PSI), Villigen, Switzerland aims to cut that difference in half with the final aimed sensitivity of measurement being $|d_\mu| < 6 \times 10^{-23} e.cm$ for phase 2 of the experiment (aimed for 2030s), while phase 1 of the experiment aims to achieve a sensitivity of $|d_\mu| < 3 \times 10^{-21} e.cm$ in the next few years. Both of these aimed sensitivities improve upon even the current indirect measurement of the muon EDM which set the upper limit of $|d_\mu| < 2 \times 10^{-20} e.cm$[10]. These measurements will be only the second fundamental particle EDM measurement made directly on the bare particle itself, with the first being the current muon EDM measurement made at Fermilab, and only the 4th ever measurement of the muon's EDM. Thus, the μEDM experiment promises to not only provide tighter constraints for the muon EDM but also develop new technology for fundamental physics experiments of the future.

1.1 Motivation to Characterize the μE1 beamline in Z-configuration

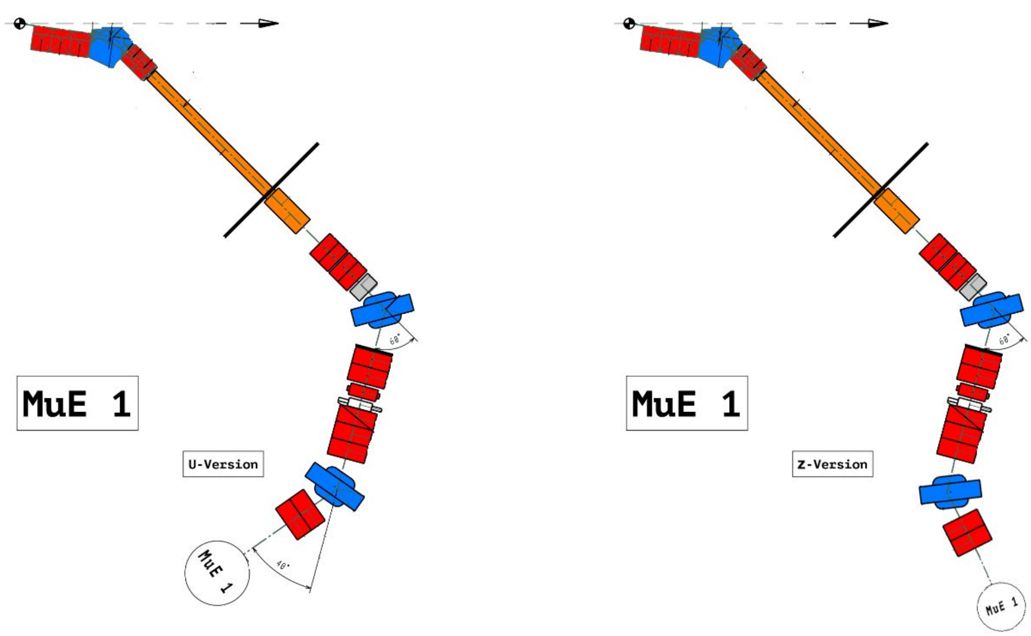

Figure 1: μE1 beamline at PSI: U-configuration [LEFT] ; Z-configuration [RIGHT].

This thesis is geared towards the characterization and modelling of the full 6D phase-space of the 'μE1' beamline at PSI[11] in its Z-configuration (see Figure 1) in order to facilitate the physics measurement of phase 2 of the μEDM experiment which is scheduled to take data in the 2030s. This phase-space characterization is required for phase 2 of the experiment, as it requires high momentum muons ($\sim$125 MeV/c muons) which the μE1 beamline can provide. The muon beam that will be input into the experiment needs to be fully understood in order to **not only estimate systematics for the final muon EDM measurement but to also have a good grasp on the input itself** which will also help better optimize the particle beam to suit the experimental needs. The characterization will also help any future experiments that might make use of the μE1 beamline in its Z-configuration, as characterization efforts of the beamline prior to this work have focused primarily on the U-configuration. As can be seen in Figure 1, the difference between the U and Z-configurations is that the last bending magnet (ASK82), also known as a dipole, has been rotated in the latter so as to bend the particles in the opposite direction to the former in order to reduce the energy dispersion in the beam (discussed in later sections).

A diagram of the whole particle beam facility (HIPA) of PSI is shown in Figure 2. The protons at PSI are produced from a hydrogen source at a frequency of 50.6 MHz which corresponds to a phase period of about 20 ns[12], which are initially accelerated using a Cockcroft-Walton accelerator as can be seen in the illustration. These protons are then accelerated further in two phases using 2 cyclotrons, the latter of which (the Ring Cyclotron) can accelerate the protons to 590 MeV kinetic energy and is a sector cyclotron[13]. These accelerated protons are then then directed onto two separate targets - a thin target (M) and a thick target (E). The μE1 beamline sources its particles from the thick target (E), hence the name μ'E'1. These particles, mainly pions (along with muons and positrons) are then focussed using quadrupoles and then directed using a dipole (which is thus the pion momentum selection dipole) bending magnet into an 8 metre long pion decay solenoid. The length of this decay channel was chosen such that pion momenta selectable by the aforementioned dipole (220 MeV/c)[11] would have lived for one lifetime at the end of the decay solenoid. As the name suggests, many of the pions then decay into muons in this solenoid, and these daughter muons (along with the other particles from the proton-on-target collision) are then focussed using 4 quadrupoles and directed into another dipole which then selects the muon momentum bite. The selected muons are then focussed using an array of quadrupoles before being directed onto the last dipole (ASK82) which then guides the muons onto the last 2 quadrupoles (QSK810 and QSK811) which apply final focussing on the muon beam and spill the beam into the experimental area. The last dipole and 2 quadrupoles can be used such that the last (ASK82) dipole turns the beam in the same direction as the ASK81 dipole (U-configuration) or in the opposite direction (Z-configuration). The U-configuration generally allows for a smaller momentum bite (thus a more mono-energetic muon beam) but lower rates and higher energy dispersion, whereas the Z-configuration allows for higher rates and a lower energy dispersion but a larger momentum spread[11].

The μE1 beamline's 4D phase-space was successfully characterized in the U-configuration by Dr. Mikio Sakurai in 2019 as a part of the μEDM collaboration[14]. This thesis is complementary to the work of Dr. Sakurai and will shed light on the 6D phase-space of the μE1 beamline in its Z-configuration for not only μEDM experiment but also any experiment that might use said configuration of the beamline in the future.

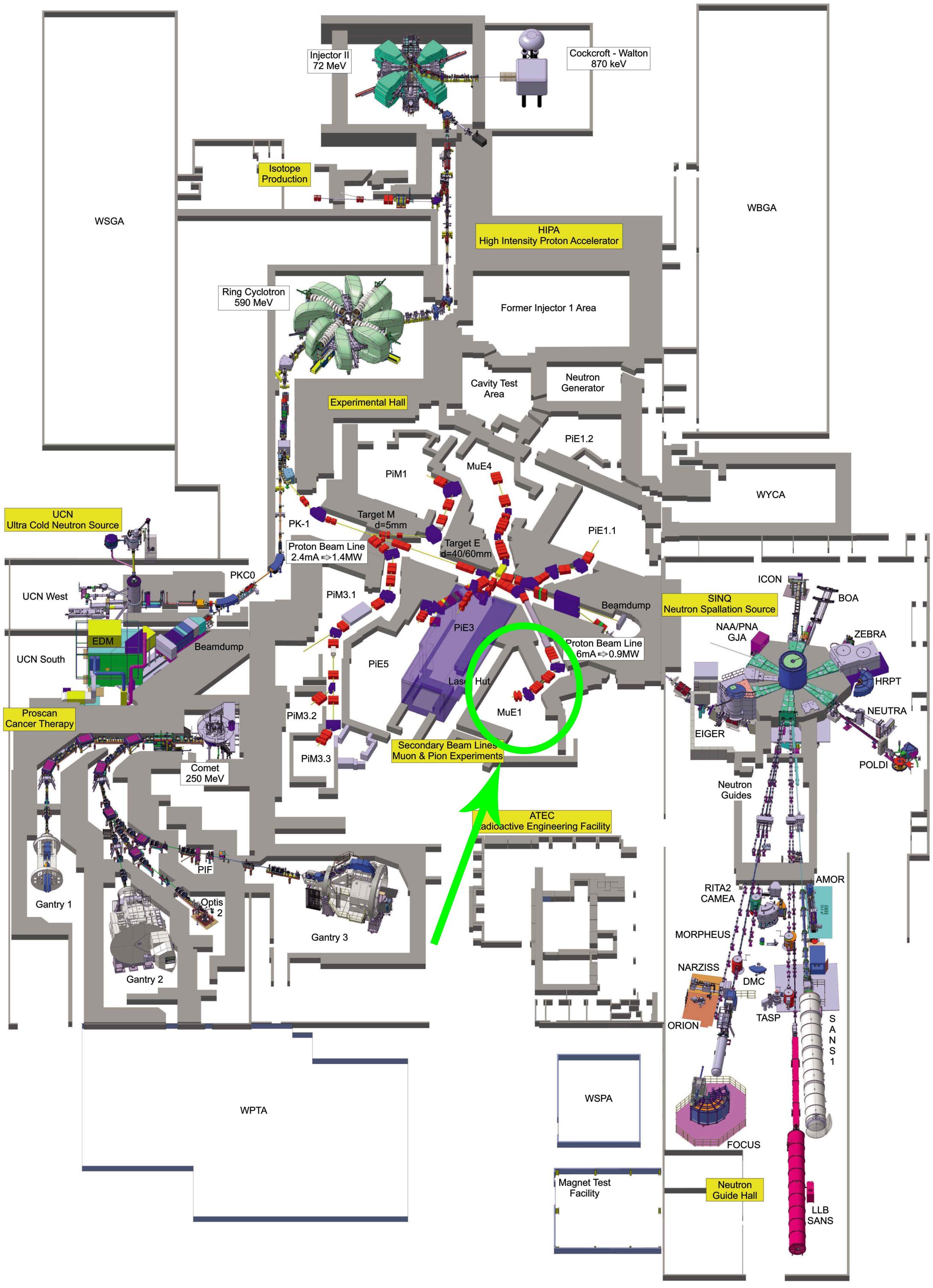

Figure 2: High-Intensity Proton Accelerator (HIPA) facility at PSI - μE1 beam area is circled in green (Image from [15]).

2 Theory and Background

This section will describe the basic idea behind the μEDM experiment in Subsection 2.1, which is the 'Frozen Spin Technique', and how said technique is employed to measure the EDM of the muons[5, 16, 17, 18], as well as the basic concepts of particle beam dynamics (or beam optics) in Subsection 2.2 summarized from [19] and [14].

2.1 Theory of μEDM

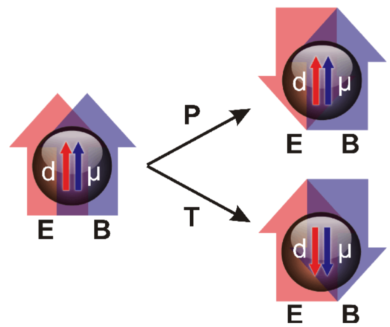

Figure 3: Behaviour of the electric dipole moment or 'EDM' ($\vec{d}$) and the magnetic dipole moment ($\vec{\mu}$) of a particle under parity (P) and time (T) reversal. CPT invariance is preserved (Image from [20]).

The Electric Dipole Moment or 'EDM' ($\vec{d}$) of a muon is given by Equation (1) whereas the magnetic dipole moment ($\vec{\mu}$) of a muon is given by Equation (2).

$$\vec{d} = \frac{\eta q}{2mc}\vec{s}, \tag{1}$$

$$\vec{\mu} = \frac{gq}{2m}\vec{s}. \tag{2}$$

Here, q is the charge and is equal to $(-e)$, m the mass and $\vec{s}$ is the spin of the muon, while c is the speed of light, g is the muon's g-factor (which is what is measured by muon g-2 experiments) and 'η' is the dimensionless EDM constant which is measured using the 'Frozen Spin Technique' in the μEDM experiment.

The relative spin precession ($\vec{\omega}$) of a charged particle (Figure 4) is given by:

$$\vec{\omega} = \vec{\omega}_a + \vec{\omega}_e \tag{3}$$

where $\vec{\omega}_a$ is the magnetic component and $\vec{\omega}_e$ is the electric component:

$$\vec{\omega}_a = -\frac{e}{m}\left\{a_\mu \vec{B} - \frac{a_\mu \gamma}{1+\gamma}\left(\vec{\beta}\cdot\vec{B}\right)\vec{\beta} - \left(a_\mu + \frac{1}{1-\gamma^2}\right)\frac{\vec{\beta}\times\vec{E}}{c}\right\}, \tag{4}$$

$$\vec{\omega}_e = -\frac{e\eta}{2m}\left\{\vec{\beta}\times\vec{B} + \frac{\vec{E}}{c} - \frac{\gamma}{c\,(1+\gamma)}\left(\vec{\beta}\cdot\vec{E}\right)\vec{\beta}\right\}. \tag{5}$$

In case of a non-zero EDM for the muon (or any other particle), the spin-precession plane tilts as shown in Figure 4 as a result of vector addition of the magnetic and electric components.

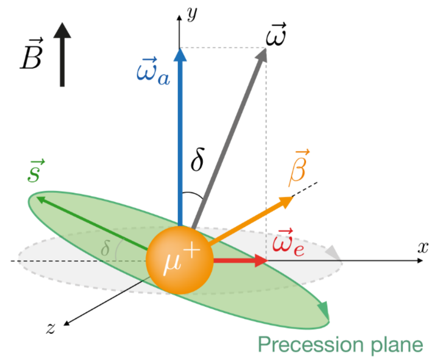

Figure 4: The muon's plane of precession tilts due to non-zero EDM (Image from [5]).

The larger the value of the EDM, the greater also is the tilt. The μEDM experiment uses this property to study the muon's EDM by trapping the muon in a storage ring using a strong kicker magnet pulse such that only the transverse motion of the muon persists owing to an externally applied solenoidal magnetic field as seen in Figure 5.

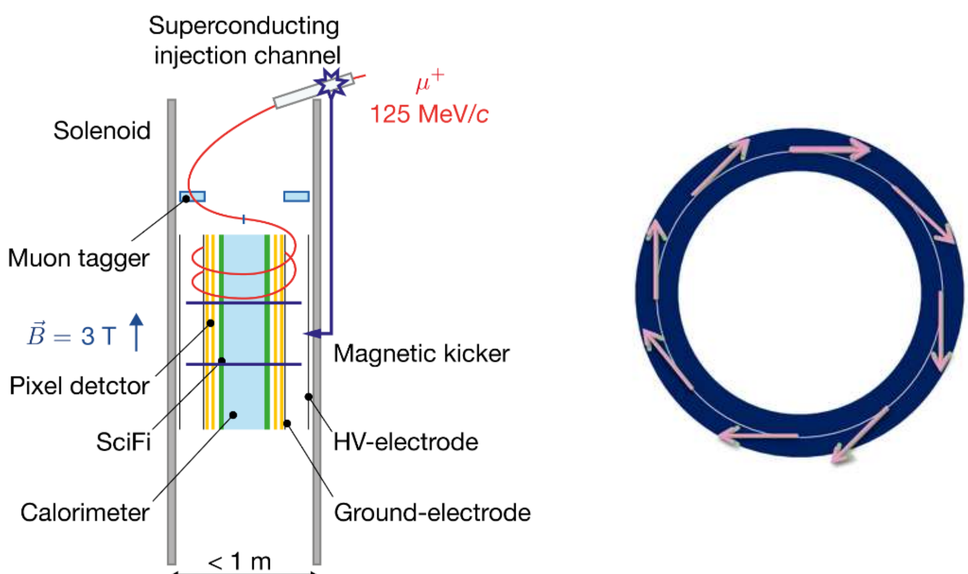

Figure 5: Concept of the μEDM experiment's setup with strength of the externally applied magnetic and electric fields chosen so as to freeze the muon's spin in the storage ring [LEFT] ; Spin-precession of the muon in the storage ring [RIGHT]. Images from [5].

At all times in the storage ring, electric and magnetic fields are applied orthogonally to the direction of motion of the stored muons ($\vec{E} \perp \vec{\beta} \perp \vec{B}$) and hence:

$$\vec{\beta} \cdot \vec{E} = \vec{\beta} \cdot \vec{B} = 0. \tag{6}$$

Equation (3) then simplifies to:

$$\vec{\omega} = -\frac{e}{m}\left[\left\{a_\mu \vec{B} - \left(a_\mu + \frac{1}{1-\gamma^2}\right)\frac{\vec{\beta}\times\vec{E}}{c}\right\} + \frac{\eta}{2}\left\{\vec{\beta}\times\vec{B} + \frac{\vec{E}}{c}\right\}\right]. \tag{7}$$

The frozen spin technique involves applying an electric field (E_f) of a strength such that the middle term cancels out with the first term of Equation (7):

$$E_f \approx a_\mu B c \beta \gamma^2, \tag{8}$$

$$a_\mu \vec{B} = \left(a_\mu + \frac{1}{1-\gamma^2}\right)\frac{\vec{\beta}\times\vec{E_f}}{c}. \tag{9}$$

Thus, Equation (3) then further simplifies to Equation (10), leaving behind only the EDM component (η):

$$\vec{\omega} = -\frac{\eta e}{2m}\left(\vec{\beta}\times\vec{B} + \frac{\vec{E}}{c}\right). \tag{10}$$

Hence, measuring the spin-precession of the muon in the storage ring under these conditions will give the direct measurement of the muon EDM. A positron detector will also be installed - either upstream or downstream - to estimate the asymmetry in the stored muons' decay to positrons in order to extract the asymmetry parameter [A(t)] which is given by Equation (11) and is proportional to the muon's EDM.

$$A(t) = \frac{N_{up} - N_{down}}{N_{up} + N_{down}} = A\ sin(\omega_e t). \tag{11}$$

Using this, the EDM and its statistical sensitivity can be given by:

$$d_\mu = \frac{a_\mu \hbar \gamma^2}{2P_0 E_f t \alpha} A(t), \tag{12}$$

$$\sigma(d_\mu) = \frac{a_\mu \hbar \gamma}{2P_0 E_f \sqrt{N} \tau_\mu \alpha}. \tag{13}$$

Here, $[A(t) = \alpha P_0 \sin(\omega t)]$ which is the measured asymmetry wherein α is the analysis power of the final polarization, and P_0 is the initial muon beam polarization[14]. Hence, it is clear that the statistical uncertainty $\left(\sigma(d_\mu)\right)$ of the EDM measurement is inversely related to the square root of the statistical number of particles analysed N and the frozen-spin electric field strength E_f, as well as the muon momentum which is inversely related to the Lorentz factor γ. Hence, ideal conditions for the experiment would be a muon beam with large momentum and high rates, to optimize the μE1 beamline for which is the aim of this thesis.

2.2 Particle Beam Dynamics

A particle in any given particle beam is usually expressed in the Frenet-Serret coordinate system which uses (x,y,l) as the base axes with ‘l’ being the direction of propagation of the beam and x and y the transverse directions. Hence, said particle can be described by 6 phase-space coordinates - x, x’ (or θ), y, y’ (or ϕ), l and δ (or momentum)[14].

$$\mathbf{X} = \begin{pmatrix} x \\ \theta \\ y \\ \phi \\ l \\ \delta \end{pmatrix}. \tag{14}$$

Using this phase-space for all particles in a beam, a 6×6 covariance matrix (also called the phase-space matrix) ‘σ’ can then be established for the whole beam[19, 21]:

$$\sigma = \begin{pmatrix} \sigma_{xx} & \sigma_{x\theta} & \sigma_{xy} & \sigma_{x\phi} & \sigma_{xl} & \sigma_{x\delta} \\ & \sigma_{\theta\theta} & \sigma_{\theta y} & \sigma_{\theta\phi} & \sigma_{\theta l} & \sigma_{\theta\delta} \\ & & \sigma_{yy} & \sigma_{y\phi} & \sigma_{yl} & \sigma_{y\delta} \\ & & & \sigma_{\phi\phi} & \sigma_{\phi l} & \sigma_{\phi\delta} \\ & & & & \sigma_{ll} & \sigma_{l\delta} \\ & & & & & \sigma_{\delta\delta} \end{pmatrix} \tag{15}$$

where, the diagonal elements are:

- $\sqrt{\sigma_{xx}}$ = Standard deviation of the horizontal beam distribution
- $\sqrt{\sigma_{\theta\theta}}$ = Standard deviation of the horizontal angular divergence distribution
- $\sqrt{\sigma_{yy}}$ = Standard deviation of the vertical beam distribution
- $\sqrt{\sigma_{\phi\phi}}$ = Standard deviation of the vertical angular divergence distribution
- $\sqrt{\sigma_{ll}}$ = Longitudinal particle beam ‘bunch’ length or phase uncertainty
- $\sqrt{\sigma_{\delta\delta}}$ = Standard deviation of the momentum spread around the central beam momentum

and the off-diagonal elements represent the covariances between the diagonal phase elements. This phase-space matrix can be acted upon by a transformation (or transfer) matrix ‘**R**’ which can be constructed using the various beamline components that the particle beam passes through such as focussing quadrupole magnets, bending dipole magnets, free drift space etc. Thus, the final phase-space matrix given the initial matrix and a transformation matrix can be algebraically expressed as:

$$\sigma_{final} = \mathbf{R}\sigma_{initial}\mathbf{R}^T \tag{16}$$

where

$$\mathbf{R} = \mathbf{R}_n\mathbf{R}_{n-1}...\mathbf{R}_3\mathbf{R}_2\mathbf{R}_1 \tag{17}$$

with $\mathbf{R}_n$ being the beamline component seen **last** by the particle beam. For a single particle with a given phase-space of **X**, the transfer matrix acts upon it according to Equation (18).

$$\mathbf{X}_{final} = \mathbf{R}\mathbf{X}_{initial}. \tag{18}$$

The full matrices for dipoles, quadrupoles and drift spaces can be found below:

- **Quadrupole Matrix:**

$$\mathbf{R}_{Quadrupole} = \begin{pmatrix} \cos(L_Q\sqrt{k}) & \frac{1}{\sqrt{k}}\sin(L_Q\sqrt{k}) & 0 & 0 & 0 & 0 \\ -\sqrt{k}\sin(L_Q\sqrt{k}) & \cos(L_Q\sqrt{k}) & 0 & 0 & 0 & 0 \\ 0 & 0 & \cosh(L_Q\sqrt{|k|}) & \frac{1}{\sqrt{|k|}}\sinh(L_Q\sqrt{|k|}) & 0 & 0 \\ 0 & 0 & \sqrt{|k|}\sinh(L_Q\sqrt{|k|}) & \cosh(L_Q\sqrt{|k|}) & 0 & 0 \\ 0 & 0 & 0 & 0 & 1 & 0 \\ 0 & 0 & 0 & 0 & 0 & 1 \end{pmatrix} \tag{19}$$

where L_Q is the length of the quadrupole and k is the focussing strength of the quadrupole (expanded upon in Section 4.1.2). This matrix is for a quadrupole that focusses in the horizontal (X) direction and defocusses in the vertical (Y) direction. Conversely, a vertically focussing and horizontally defocussing quadrupole can be described by interchanging the first 2 diagonal (non-zero) 2×2 matrices.

- **Dipole Matrix:**

$$\mathbf{R}_{Dipole} = \begin{pmatrix} \cos\alpha & r\sin\alpha & 0 & 0 & 0 & r(1-\cos\alpha) \\ -\frac{1}{r}\sin\alpha & \cos\alpha & 0 & 0 & 0 & \sin\alpha \\ 0 & 0 & 1 & r\alpha & 0 & 0 \\ 0 & 0 & 0 & 1 & 0 & 0 \\ -\sin\alpha & -r(1-\cos\alpha) & 0 & 0 & 1 & -r(\alpha-\sin\alpha) \\ 0 & 0 & 0 & 0 & 0 & 1 \end{pmatrix} \tag{20}$$

where α is the bending angle and r is the bending radius which, along with the applied magnetic field strength (B), selects the momentum of the beam particles (P) as $\left[r = \frac{P}{qB}\right]$.

- **Drift Space Matrix:**

$$\mathbf{R}_{Drift} = \begin{pmatrix} 1 & L_D & 0 & 0 & 0 & 0 \\ 0 & 1 & 0 & 0 & 0 & 0 \\ 0 & 0 & 1 & L_D & 0 & 0 \\ 0 & 0 & 0 & 1 & 0 & 0 \\ 0 & 0 & 0 & 0 & 1 & L_D/\gamma^2 \\ 0 & 0 & 0 & 0 & 0 & 1 \end{pmatrix} \tag{21}$$

where L_D is the length of the drift space and γ is the lorentz factor of the central momentum reference particle.

The transverse or 4D phase-space of a particle beam can expressed as 2 sets of 4 Courant-Snyder or Twiss parameters[22], namely (α, β, γ and ε). The description of these Twiss parameters and how they can be measured are discussed extensively in Section 4.1.2. Comprehensive information on particle beam optics can be found in [19] and [21].

3 Beamtime Preparation and Experimental Setup

Input from experimental data is essential in order to model a beamline, as simulation modelling involves a number of unknown variables and relies heavily upon the input phase space. Ideally, the phase space would be measured at the input of the beamline itself, however this is simply not possible. To reconstruct the input phase space, the phase space at the end of the beamline must be analysed from data and then projected backwards through the beamline to its beginning, hence making experimental input invaluable.

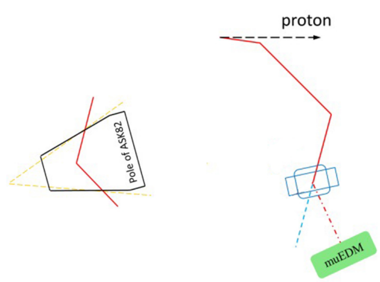

Figure 6: Configuration used to characterize μE1's muon beam in June 2024 (Courtesy: C. Cong)

The data for modelling of the μE1 beamline at PSI was collected during the first week of June 2024 by the μEDM group of PSI over the course of a week-long beamtime at PSI. The μE1 beamline was operated in the Z-configuration with the ASK82 dipole rotated 20° counter-clockwise from the straight configuration such that a 35° fringe field angle on both the entrance and exit of ASK82 is observed with the shorter side of the horseshoe pole of the ASK82 dipole on the right side with respect to the direction of propagation of the beam so as to induce a weak fringe field (Figure 6). The ASK82 dipole deflects the central trajectory of the beam by 40°, while the upstream ASK81 dipole deflects the central trajectory by 60°. A schematic of the experimental setup, including the detectors and collimators used, after ASK82 is shown in Figure 7.

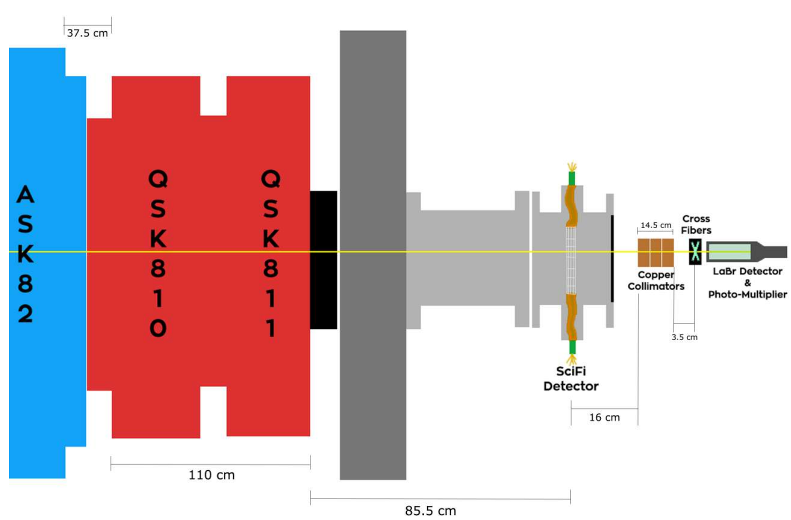

Figure 7: Schematic of the Experimental Setup after the ASK82 dipole magnet

To collect the data, two sets of detectors were used - a scintillating fibre (SciFi) mesh detector[23] which recorded particle hits above a tuned threshold so as to avoid noise (Figure 11) and two crossed plastic scintillation bars (SciCross) attached to a Lanthanum Bromide (LaBr) crystal calorimeter, both of which recorded waveforms, for 5-point coincidence (which is to say that the particles that were recorded passed through the 1cm^2 overlap of the SciCross bars, thus entering the LaBr through the cenrtal axis). Besides the detectors, 3 copper collimators of 5cm thickness each and 4 interchangeable collimation holes of radii 4mm, 3mm, 2mm and 1mm were also used to decrease the rate of the muons incident upon the LaBr calorimeter so as to avoid pileup (Figure 8). The DAQ system used to acquire all the data was the WaveDAQ system[24] which is made of 16-channel WaveDREAM boards that were developed at PSI[25].

Figure 8: Copper Collimators used during the beamtime. Each of the 3 collimators are 5cm thick and have 4 interchangeable collimation holes of radii 4mm, 3mm, 2mm and 1mm.

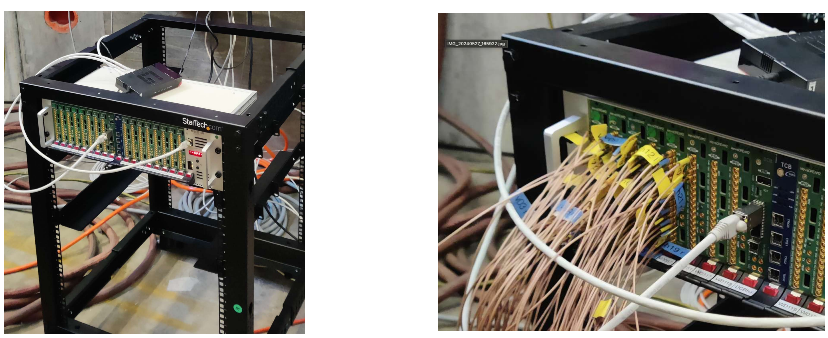

Figure 9: WaveDAQ system: before connections [LEFT], after connections - 6 WaveDREAM boards were connected to the 84 SiPM ends of the SciFi detector and a separate WaveDREAM board was connected to the 4 ends of the SciCross, the LaBr and the HIPA proton current [RIGHT].

Prior to the beamtime, efforts were made to optimize the beamline using the ‘Transport’ software developed by CERN[26], however upon setting the μE1 beamline’s magnet currents to be in accordance with the Transport optimization (shown in Figure 10), very low rates were observed. This is most likely due to the fact that the input phase space used in the simulation was an empirical estimate and not derived from experimental data, further highlighting the importance of this measurement. Hence, the **Transport optimization was abandoned in favour of manual optimization** during the beamtime which then yielded much higher rates.

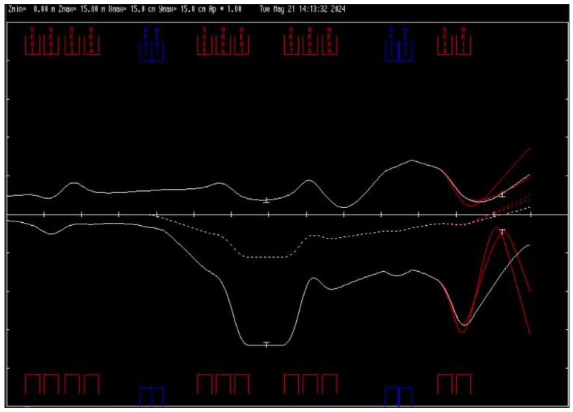

Figure 10: Pre-beamtime optimization of 100 MeV/c muons in the μE1 beamline with [$\delta P/P = 3\%$] (Yielded very low rates upon use and was thus **NOT used**). The red and blue rectangles at the top and bottom represent quadrupoles and dipoles along the μE1 beamline respectively, the central line represents the direction of propagation (Z), the top and bottom-half white curves represent the 1σ spread of the beam in the vertical (Y) and horizontal (X) directions respectively. The dotted white curve shows the energy dispersion along X through the beamline. The red curves represent another optimized configuration wherein an attempt was made to minimize the beam spread in X, while the white curves minimized the dispersion.

The following subsections will discuss the detectors and the measurements made during the beamtime.

3.1 Scintillating Fiber (SciFi) Detector

The scintillating fiber (SciFi) detector that was used in June 2024 was a plastic scintillator mesh detector developed at the University of Pisa based on the concept mentioned in [23]. The detector itself comprises a 21 x 21 grid of 0.5mm thick scintillating fibers, the ends of which are connected to silicon photomultipliers (SiPMs) which then relay the particle signal to the DAQ system. Each grid point (where a horizontal and a vertical fiber cross each other) is taken as the centre of a $(5x5)mm^2$ square to make up a 105mm-side square of detection area that can detect the rate of the particles incident upon it (Figure 11).

Figure 11: Scintillating Fiber (SciFi) detector horizontally laser aligned with the beam [LEFT] ; Position of SciFi after QSK811 magnet with 855mm of drift space [RIGHT].

β particles from a strontium-90 (Sr90) radioactive source were used to calibrate the SciFi detector. The SciFi was mounted at a distance of (855 ± 3)mm from the end of the QSK811 quadrupole. The data collected at the SciFi detector was converted to MIDAS (.mid) files and saved for analysis.

3.2 Scintillation Cross (SciCross) Detector

The scintillation cross (SciCross) detector was made up of two (90 x 10 x 5)mm^3 plastic scintillator bars stacked on top of each other in a cross-shape as seen in Figure 12 with their ends attached to an SiPM each using optical cement, the output from which was connected to different channels of a WaveDREAM board for coincident muon detection with LaBr. The SciCross DAQ stores waveforms, the number of which is proportional to the energy lost through ionisation of the detected particle on its path through the material[27]. Since the bars were not thick enough to stop the particles, the gathered data shows energy deposited in the bars rather than total energy of the particle.

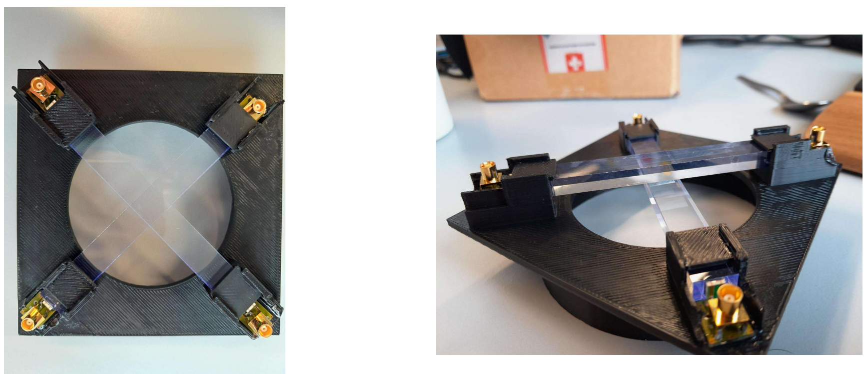

Figure 12: Plastic Scintillating Cross (SciCross) Detector

The holder for the SciCross was designed using CAD Onshape software[28] by the author of this thesis and then 3D printed for use in the experiment. To block ambient light from reaching the SciCross, the whole cross was covered from the top and bottom using a black, optically opaque filter sheet as seen in Figure 13. The 4 ends of the 2 bars were attached to channels 1, 2, 3, and 4 of the WaveDREAM board used for the SciCross-LaBr compound detector DAQ, and the back end of the holder was attached onto the LaBr calorimeter as designed for use in the experiment.

Figure 13: Covered SciCross to filter light from the ambient environment out [(half) LEFT ; (final) MIDDLE & RIGHT].

3.3 Lanthanum-Bromide (LaBr) Detector

The lanthanum bromide detector (LaBr) is a calorimeter made up of $LaBr_3$ and has been used extensively as a scintillator and as a calorimeter in physics[29, 30, 31, 32]. The LaBr used for this thesis had a diameter of 82.6mm and a length of 100mm, with simulations made prior to the beamtime confirming that all muons (100 MeV/c, 125 MeV/c and 140 MeV/c) coincident upon the SciCross and the LaBr would stop well before the 100mm end of the LaBr and deposit all their energy.

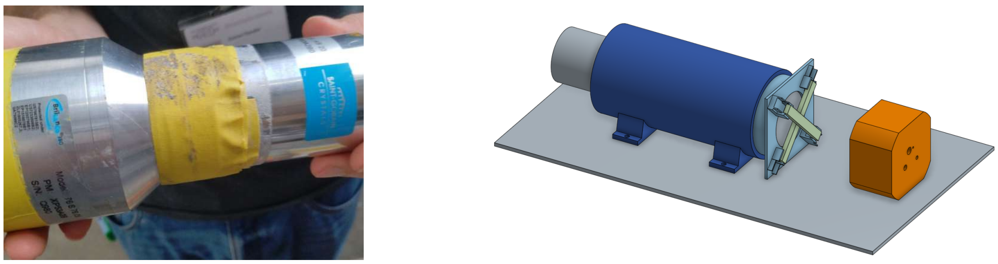

Figure 14: Lanthanum Bromide (LaBr) Calorimeter [LEFT] ; LaBr assembled with the SciCross and holders in OnShape [RIGHT].

The LaBr is fitted with a photomultiplier tube (PMT) which transforms the light into an electric pulse which is recorded by the WaveDAQ after being digitized using an ADC. During data taking, the LaBr's signal was fed into the channel 15 of the WaveDREAM board that was used.

The holder for the LaBr (Figure 15) was designed by the author using CAD Onshape as in the case of the SciCross' holder, and leverages the conical bend in the LaBr apparatus as shown in Figure 14 to fix the LaBr in between the holder and the SciCross. The holder of the LaBr was then screwed onto the aluminium plate base which was then attached to the XYZ table so as to allow movement of the SciCross-LaBr compound detector across the beam.

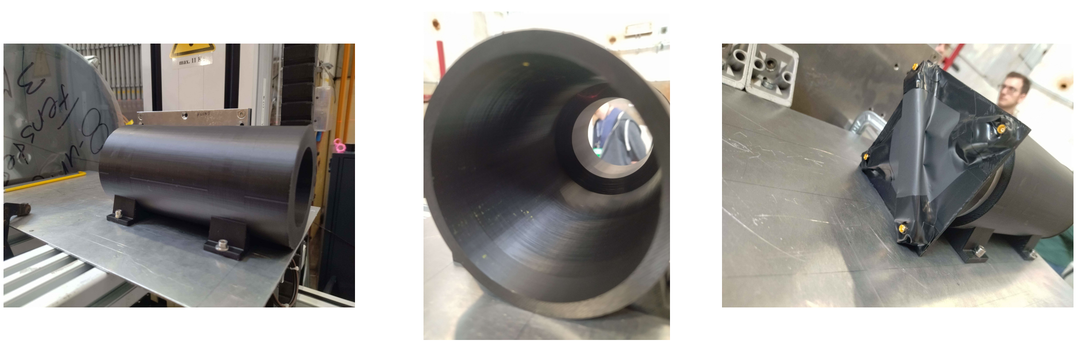

Figure 15: LaBr Holder [LEFT & MIDDLE] ; LaBr assembled with the SciCross [RIGHT].

All data from the SciCross and the LaBr were obtained and saved in the wavedream (.wd) format for analysis. The 'home position', or relative (0,0,0), of the SciCross-LaBr compound on the XYZ table as per the centre of the beam pipe was initially found to be at absolute (311,164,10), where absolute (0,0,0) is when the XYZ table is as close to the beam pipe as possible and as far left and low as possible. It is to be noted that it was known prior to data taking that **the energy resolution of the LaBr was degraded due to neutron exposure, and efforts were made in the analysis, largely successful, to recover the energy and time resolutions of the LaBr.**

3.4 Measurements

The final set up with and without the LaBr mounted on the XYZ table can be seen in Figure 16.

Figure 16: SciFi setup with Tedlar layer for vacuum protection [LEFT] ; Final setup with SciCross-LaBr mounted on the XYZ table [MIDDLE] ; LaBr aligned with the beam on XYZ table [RIGHT].

Phase space measurements were made for 173 MeV/c and 216 MeV/c momentum pions **backward decaying** to muons of **100 MeV/c and 125 MeV/c** momenta respectively, as well as for 127 MeV/c pions **forward decaying** to **140 MeV/c muons**. These measurements included quadrupole scans of the last 2 quadrupoles after the ASK82 dipole - namely QSK810 and QSK811 - for 4D phase space and LaBr scans using the XYZ table of the beam for energy and dispersion measurements, as well as time of flight (ToF) measurements . A summary can be found in Table 1.

Pion Momentum	Muon Momentum	Beam Tune	Purpose
173 MeV/c	100 MeV/c	mue1_p100_Jun_2024_Z-Config-V1_TRANSPORT_Tune6.sp	5mm Square - Closed Slits Quadrupole Current Scans
			5mm Square - Closed Slits Cross-LaBr Scans
			Open Slits Quadrupole Current Scans
216 MeV/c	125 MeV/c	mue1_p125_Jun_2024_Z-Config-V1_Tune1.sp	Open Slits Quadrupole Current Scans
			5mm Square - Closed Slits Cross-LaBr Scans - X only
		mue1_p125_Jun_2024_Z-Config-MUSR_TunePion_v3.sp	Open Slits Quadrupole Current Scans
			5mm Square - Closed Slits Cross-LaBr Scans - X only
127 MeV/c	140 MeV/c	mue1_pi127_mu140_Jun_2024_Z-Config-MUSR_Tune1.sp	4mm Square - Closed Slits Cross-LaBr Z Scans - X only
			Open Slits Cross-LaBr Z Scans
			TOF Studies
			5mm Slits Z Scan Cross-LaBr Scans
			20mm Square Slits Cross-LaBr Z Scans

Table 1: Summary of measurements made during the June 2024 beamtime

Beam Tune File Name	**Purpose**
mue1_p100_Jun_2024_Z-Config-V1_TRANSPORT.sp mue1_p100_Jun_2024_Z-Config-V1_TRANSPORT_PrelimTune.sp mue1_p100_Jun_2024_Z-Config-V1_TRANSPORT_Tune2.sp mue1_p100_Jun_2024_Z-Config-V1_TRANSPORT_Tune3.sp mue1_p100_Jun_2024_Z-Config-V1_TRANSPORT_Tune4.sp mue1_p100_Jun_2024_Z-Config-V1_TRANSPORT_Tune5.sp	Beam tune optimization.
mue1_p100_Jun_2024_Z-Config-V1_TRANSPORT_Tune6.sp	LaBr quadrupole scans (100MeV/c). Also the only tune used for the low rates data when the upstream solenoid was hot due to lack of Helium. SciFi quadrupole scans (100MeV/c) with all slits fully open. Estimation of the efficiency of the SciFi for 100MeV/c.
mue1_p125_Jun_2024_Z-Config-V1_Initial.sp	Initial scaled 125MeV/c beam tune.
mue1_p125_Jun_2024_Z-Config-V1_Tune1.sp	125MeV/c optimized beam tune. Used for SciFi quadrupole scans (125MeV/c), and for LaBr + SciFi quadrupole scans (125MeV/c) X scan with 5mm Y slit.
mue1_Pion120_Mu125_fd_Jun_2024_Z-Config-V1_Tune1.sp mue1_Pion125_Mu125_fd_Jun_2024_Z-Config-V1_Tune1.sp mue1_Pion125_Mu120_fd_Jun_2024_Z-Config-V1_Tune1.sp mue1_Pion125_Mu115_fd_Jun_2024_Z-Config-V1_Tune1.sp mue1_Pion125_Mu130_fd_Jun_2024_Z-Config-V1_Tune1.sp mue1_Pion125_Mu135_fd_Jun_2024_Z-Config-V1_Tune1.sp	Time of Flight (TOF) studies for forward decay.
mue1_p100_Jun_2024_Z-Config-MUSR_Initial.sp mue1_p90_Jun_2024_Z-Config-MUSR_TunePion.sp mue1_p100_Jun_2024_Z-Config-MUSR_TunePion.sp mue1_p125_Jun_2024_Z-Config-MUSR_TunePion.sp	MuSR Beamtune The 4 beam tunes are for 4 different muon momenta, with the currents simply scaled from the initial MuSR beam tune.
mue1_p125_Jun_2024_Z-Config-MUSR_TunePion_v1.sp	125MeV/c (backward decay) beam tune optimization.
mue1_p125_Jun_2024_Z-Config-MUSR_TunePion_v3.sp	LaBr + SciFi quadrupole scans (125MeV/c) X scan with 5mm Y slit, SciFi quadrupole scans (125MeV/c) with all slits fully open and to estimate the efficiency of the SciFi for 125MeV/c.
mue1_pi127_mu140_Jun_2024_Z-Config-MUSR_EdgeInitial.sp mue1_pi127_mu142_Jun_2024_Z-Config-MUSR_Tune1.sp mue1_pi127_mu145_Jun_2024_Z-Config-MUSR_Tune1.sp mue1_pi127_mu150_Jun_2024_Z-Config-MUSR_Tune1.sp mue1_pi127_mu147_Jun_2024_Z-Config-MUSR_Tune1.sp	TOF studies in order to obtain 140MeV/c muons via pion forward decay.
mue1_pi127_mu140_Jun_2024_Z-Config-MUSR_Tune1.sp	LaBr + SciFi quadrupole scans (140MeV/c) X scan with 4mm Y slit. LaBr + SciFi quadrupole scans (140MeV/c) Y scan with 4mm X slit. To obtain TOF measurement for 140MeV/c with ALL slits closed to (2.5+2.5)mm 140MeV/c tests to see best approach to take measurements. LaBr + SciFi quadrupole scans (140MeV/c). A single copper collimator was installed downstream of the cross-scintillators to reduce rate on LaBr. LaBr + SciFi quadrupole scans (140MeV/c) with upstream slits in a (5x5)mm square and downstream slits fully open. TOF spectra measurements for 140MeV/c forward decay at various Z positions and trigger threshold values. TOF measurements with no collimators (not even in between the cross and LaBr). LaBr + SciFi Z scans (140MeV/c) - X scan with 5mm horizontal slit and Y scan with 5mm vertical slit.

Table 2: List of all the beamtunes developed and used during the June 2024 beamtime - the 4 main beamtunes used for phase space measurments are highlighted in bold.

The slits mentioned above refer to the **2 slit systems** that the μE1 beamline was equipped with during the June 2024 beamtime: one upstream of the ASK82 (named 'FS81') and one in between the QSK811 quadrupole and the SciFi detector (named 'FS00'). These are divided up into 4 parts each - Left (L), Right (Right), Up (O) and Down (U) - which can range in position from 0mm (closed) to 140mm (fully open). The slits allow the rates to be constrained by excluding tails of the beam envelope along the transverse directions which helps avoid pile-up in the WaveDAQ.

As is seen in Table 1, phase space measurements were also made for the beamtune used by the Muon Spin Resonance (μSR) group at PSI in order to compare the new beamtune that was manually optimized during the June 2024 beamtime with the μSR beamtune to check if the former was more or less favourable for μEDM's phase 2 measurement than the latter. Since the magnets in the μE1 beamline were not (at the time of measurement) equipped to be able to steer pions of momenta greater than 220 MeV/c as required for sufficient statistics of pions backward decaying into muons with momenta greater than 125 MeV/c, ToF studies were conducted on muons from forward decaying pions for various combinations of pion and muon momenta. In the end, to access muon momenta above 125 MeV/c, data was taken using forward decaying pions with a momentum of 127 MeV/c. As mentioned earlier, the beamtunes used for the measurements were optimized manually during the June 2024 beamtime and were stored in the μE1 beamline control room monitoring system as well as with the author and can be made available upon request. The list of the beamtunes and how they were used during the beamtime can be obtained from Table 2.

The measurements were taken during the first week of June 2024 which was also the first week of beam operation at PSI in 2024. The muon beam **did not** have any dips due to the proton beam periodically being redirected towards the Ultra-Cold Neutron (UCN) facility at PSI as it was not operating during the course of the June 2024 μEDM beamtime. As mentioned in Table 2, there was a period during the beamtime during which the pion decay solenoid of the beamline was insufficiently cooled due to lack of helium coolant, and so very low rates were observed for a few hours during the 100 MeV/c muon momentum LaBr scans (with SciFi also active). This data was taken as a curiosity nonetheless, however further analysis did not show anything peculiar or significantly different from the 'normal' data.

The optimal current settings for the last 2 quadrupoles, QSK810 and QSK811, around which the quadrupole current scans were performed (by keeping 1 of the quadrupoles at the optimal current and taking data for the currents around the optimal of the other quadrupole and vice-versa) are summarized in the table below:

Muon Momentum	Optimal Current (A)	
	QSK810	QSK811
100 MeV/c	-87.2	123.7
125 MeV/c	-109.6	155.4
125 MeV/c (μSR)	-114.8	158.2
140 MeV/c	-126.2	178.5

Table 3: Optimal current configurations of QSK810 and QSK811 quadrupoles for each beamtune used for data

4 Methodology

This section will expand upon the various techniques used to extract the phase space of the beam-tunes used from the data collected during the June 2024 beamtime. In addition, efforts were made to characterize the energy resolution of the LaBr which was known to have degraded due to neutron exposure from prior use (see Section 3.3) in order to extract accurate results. The methodology of this characterization will be expanded upon in Section 4.2.

Analysis of the data collected during the June 2024 beamtime was performed using ROOT (C++), Python and PyROOT with aid of Geant4. Modifications to code developed by Dr. Diego Alejandro Sanz Becerra were made by the author in order to read the SciFi (.mid) and SciCross-LaBr (.wd) data files and extract ROOT (.root) files for analysis. Said code can be found on the muEDM GitLab page (`https://gitlab.psi.ch/muEDM`) under the 'dev-harrsh' branch of the 'SCIFIReader' repository for the SciFi (.mid) file conversion, and under the 'main' branch of the 'muEDMTest-BeamTools' repository for the SciCross-LaBr (.wd) file conversion. Instructions for conversion of both file types, as well as for the use of the other code files on the 'dev-harrsh' branch of the 'SCIFIReader' repository, are provided on the respective'README.md' files . Similarly, all the code used for the analysis of the extracted data and the modelling of the results have been uploaded to the muEDM GitLab page in a new repository - `https://gitlab.psi.ch/muEDM/analysis/mue1_z_june2024` - including appropriate README.md files. It is to be noted that access to the GitLab repository is restricted to users approved by PSI.

4.1 Phase Space Extraction Techniques

For each muon beam setting, 5 different analytical techniques were used to obtain the most important and necessary elements of the phase space matrix mentioned in Equation (15). These techniques and the subsequent matrix elements obtained using them are summarized in Table 4.

Technique	Detector	Matrix Elements Obtained
Transverse Beamspots	SciFi	σ_{xx}, σ_{xy}, σ_{yy}
Quadrupole Scans	SciFi	σ_{xx}, $\sigma_{x\theta}$, $\sigma_{\theta\theta}$, σ_{yy}, $\sigma_{y\phi}$, $\sigma_{\phi\phi}$
Z Scans**	SciCross-LaBr	σ_{xx}, $\sigma_{x\theta}$, $\sigma_{\theta\theta}$, σ_{yy}, $\sigma_{y\phi}$, $\sigma_{\phi\phi}$
ToF-Energy Distribution	SciCross-LaBr	σ_{ll}, $\sigma_{l\delta}$, $\sigma_{\delta\delta}$
Position-Momentum Slicing	SciCross-LaBr	$\sigma_{x\delta}$, $\sigma_{y\delta}$*

*Only available for 100 MeV/c muon momentum

**Used only for 140 MeV/c due to lack of Quadrupole Scan Data

Table 4: Various techniques used for analysis of the 6D phase space

The basic concepts behind each of the 5 techniques used for phase space extraction are expanded upon in the subsections below.

4.1.1 Transverse Beamspots

2D transverse beam profiles are extracted from the SciFi mesh's hit data which can be used to determine the beam's spread along the horizontal (σ_{xx}) and the vertical (σ_{yy}), as well as correlation (beamspot tilting - σ_{xy}) between the 2 transverse axes.[1] No gaussian fits were used on the beamspots as very large χ^2 values were observed, and all results are from the statistics of the histograms.

4.1.2 Quadrupole Scans

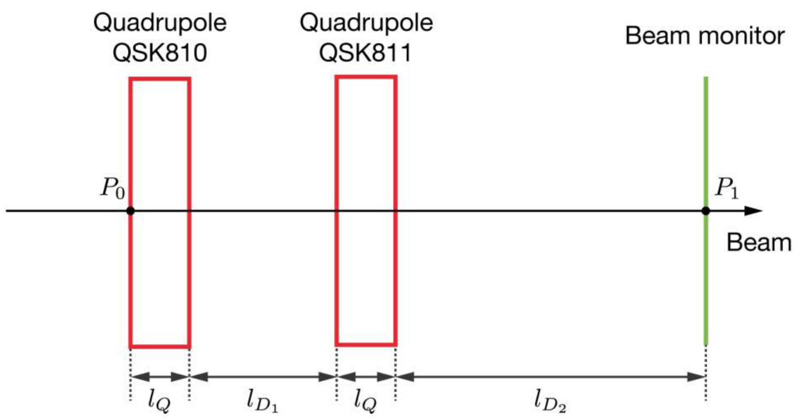

Figure 17: Quadrupole scan technique using QSK810 and QSK811 quadrupoles. Beamspots for various current settings of the 2 quadrupoles are obtained at point P_1 (SciFi in case of June 2024 beamtime). This current dependence of the beamspots is used to project the beam back to before the quadrupoles using matrix multiplication to obtain the full transverse phase space at P_0. Image from [14].

Quadrupole scans are a well known and widely used technique to obtain transverse (4D) phase spaces[14, 21, 33]. It involves measuring the beamspots, and thus the σ_{xx} and σ_{yy}, of a particle beam for a range of current settings of a single quadrupole or more (ideally at least 2) around their respective optimal current settings while keeping the other quadrupole(s)' currents at their optimal value if more than one quadrupole is being used. Then, the current profiles of the transverse spreads for all the quadrupoles used are plotted and fitted simultaneously according to Equation (31), separately for X and Y, in order to obtain 3 phase space parameters. These can be used to extract the Courant-Snyder or Twiss parameters[21, 22] (in case of zero dispersion) and express the transverse phase space in the form of 2 phase space ellipses, one for the horizontal (X) and one for the vertical (Y). An example of such a phase space ellipse is shown in Figure 18.

[1] This was performed by using the 'ReadEventsSCIFINoFit.py' code on the GitLab repository (https://gitlab.psi.ch/muEDM/analysis/scifireader/-/tree/dev-harrsh) which simply reads the MIDAS files and maps the rates observed on each fiber crossing onto a pixel in a 21x21 grid. Instructions for use are provided in the 'README.md' file.

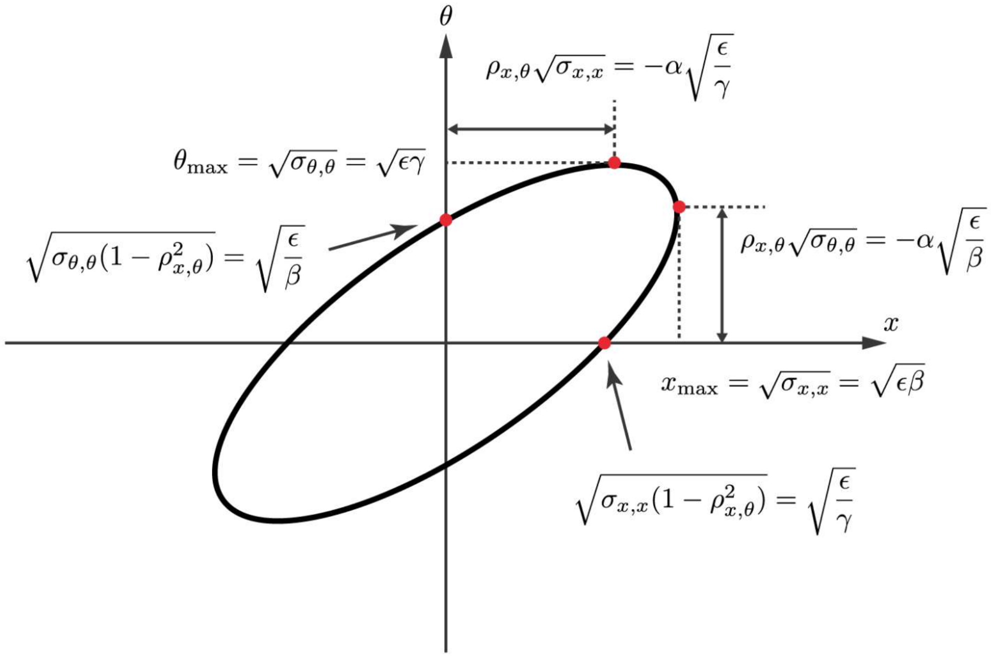

Figure 18: Example of a transverse phase space ellipse in the horizontal (X) plane. It is expressed using 3 phase space parameters - σ_{xx}, $\sigma_{x\theta}$ and $\sigma_{\theta\theta}$. The red points represent characteristic points - x_{max} and θ_{max} represent the std. dev. (1σ) of the horizontal beam size and beam divergence distribution respectively. The parameters can also be expressed in terms of the corresponding Courant-Snyder or Twiss parameters (ε, α, β, γ). These parameters have units of: $\varepsilon\,[m \cdot rad]$, $\alpha\,[dimensionless]$, $\beta\,[m/rad]$ and $\gamma\,[rad/m]$, with ε being the determinant of σ_X and is known as 'emittance'. Image from [14]

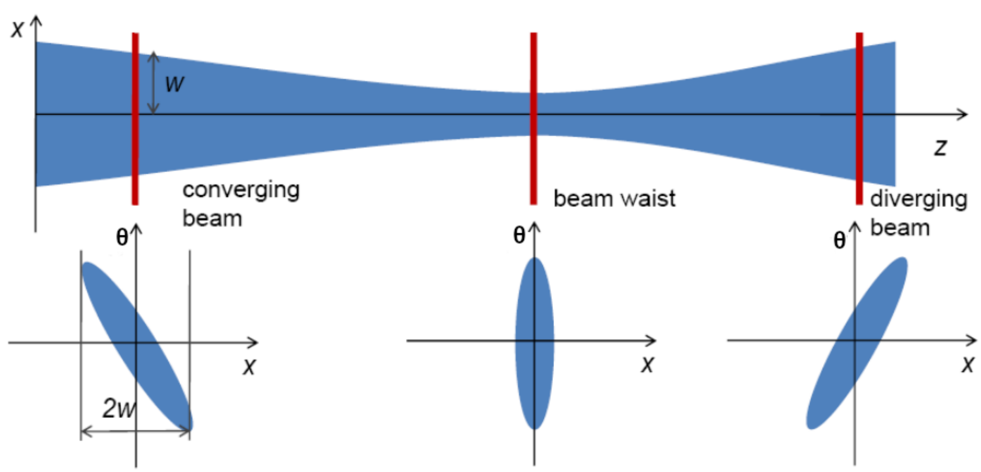

Figure 19: Illustration of the physical interpretation behind the correlation between x and θ $(\rho_{x\theta})$. Negative correlation implies that the beam is converging, positive correlation implies that the beam is diverging and zero correlation implies that the beam is at its waist. Image adapted from [34].

To understand the mechanism behind the quadrupole scan technique, let us focus on the horizontal phase space of (x,θ); the vertical phase space (y,ϕ) can be obtained identically to the horizontal. Given the horizontal phase space matrix[21]:

$$\sigma_X = \begin{pmatrix} \sigma_{xx} & \sigma_{x\theta} \\ \sigma_{x\theta} & \sigma_{\theta\theta} \end{pmatrix} = \begin{pmatrix} x_{max}^2 & \rho_{x\theta} x_{max}\theta_{max} \\ \rho_{x\theta} x_{max}\theta_{max} & \theta_{max}^2 \end{pmatrix} = \varepsilon \begin{pmatrix} \beta & -\alpha \\ -\alpha & \gamma \end{pmatrix} \tag{22}$$

where $[\sqrt{\sigma_{xx}} \equiv x_{max}]$, $[\sqrt{\sigma_{\theta\theta}} \equiv \theta_{max}]$ and $\rho_{x\theta}$ is the correlation between σ_{xx} and $\sigma_{\theta\theta}$. Using Equation (22), the Twiss parameters (ε, α, β, γ) can be found from the phase space measurement and vice-versa. These parameters have units of: $\varepsilon\,[m \cdot rad]$, $\alpha\,[dimensionless]$, $\beta\,[m/rad]$ and $\gamma\,[rad/m]$, with ε being the determinant of σ_X and is known as 'emittance'. ε is directly related to the area of the 1σ phase ellipse, A_X, as:

$$\varepsilon = \sqrt{|\sigma_X|} = \frac{A_X}{\pi}. \tag{23}$$

Now, using the transfer matrix $\mathbf{R}$, the phase space at P_1 and P_0 of Figure 17 can be equated as:

$$\sigma_X(P_1) = \mathbf{R}\sigma_X(P_0)\mathbf{R}^T \tag{24}$$

where $\mathbf{R}^T$ is the transpose of the transfer matrix $\mathbf{R}$ and comprises of all the beamline elements between P_0 and P_1.

$$\mathbf{R} = \mathbf{R}_{Q_d}\mathbf{R}_{drift}\mathbf{R}_{Q_f}\cdots \tag{25}$$

$\mathbf{R}_{Q_d}$ and $\mathbf{R}_{Q_f}$ are the transfer matrices for a horizontal **de-focusing** and horizontal **focusing** quadrupoles of length L_Q each respectively, and $\mathbf{R}_{drift}$ is the transfer matrix of free drift space of length L_D.

$$\mathbf{R}_{drift} = \begin{pmatrix} 1 & L_D \\ 0 & 1 \end{pmatrix}, \tag{26}$$

$$\mathbf{R}_{Q_f} = \begin{pmatrix} \cos(L_Q\sqrt{k}) & \frac{1}{\sqrt{k}}\sin(L_Q\sqrt{k}) \\ -\sqrt{k}\sin(L_Q\sqrt{k}) & \cos(L_Q\sqrt{k}) \end{pmatrix}, \tag{27}$$

$$\mathbf{R}_{Q_d} = \begin{pmatrix} \cosh(L_Q\sqrt{|k|}) & \frac{1}{\sqrt{|k|}}\sinh(L_Q\sqrt{|k|}) \\ \sqrt{|k|}\sinh(L_Q\sqrt{|k|}) & \cosh(L_Q\sqrt{|k|}) \end{pmatrix}. \tag{28}$$

Here, k is the **focusing strength of the quadrupole** and is dependent upon the current (I) applied to the quadrupole ($k \propto I$), thus dictating the relation between the transverse spread of the beam and the quadrupole current[19, 14]. This focusing strength, k, of a quadrupole can be calculated using the equation below (units of the variable involved are given in square brackets []):

$$k[\mathrm{m}^{-2}] = 0.2994\frac{B_0[\mathrm{T/A}] \cdot I[\mathrm{A}]}{a[\mathrm{m}] \cdot p[\mathrm{GeV/c}]} = 0.2998\frac{g[\mathrm{T/m}]}{\beta \cdot E[\mathrm{GeV}]} \tag{29}$$

where 'B_0' is the current gradient of the quadrupole, 'g' is the radial gradient of the magnet, 'p' and 'E' are the momentum and energy of the particles being acted upon by the quadrupole and 'a' is the aperture (pole-tip radius) of the quadrupole.

For the QSK quadrupole magnets used in for the measurement of this thesis, the aperture is $[a = 0.125m]$ and the current gradient is $\left[B_0 = (1.8246 \times 10^{-3})\frac{\mathrm{T}}{\mathrm{A}}\right]$.

Hence, using Equation (24), the first matrix element of σ_X can be equated to the first matrix element of the product matrix of the RHS to give:

$$\sigma_{xx}(P_1) = \mathbf{R}_{11}^2 \sigma_{xx}(P_0) + 2\mathbf{R}_{11}\mathbf{R}_{12}\sigma_{x\theta}(P_0) + \mathbf{R}_{12}^2 \sigma_{\theta\theta}(P_0) \tag{30}$$

OR

$$x_{max}^2(P_1) = \mathbf{R}_{11}^2 x_{max}^2(P_0) + 2\mathbf{R}_{11}\mathbf{R}_{12}\rho_{x\theta} x_{max}\theta_{max}(P_0) + \mathbf{R}_{12}^2 \theta_{max}^2(P_0) \tag{31}$$

wherein the **R** matrix elements are current dependent due to focusing strength 'k'. The parameters $x_{max}(P_0)$, $\theta_{max}(P_0)$ and $\rho_{x\theta}(P_0)$ are then fitted on a 'Quadrupole Current vs Spread ($x_{max}^2(P_1)$)' distribution. Since 2 quadrupoles (QSK810 and QSK811) were varied for this measurement, the aforementioned parameters were fit simultaneously on the 'QSK810 current vs $x_{max}^2(SciFi)$' and 'QSK811 current vs $x_{max}^2(SciFi)$' distributions using the combined χ^2 method. This hence yields the horizontal phase space [(x,θ) or σ_X] of the beam before the 2 quadrupoles (P_0) which can then be easily propagated via matrix multiplication to obtain the phase space at the SciFi (P_1). The vertical phase space [(y,ϕ) or σ_Y] can be obtained similarly. It is to be noted that the fits seemed to improve drastically when second order effects of the quadrupoles[19] were included compared to just the first order, however orders higher than the second order did not show any further improvements.

4.1.3 Z Scans

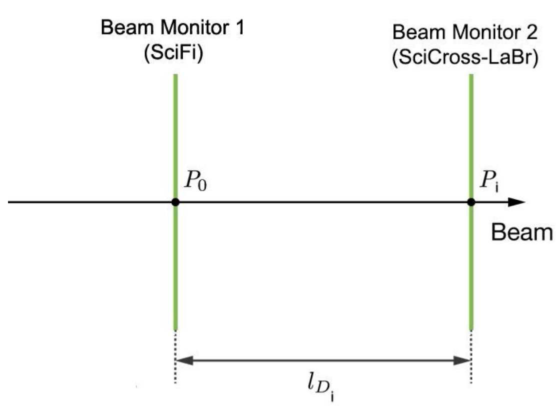

Figure 20: Z scan technique using SciFi and LaBr - beamspots are obtained at the SciFi (P_0) followed by beam profile scans after some free drift space using the SciCross-LaBr compound detector (P_i). Matrix multiplication is then used similarly to the quadrupole scan technique to obtain the transverse phase space at the SciFi (or at LaBr).

The Z scan method follows the same matrix multiplication concept to extract the phase space as the quadrupole scan technique, however in this case there are no quadrupoles involved but simply beam profile scans after some free drift space. As this method requires at least a translatable beam monitor, it remains less popular than the quad-scan method. The horizontal and vertical spreads are measured at both the beam monitors, with the translatable beam monitor (LaBr in this case) being moved slightly in the direction of propagation of the beam (Z) followed by beam profile cross-scans at that location. Then, the phase space parameters (elements of σ_X) are fit as in the quadrupole scan method using equation (33). The precision of the measurement increases with increasing number of beam profile measurements along Z, as the mean of all obtained phase spaces is taken to be the final phase space measurement. In this method, the transfer matrix **R** is made up of only a single drift space matrix for each Z position used. For 'N' position profiles scanned:

$$\mathbf{R}_i = \begin{pmatrix} 1 & L_{D_i} \\ 0 & 1 \end{pmatrix} \tag{32}$$

where i ranges from 1 to N. The equation to be fit for each Z position (using (31)) hence becomes:

$$x^2_{max}(P_0) = x^2_{max}(P_i) + 2L_{D_i}\rho_{x\theta}x_{max}\theta_{max}(P_i) + L^2_{D_i}\theta^2_{max}(P_i) \tag{33}$$

for the horizontal (X) phase space at the SciFi (P_0). The vertical phase space can be similarly obtained using the Z scan technique.

4.1.4 ToF-Energy Distribution

In this technique, the momentum (related to energy) in the form of $\Delta P/P$ is plotted against the time of flight (ToF) of the muons (or other particles). The momentum or energy is obtained from the charge deposited by each particle in the LaBr detector. The ToF is expressed in nanoseconds (ns) and is calculated by matching the phase of the particle incident upon the detector (SciCross or LaBr) with the 20ns long proton bunch window of the continuous beam HIPA facility of PSI[15] and then rescaling the phase to nanoseconds. This distribution was initially extracted from the SciCross-LaBr data for the 140 MeV/c forward decay muon momentum in order to gain insight into the various particle species that would enter the experiment if a similar forward decay beam were to be used for μEDM phase 2, however it was later understood that given the μE1 beamline's pion decay solenoid[11], any notion of a bunch-length would be lost for the particle beams, and that the ToF in terms of the 20ns phase of the proton current of HIPA would be the most meaningful way to express the 5th dimension of the phase space of the particle beam. Hence, the ToF-Energy distribution was subsequently used to obtain the length-energy phase space (σ_{ll}, $\sigma_{l\delta}$, $\sigma_{\delta\delta}$) of the beamtunes used. The aforementioned ToF-Energy distribution of the 140 MeV/c forward decay muon setting (with energy expressed in arbitrary units and not $\Delta P/P$ as per the final phase space measurement) is shown in Figure 21. It is to be noted that since it is a phase, the distribution has right-left periodic boundary conditions.

The example describes the distinct particle species seen in the forward decay settings owing to similar momenta of the particles produced the PoT collisions and this is discussed in depth in Section 5.4. In case of the backward decay settings, the muons reaching the experimental area from the pion decays have a large difference in energy when compared to the particle produced from the

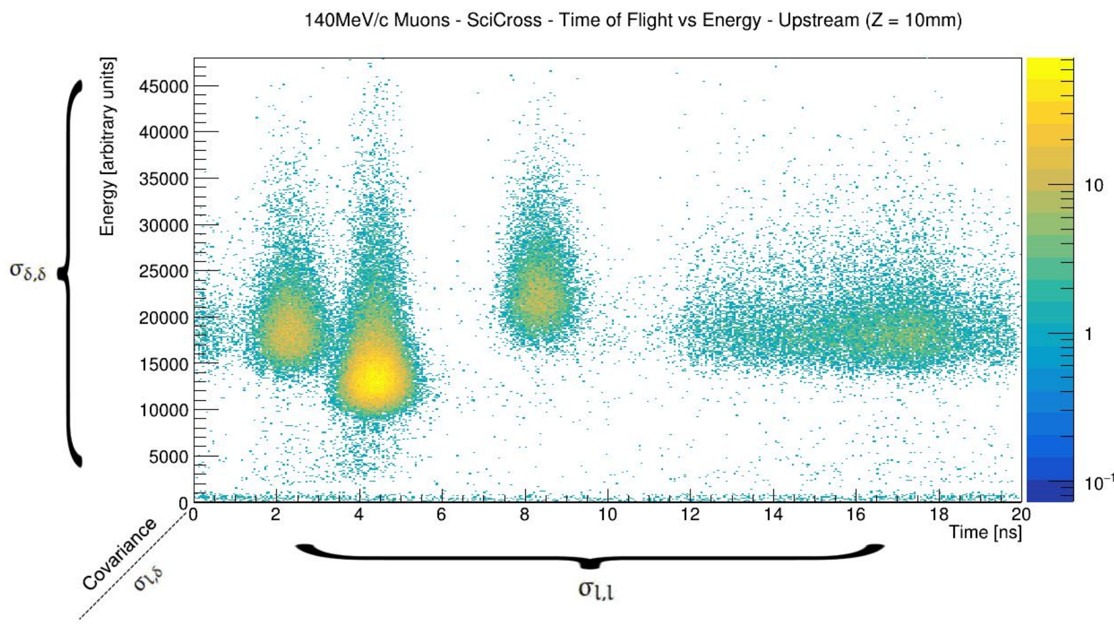

Figure 21: Time of Flight (ToF) vs energy distribution of the 140 MeV/c forward decay muons with 3 particle species (explained in Section 5.4). The ToF-Energy distribution is used to find σ_{ll} from the std. dev. of the X axis (ToF), $\sigma_{l\delta}$ is found by simply calculating the covariance of the distribution (for 1 particle species only) and $\sigma_{\delta\delta}$ is found by getting the standard deviation of the total Energy (E) and then converting to $\Delta P/P$.

proton on target (PoT) collisions (unlike in the forward decay case). Hence, in those cases only a single cluster of muons can be observed in the Tof-Energy distribution as the other particles get lost at the dipole bends owing to different bending radii that don't match the transmission condition.

For a single particle species, the statistics of the ToF-Energy distribution are used to find σ_{ll} from the standard deviation of the X axis and is expressed in units of nanoseconds (ns). For the same single particle distribution, the Y axis which is originally in terms of charge 'Q' ('charge' is the integrated voltage, which is proportional to the energy deposited through ionisation in the detector) is converted to '$\Delta P/P$' by taking the mode of the Y projection histogram as the central momentum (125 MeV/c in case of the 125 MeV/c muon momentum beamtune for example) and then rescaling in order to obtain $\sigma_{l\delta}$ by simply calculating the covariance of the ToF-Δ distribution. Finally, the energy spread ($\sigma_{\delta\delta} \equiv \Delta P/P \equiv \Delta$) of the mono-particle beam is found by getting the standard deviation of the kinetic Energy (E_k) and then converting to $\Delta P/P$. The equation to convert the charge (Y axis) to $\Delta P/P$ is as below:

$$\frac{\Delta P}{P} = \frac{\sqrt{\left(\frac{Q}{Q_M}E_k' + m\right)^2 - m^2} + (P - P')}{P} - 1 \tag{34}$$

where P is the central momentum of the particle for a set beamtune in MeV/c, Q is the variable charge deposited in the LaBr with Q_M being the **mode** of said variable charge, m is the mass of the particle in MeV/c^2, E_k' is 'corrected' kinetic energy of the central momentum particle (in

MeV) after energy losses incurred while passing through the SciCross and/or any other material (aluminium cover of LaBr, teflon beam cover and SciCross in this case) and P' is the corresponding corrected momentum (in MeV/c) of the central momentum particle associated with the corrected kinetic energy (E_k'). Similarly, the charge axis can also be rescaled to kinetic energy for an accurate calculation of the energy spread ($\Delta P/P$) using:

$$E = \frac{Q}{Q_M} E_k'. \tag{35}$$

The standard deviation of this rescaled kinetic energy distribution is then obtained in % which is converted to $\Delta P/P$ for the final energy spread measurement. Initially the spread was attempted to be obtain directly from the $\Delta P/P$ distribution, however upon further investigation it was found that said method would systematically overestimate the energy spread and hence would not be accurate. Using the kinetic energy spread to determine $\sigma_{\delta\delta}$ was more accurate in estimating the energy spread as it would avoid the inflation of the spread measurement as in the case of directly using the momentum, and hence the kinetic energy was used in the end to determine the 1σ fractional energy spread of the beam.

4.1.5 Position-Momentum Slicing

The position-momentum slicing technique was developed in order to extract the horizontal and vertical energy dispersion measurements at the monitor position, which are closely related to $\sigma_{x\delta}$ and $\sigma_{y\delta}$ respectively, as the data taken during the June 2024 beamtime was inadequate to use the traditional dispersion methods described in [35] and [36].

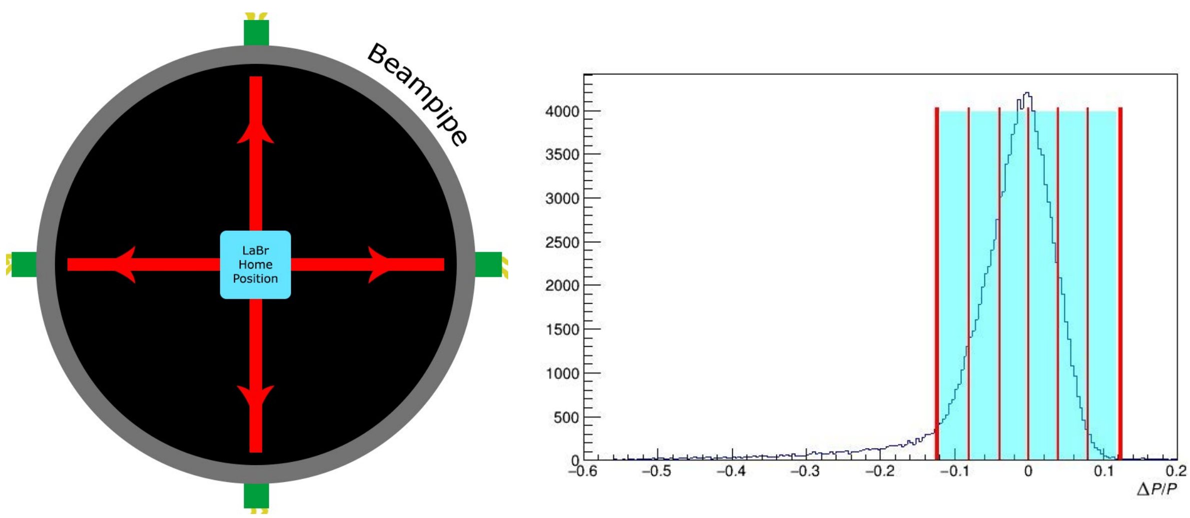

Figure 22: Position-Momentum slicing technique for energy dispersion calculation - Cross scans are performed to obtain beam profile data as in the case of the Z scan technique [LEFT] ; Cuts are performed on the momentum distribution with small momentum windows plotted against each scanned position (Note: Slices shown here are not to scale) [RIGHT].

In this method, position scans are performed using the SciCross-LaBr compound detector horizontally and vertically in and around the mean position (see Figure 22) with both the slits in a (5 x 5)mm^2 square configuration in order to avoid pile-up in the WaveDAQ. The momentum or

$\Delta P/P$ distribution is obtained using Equation (34) on which cuts are performed such that small momentum windows are plotted against each of the scanned positions (separately for horizontal and vertical) so as to obtain a position-momentum distribution as shown below:

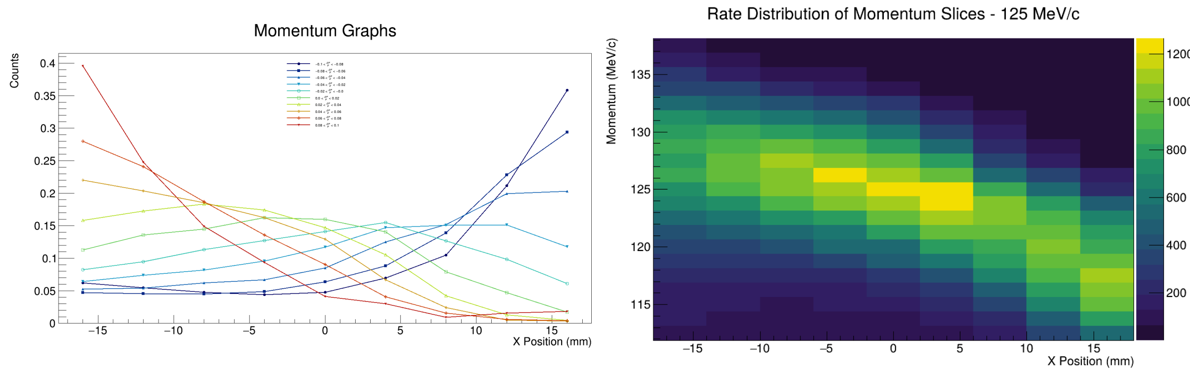

Figure 23: Example of position-momentum sliced dispersion for dispersion measurement in 1D [LEFT] and 2D [RIGHT].

After the position-momentum sliced distribution has been obtained, the range around $[\Delta P/P = 0]$ that contains meaningful particles and NOT the low momentum tail as seen in Figure 22 is retained while the top and bottom edges of the distribution are cut out, and finally the covariance of this final distribution is calculated, thus giving the measurement of $\sigma_{x\delta}$ (horizontal) and $\sigma_{y\delta}$ (vertical) elements of the phase space of the particle beam. Then, the dispersion $[D_x(\delta)$ and $D_y(\delta)]$ functions are calculated using a simple relation:

$$\sigma_{x\delta} = Cov(x,\delta) = \sigma_{\delta\delta}^2 \cdot D_x(\delta), \tag{36}$$

$$D_x(\delta) = \frac{\sigma_{x\delta}}{\sigma_{\delta\delta}^2} \tag{37}$$

which is isomorphic for vertical $[D_y(\delta)]$ dispersion. The tail of the momentum distribution is removed as it represents the particles that were either only partially stopped in the LaBr, passed through the LaBr obliquely so as to deposit only a small amount of their energy or are of a different particle species than the one desired, and is a well known phenomenon in detector physics[37].

It is worth mentioning all the **ideas that were tried, but did NOT work**, to obtain the dispersion prior to arriving at this simple yet effective solution so as to inform future work. The dispersion was initially attempted to be calculated using equations mentioned in [35] and [19]:

$$x^2 = x_0^2 + D_x^2(\delta) \cdot \delta^2, \tag{38}$$

$$x = D_x(\delta) \cdot \delta \tag{39}$$

using $D_x(\delta)$ as a fit parameter. However, the fits were found to be extremely unstable with very different values of dispersion being obtained for even small changes made to the distribution. At times, the fits yielded values for $D_x(\delta)$ that when used to calculate the increase in the spread of X due to dispersion where even exceeding the total spread in X. Fits were tried using both taking δ as a function of x and taking x as a function of δ, but neither method yielded stable results. Thus, the fit method was abandoned in favour of the covariance method when the energy spread measurement was made using the Tof-Energy method which then provided reliable estimates of the dispersion function. Data was also taken for the dispersion's dependence on the quadrupole strength, however no significant dependence could be established. The null-hypothesis of zero dependence could not be rejected.

4.1.6 Other Phase Space Parameters

As one may have deduced, the methods described in Table 4 only mention 12 of the 21 phase space parameters seen in Equation (15). This is for a few different reasons:

- Certain parameters - namely $\sigma_{x\phi}$, $\sigma_{x\theta}$ and $\sigma_{\theta\phi}$ - are generally 0 if the parameter σ_{xy} is 0 since x and θ have non-zero correlation due to one being a derivative of the other as is the case for y and ϕ. Hence, in the case that x and y have no correlation (indistinguishable from the null hypothesis), it is reasonable to assume that the 3 aforementioned elements also have null value. This is supported by the principles of beam dynamics[38, 19, 21].
- Parameters σ_{xl}, $\sigma_{\theta l}$, σ_{yl} and $\sigma_{\phi l}$ do not provide significant insight for the μEDM experiment and thus were excised from data taking as well as analysis. If one were to try to estimate said parameters, a covariance technique similar to those used in Sections 4.1.4 and 4.1.5 can be used by plotting the phase uncertainty (l) against the desired parameter (x, y, θ or ϕ) and then calculating the covariance.
- Finally, parameters $\sigma_{\theta\delta}$ and $\sigma_{\phi\delta}$ are usually estimated by using the 'Dipole Current Scan' technique which is similar to the quadrupole scan technique described in Section 4.1.2 except that the dipoles' current (ASK81 and ASK82 in case of the μE1 beamline) are varied instead of the quadrupoles' currents[19]. However, due to lack of time during the June 2024 beamtime, these measurements were unable to be made and so the 2 parameters remain elusive for the time being.

The following subsections will describe the estimation of the rates at the SciFi and the characterization of the LaBr calorimeter using the 140 MeV/c forward decay muon ToF measurements.

4.2 Characterization of the LaBr Calorimeter

The LaBr calorimeter used during the June 2024 beamtime was graciously provided by the $\mu - e\gamma$ 2 (MEG II) collaboration at PSI. It was known at the time that prolonged exposure to neutrons during the calibration of the MEG II apparatus (which is its primary use) had degraded the LaBr, and thus to obtain accurate results from the data collected during the June 2024 beamtime from the LaBr, it would need to be characterized. The broadening of the energy distribution due to the LaBr in particular was essential to be studied in order to extract accurate values for the 6th dimension of the phase space ($\Delta P/P$).
Initially, the energy spread for the 125 MeV/c beamtunes was found to be 3.60% and that for the 100 MeV/c beamtunes was found to be 2.98%. These values were taken to be the upper limits of the energy spread due to the aforementioned reasons, and a few methods were attempted in the

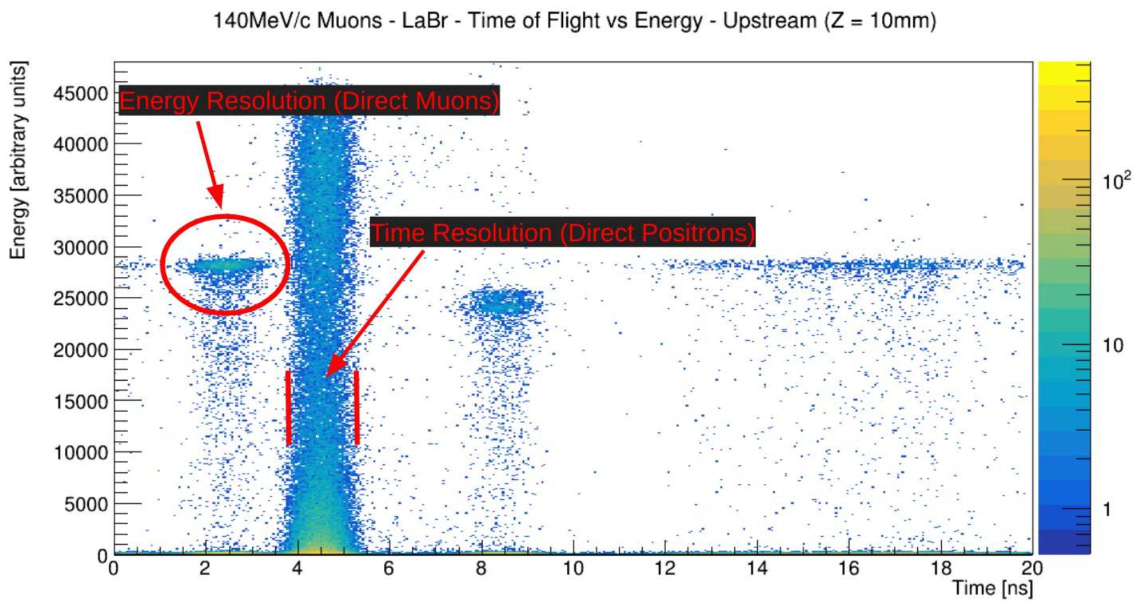

Figure 24: Time of Flight (ToF) vs energy distribution of the 140 MeV/c forward decay muons at the LaBr for 10mm Z position. The positron line that runs parallel to the Y-axis is caused due to Bragg's energy deposition law as the positrons deposit all of their energy in the calorimeter. The positron line should theoretically be a delta function and thus measuring the σ of the line would provide the inherent ToF broadening of the LaBr + PoT uncertainty. Later on, it was realized that the energy spread resolution (broadening) can easily be extracted by comparing the deconvoluted energy spread from the ToF and measured energy spread of the direct muons (Y-axis), thus foregoing the need for the MC simulation.

quest to extract the real energy spreads. The first method was to try to match the time of flight (ToF) data for the backward decay beamtunes to a Monte-Carlo (MC) setup as the spread in the ToF is closely linked with the energy spread of the beam as faster particles have smaller ToF values and vice-versa, however the ToF spread is also affected by a few factors other than the energy spread such as:

- the trajectory of the particle (the further away from the centre of the beam the particle was travelling, the larger will its ToF be due to longer path lengths). Accounted for by introducing a small angle cosine factor into the MC simulation.
- the energy spread of the pions that decay to the muons. Estimated to be around 3%.
- the uncertainty in position of decay of the pions along the beamline (since in backward decay mode the pions are travelling faster than their daughter muons, the later the pions decay the shorter the ToF will be). Implemented into the MC by adding the decay probability spectrum of the pions of central momentum and generating positions of pion decay accordingly between ASX81 (pion momentum bit selection dipole) and ASK81 (muon momentum bit selection dipole) including the 8m long pion decay solenoid[11].
- the length of the proton spill onto the target (at HIPA it is about 100ps[15]). Implemented implicitly in the time resolution (see below).

- the time resolution of the LaBr. Found using 140 MeV/c positrons in the 140 MeV/c forward decay muons ToF spectrum (expanded upon below).

For the time resolution of the LaBr, the ToF spectrum of the 140 MeV/c forward decaying muons was used as the positrons that came directly from the PoT collision onto the LaBr were of 140 MeV/c and should have thus theoretically had the same ToF except for the broadening of their ToF due to the time resolution of the LaBr as well as the uncertainty in the PoT collision time. Hence, measuring the width of the positron line (see Figure 24) deftly provided the broadening of the ToF spread in the LaBr due to the PoT spill uncertainty and the inherent broadening due to the LaBr. The **time resolution broadening was found to be** (347.7 ± 1.1)**ps**.

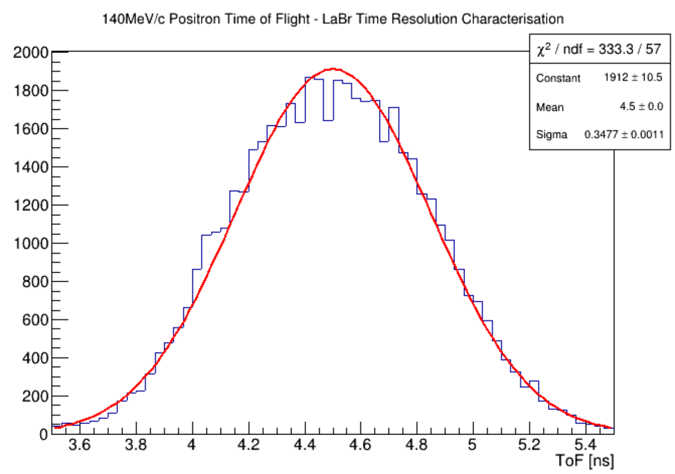

Figure 25: Time resolution of the LaBr using 140 MeV/c positrons was found to be (347.7 ± 1.1)ps.

Using this result as input, the MC simulation was set up such that the factors mentioned in the bullet points above are accounted for and the **muon energy spread is given as a user input** (and is shown in the title of [RIGHT] of Figure 26) in order to output the ToF spectrum of the desired muon momentum in order to directly extract the energy spread of a particular muon momentum without requiring the energy broadening characterization of the LaBr. The results of this method for 100 MeV/c muons is shown below:

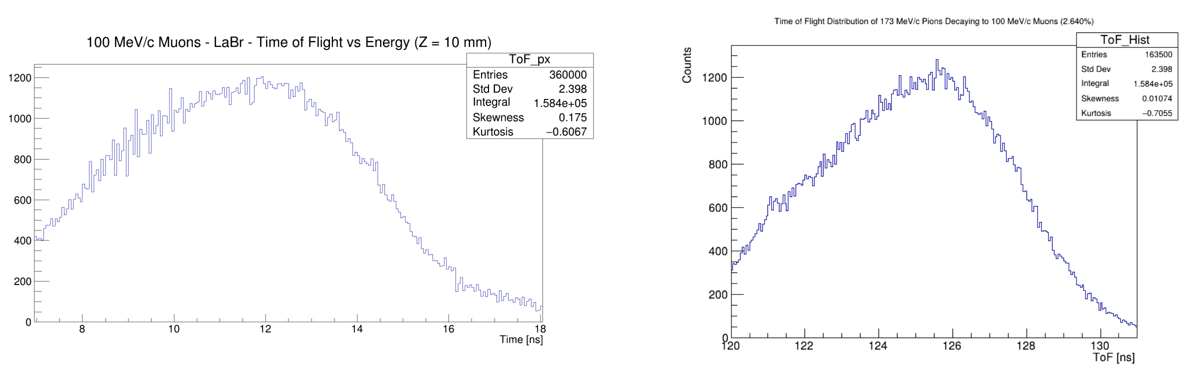

Figure 26: 100 MeV/c muon momentum Monte-Carlo simulation compared to data - ToF spectrum from data [LEFT] ; ToF spectrum generated from the MC simulation given muon momentum spread as input (2.640% seen in the title) [RIGHT].

As can be seen by comparing the respective stat-boxes, the spectra resemble each other closely which would suggest that the energy spread of the 100 MeV/c muon beam is 2.640%, and this results wasn't too far off from the actual value as will be seen later. However, the same method yielded unreliable results in case of the 125 MeV/c muon beam and thus a more robust method was sought. That is when the idea of using the direct 140 MeV/c muons from PoT production as seen in Figure 24 was devised, as the actual energy spread of that bunch of muons could easily be estimated using the time resolution result. This actual energy spread can then be used to deconvolute the apparent energy spread of the same bunch of muons obtained by measuring the 1σ of its energy distribution in order to extract the energy broadening resolution of the LaBr calorimeter. Thus, the actual energy spread of the 140 MeV/c direct muons was extracted using the MC simulation method:

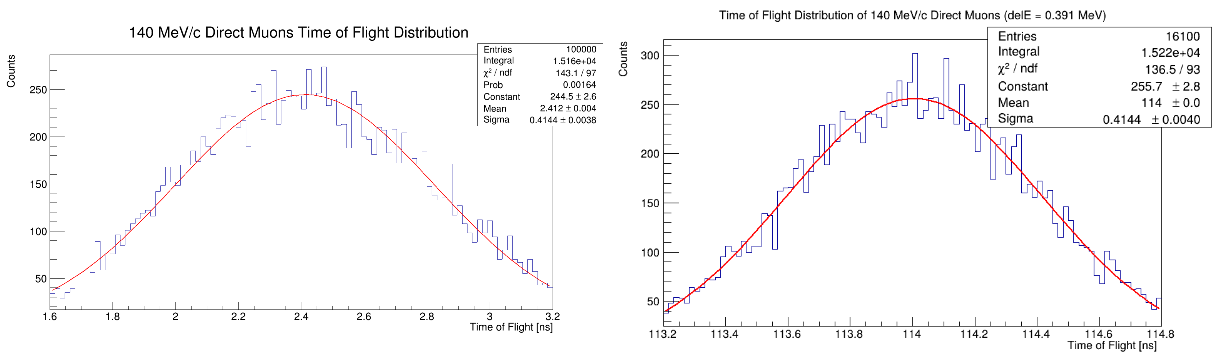

Figure 27: Actual energy spread of the 140 MeV/c direct muons - ToF spectrum from data [LEFT] ; ToF spectrum generated from the MC simulation given muon kinetic energy spread as input ($\Delta E_k = 0.391$ MeV as seen in the title) [RIGHT].

$\Delta E_k = (0.391 \pm 0.006)$ MeV was found to be the actual kinetic energy spread of the 140 MeV/c direct muons. Next, the loss in kinetic energy of said muons had to be estimated due to traveling through the SciCross and the covering of the LaBr had to be estimated to obtain the accurate kinetic energy of the muons when they reach the LaBr. This was done successfully using **Geant4**[39] simulation software, and it was found that the 140 MeV/c momentum direct muons lose about 5.7 MeV of kinetic energy before reaching the LaBr.

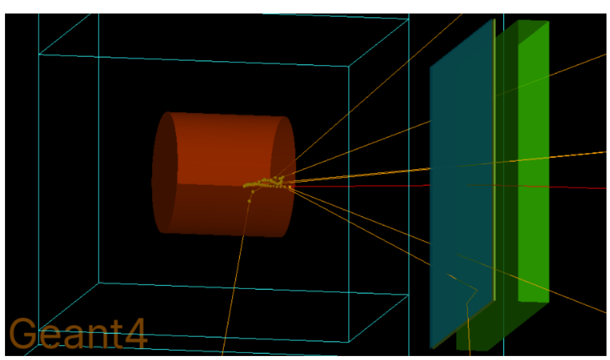

Figure 28: Geant4 simulation of loss in kinetic energy of 140 MeV/c muons before reaching LaBr calorimeter crystal due to SciCross and the cover of the LaBr.

The materials passed through by the particles en route to the LaBr was 2cm of polystyrene (Sci-Cross) and 0.5mm of Al and 0.1mm of Tedlar (LaBr Cover). Thus

$$(E_k - E_k')(140\text{MeV/c}\ \mu^+) \equiv \delta E_k^{(\mu)}(140\text{MeV/c}\ \mu^+) = 5.7\ \text{MeV}. \tag{40}$$

Given that 140 MeV/c momentum muons possess a kinetic energy of [$E_k = 69.7$ MeV], kinetic energy of said muons post energy loss (E_k') is:

$$E_k'(140\text{MeV/c}\ \mu^+) = (69.7 - 5.7) = 64.0\ \text{MeV}, \tag{41}$$

$$\therefore Real\ \ \Delta E_k/E_k(140\text{MeV}\ \mu^+) = (0.61 \pm 0.01)\%. \tag{42}$$

This result was then used to get $\Delta E_k/E_k$ of the 140 MeV/c muon beam using its energy spectrum.

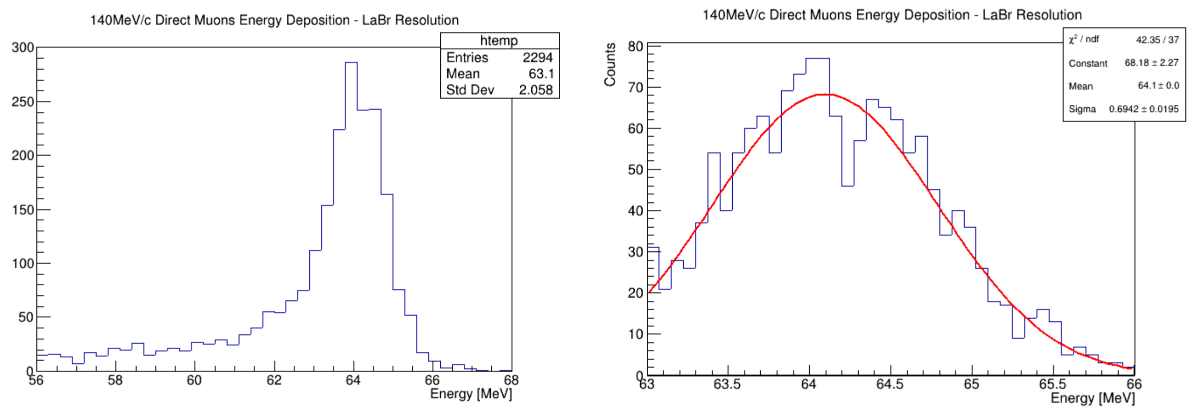

Figure 29: Apparent energy spread of the 140 MeV/c direct muons from kinetic energy spectrum found to be (0.69 ± 0.02) MeV

$$Apparent\ \ \Delta E_k/E_k(140\text{MeV}\ \mu^+) = (1.08 \pm 0.03)\%. \tag{43}$$

Thus, comparing Equations (42) and (43) in order to obtain the deconvolution factor, the equation to find **the energy broadening resolution of the LaBr used during the June 2024 for a muon beam of post-energy loss kinetic energy 'E_k''** in accordance with the energy-resolution principles mentioned in [40] is:

$$ER_{LaBr} = \left[(0.89 \pm 0.04)\sqrt{\frac{64}{E_k'}}\right]\%. \tag{44}$$

This result will remain accurate to describe the broadening of the energy spectrum of a particle beam due to the LaBr crystal used until further degradation.

5 Analysis and Results

The following sections will describe the rates and the phase space results from the June 2024 beamtime for the various beamtunes. The systematics that have been taken into account are the quadrupole current fluctuations ($\pm$0.3A) for the quadrupole scan technique, the uncertainty in the measured drift space ($\pm$3mm), the time and energy resolution of the LaBr described earlier, deviation of the the beam from the straight trajectory and the resolution of the SciFi detector. The results have been grouped together as per muon momenta, beamtunes, and settings used to acquire the data, and each subsection provides all the 6D phase space measurements obtained from analysis for that particular setting. However, this differs from the chronological order in which the results were obtained.

5.1 Rates @SciFi

The rates of the various beamtunes used are essential pieces of information in the context of the μEDM experiment (as it is in most particle physics measurements) as the final statistical sensitivity of the measured EDM of the muon is directly proportional to the number of particles studied. Thus, the measured rates need to ideally be as high as possible in order to achieve the highest sensitivity. These rates were estimated for the beamtunes used during the June 2024 beamtime by first measuring the total rates at the SciFi, then measuring the rates at the cross-section of the SciCross (which is a diamond with $\sqrt{2}$cm length diagonals) summed over the whole acceptance area of the beampipe (see Figure 30). Since the rate of particles passing through the whole acceptance area should be the same at the SciFi and at the SciCross, comparing the two measured rates thus allows one to extract an efficiency measurement of the SciFi detector.

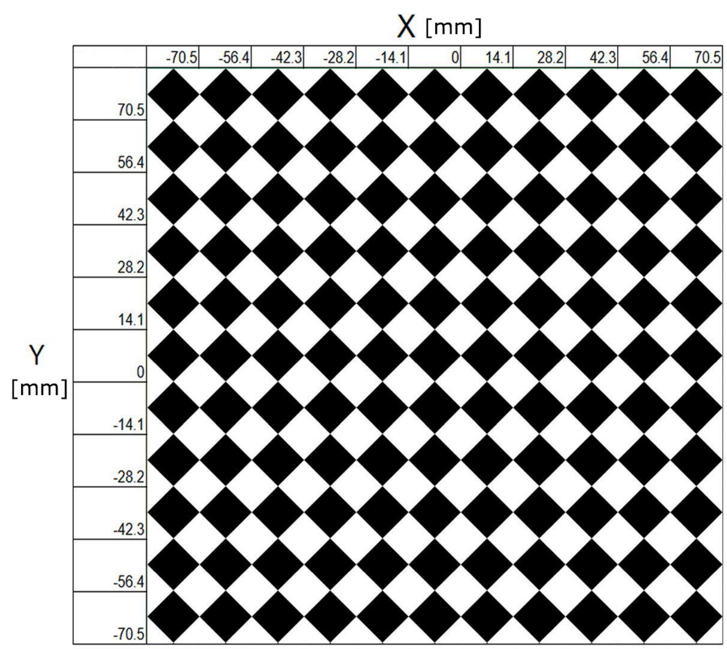

Figure 30: Efficiency measurement of the SciFi detector - black diamonds depict where the cross-section of the SciCross was placed. The black diamonds cover exactly **half** the area of the SciFi.

Thus, the efficiency of the SciFi detector, denoted by 'η_{SciFi}' was found to be:

$$\eta_{SciFi} = \frac{Total\ Rate\ @SciFi}{2 \times Total\ Rate\ @SciCross} = (1.12 \pm 0.07)\% \tag{45}$$

where the denominator is multiplied by 2 as the area covered by the SciCross cross-section is exactly half of the area of the square. Using this, the total rates for all the beamtunes were found using the SciFi measurements, and are summarized in Figure 31 which also includes the rates from the 2019 beamtime described in [14] for the U-configuration of the μE1 beamline.

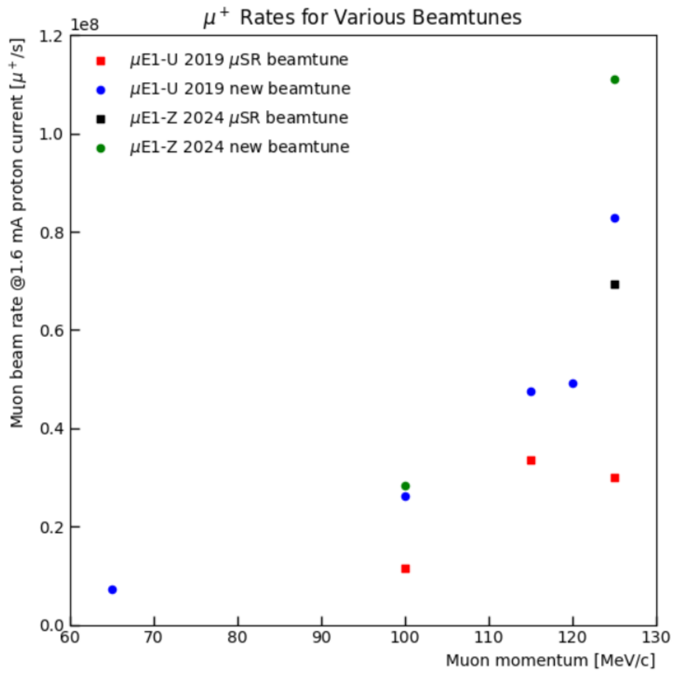

Figure 31: Total rates of all beamtunes used in the 2019 and June 2024 beamtime save for the 140 MeV/c beamtune. Adapted from [14]. Z-configuration points are not entirely accurate as the rates were not mentioned

The 140 MeV/c forward decay beamtune's muon rates are not included in this plot as it was found to have extremely low rates with large uncertainties. Using the time of flight (ToF) data, it was found that only 34.9% of the particles were muons which gave a total rate of (0.222 ± 0.013) MHz/mA of muons for the 140 MeV/c forward decay beamtune. This extremely low rate when compared to the backward decay beamtunes, coupled with the fact that the beam was contaminated by positrons and pions which would introduce undesirable systematics in the physics measurement of μEDM's phase 2, led to the forward decay beamtune being discarded from analyses beyond extraction of the 4D transverse phase space. This is discussed further in Section 5.4.

As can be seen from the plot, the new, manually optimized 125 MeV/c beamtune in the Z-configuration during the June 2024 beamtime has the highest muon rate of (68.8 ± 4.0) MHz/mA which would be very desirable for the experiment. It can be assumed that the new optimized 125 MeV/c beamtune in the Z-configuration owes its higher rates when compared to the optimized 125 MeV/c beamtunes in the U-configuration during the 2019 beamtime to the higher degree of energy spread of the muons (discussed in greater detail later). This is because the large $\Delta P/P$ muons that would be lost during the ASK82 bend in the U-configuration recombine instead in the Z-configuration. An excellent illustration of this concept is shown below by the courtesy of C. Cong:

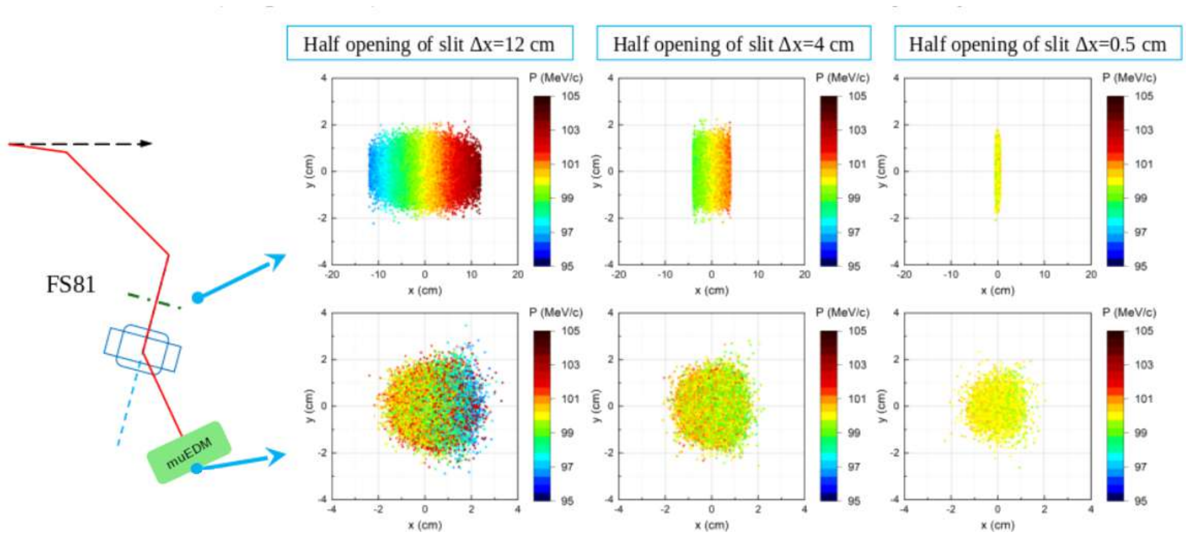

Figure 32: Re-convergence of a muon beam containing a large energy spread at the ASK82 dipole magnet in the Z-configuration of the μE1 beamline. Courtesy of C. Cong[41].

However, since large energy spreads decrease the sensitivity of the EDM measurement, further simulation studies need to be conducted based on the results of the June 2024 beamtime in order to determine which beamtune will be ideal for the final phase 2 muon EDM measurement.

5.2 100 MeV/c Backward Decay Muons - Phase Space

Beamtune: mue1_p100_Jun_2024_Z-Config-V1_TRANSPORT_Tune6.sp

The 100 MeV/c beamtune used to collect data during the June 2024 beamtime was operated in two settings - one with both the slit systems (FS81 and FS00) in the formation of a $(5 \times 5)\text{mm}^2$ square shape at the center (thus with each of the slabs at 2.5mm setting) and one setting with both the slits completely open. The following subsection will describe the results for both the aforementioned settings.

5.2.1 Fully Open Slits

Both slits were kept completely open for the set of data that will be presented in this section. The transverse beamspot at the SciFi is shown in Figure 33. The correlation between the two transverse axes that is closely related to the phase matrix element σ_{xy} (covariance) was not high enough to discard the null hypothesis of $[\sigma_{xy} = 0]$. The beamspot also provides values of $\sqrt{\sigma_{xx}}$ and $\sqrt{\sigma_{yy}}$ in the form of the standard deviations. Further confirmation of these elements as well as the measurements of the remaining elements of the 4D phase space elements can be obtained from the quadrupole scan technique's results as seen in Figures 34 and 35 with the **Twiss parameters at the SciFi** summarized in Table 5. The total rate of this beam setting is 17.784 MHz/mA.

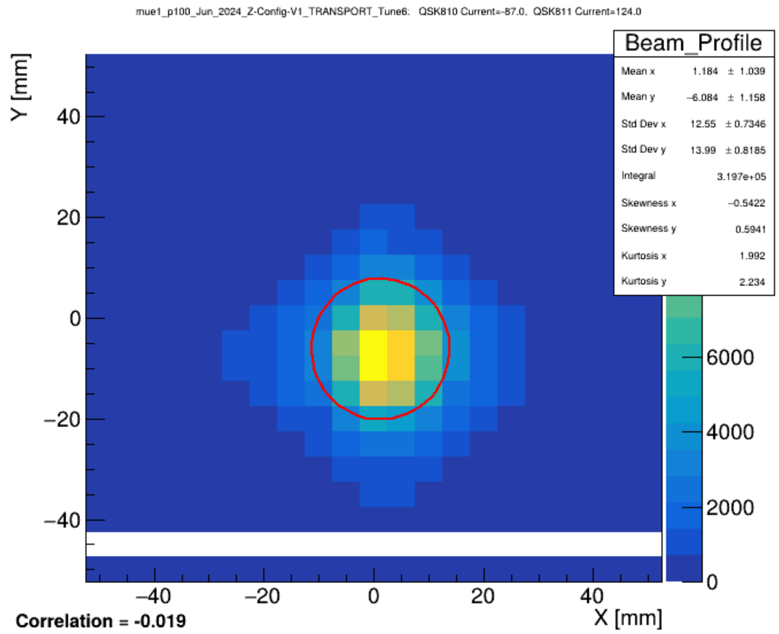

Figure 33: Beamspot of the 100 MeV/c beamtune with open slits. Correlation between X and Y (σ_{xy}) is not sufficiently high to disregard null hypothesis of [$\sigma_{xy} = 0$]. All kurtosis shown is excess kurtosis. Total rate of this beam setting is 17.784 MHz/mA.

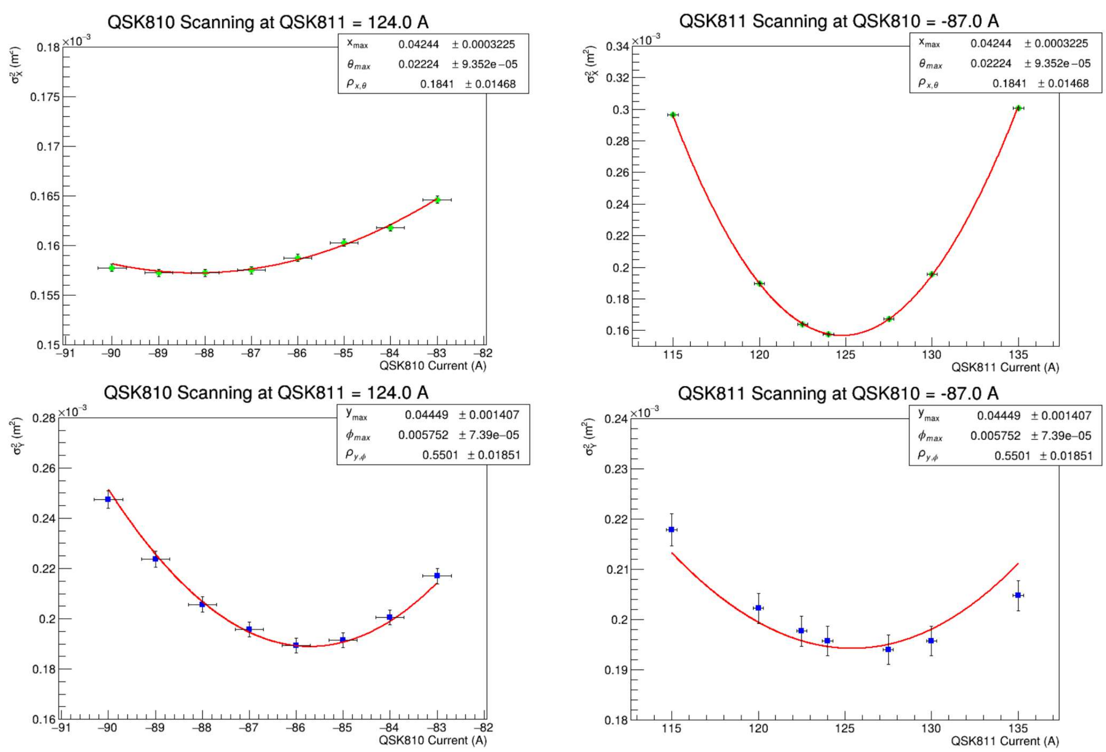

Figure 34: Phase space simultaneous fits of the quadrupole scan data for the 100 MeV/c open slits setting - horizontal (X) [TOP] and vertical (Y) [BOTTOM].

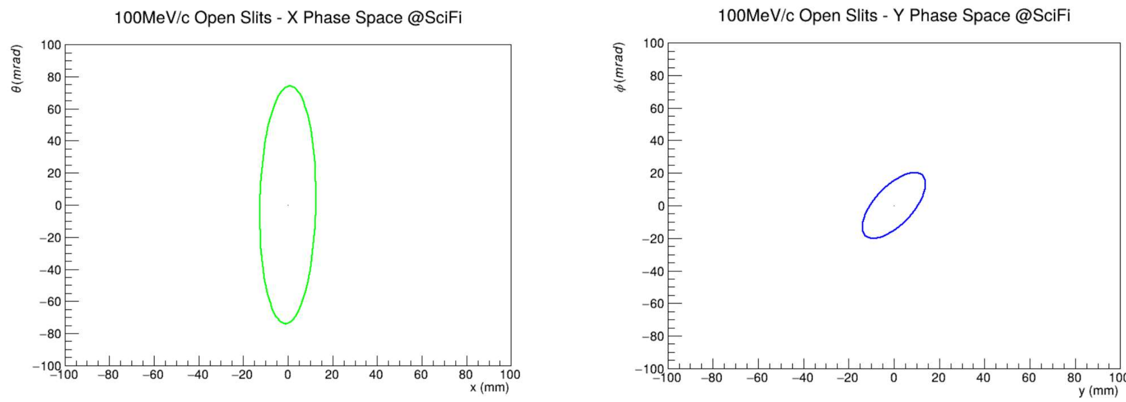

Figure 35: Transverse phase space ellipses of the 100 MeV/c open slits setting at the SciFi. X phase space is in green and Y phase space is in blue.

Parameter [units]	Horizontal (X)	Vertical (Y)
α []	-0.0753 ± 0.0063	-0.8635 ± 0.1004
β [m/rad]	0.1699 ± 0.0086	0.9105 ± 0.2026
γ [rad/m]	5.9190 ± 0.0149	1.9172 ± 0.0140
ε [mm.mrad]	927.606 ± 23.653	213.693 ± 45.482

Table 5: Twiss parameters of the 100 MeV/c open slits setting at the SciFi. Note that the emittance (ε) here is the area of the ellipses.

The ToF-energy distribution for the 100 MeV/c beamtune is shown in Figure 36 yielding values of σ_{ll} and $\sigma_{l\delta}$ given in Equations (46) and (47) respectively. The uncertainties of these values were obtained purely from statistics.

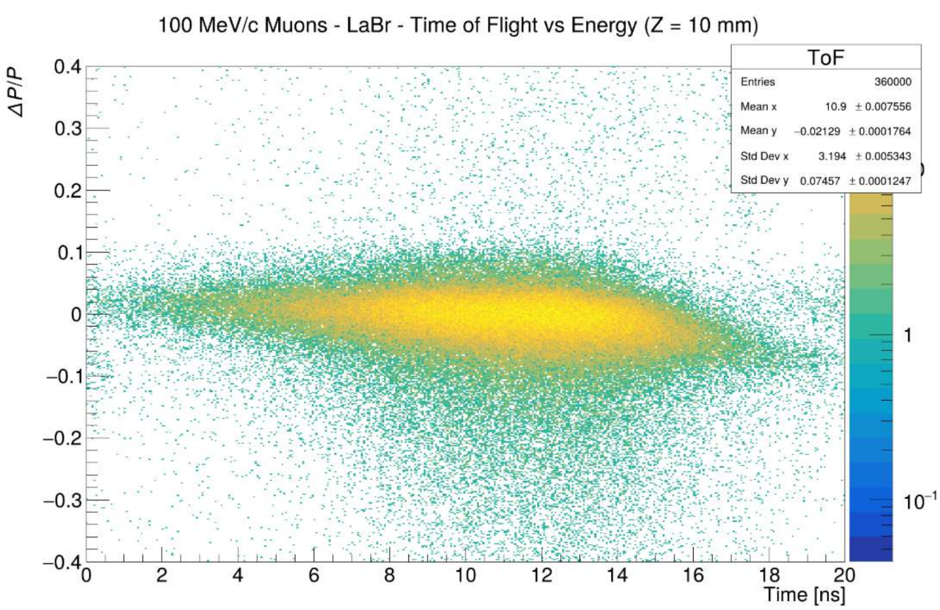

Figure 36: ToF-energy distribution for the 100 MeV/c open slits setting.

$$\sqrt{\sigma_{ll}} = (3.194 \pm 0.005) \text{ ns}, \tag{46}$$

$$\sigma_{l\delta} = (-0.035 \pm 0.002) \text{ ns}. \tag{47}$$

The momentum or energy spread ($\Delta P/P$) was found using the kinetic energy spread (Figure 37) after taking broadening effects according to Equation (44) into account. Using the same Geant4 energy loss simulation as described in Figure 25, it was found that the 100 MeV/c muons initially of kinetic energy $E_k = 39.8$ MeV lose about 7.7 MeV of kinetic energy before reaching the LaBr, making the corrected kinetic energy:

$$E'_k = 32.1 \text{ MeV}, \tag{48}$$

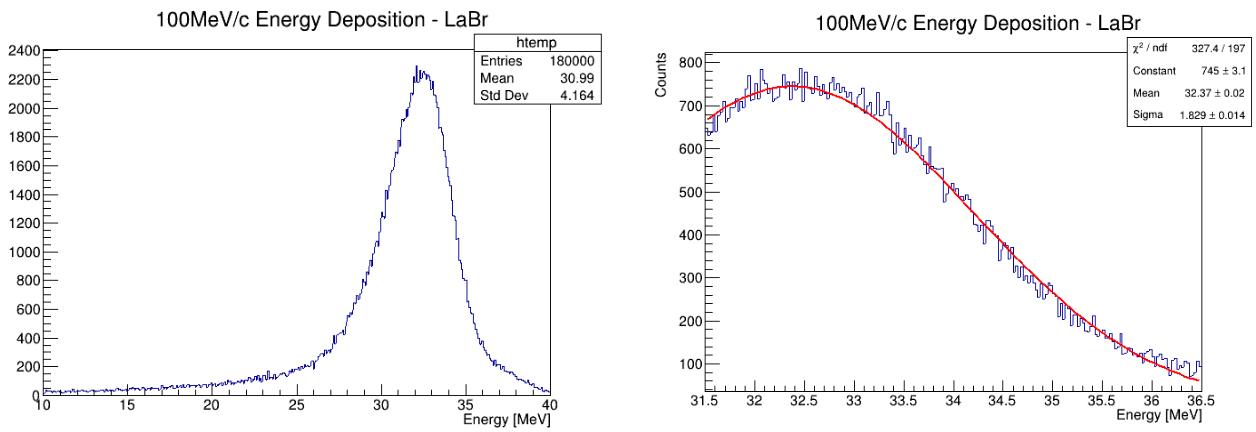

Figure 37: Post-energy loss kinetic energy (E'_k) spread of the 100 MeV/c muon beamtune used to calculate $\Delta P/P$.

$$\frac{\Delta P}{P}^{(5mm)}_{100\text{MeV/c}} = (2.51 \pm 0.14)\%. \tag{49}$$

Notice that this is the energy spread for the **(5×5)mm^2 square slit** setting as all the energy measurements were made with this setting so as to avoid pile-up in the WaveDAQ used to collect data from the SciCross and LaBr. Comparing the rates of the 5mm square slit setting and the open slits setting and then simply extrapolating the energy spread while preserving Gaussian properties, a total energy spread of $(3.15 \pm 0.17)\%$ was obtained for the open slits. However, such an extrapolation remains contentious but has been included here nonetheless to inform future work*.

$$\frac{\Delta P}{P}^{(Open)}_{100\text{MeV/c}} = (3.15 \pm 0.17)\% \qquad (?)^* \tag{50}$$

The energy dispersion function ($D(\delta)$) was then calculated for the horizontal and vertical transverse axes and have been described in Figure 38. The covariances ($\sigma_{x\delta}$ and $\sigma_{y\delta}$) were calculated using the position-momentum slicing method to be:

$$\sigma_{x\delta} = (-0.0574 \pm 0.0039) \text{ mm}, \tag{51}$$

$$\sigma_{y\delta} = (-0.0736 \pm 0.0057) \text{ mm}. \tag{52}$$

The corresponding dispersion functions using Equation (37) are thus:

$$D_x(\delta) = (-91.05 \pm 6.25)\ \text{mm}, \tag{53}$$

$$D_y(\delta) = (-116.88 \pm 9.04)\ \text{mm}. \tag{54}$$

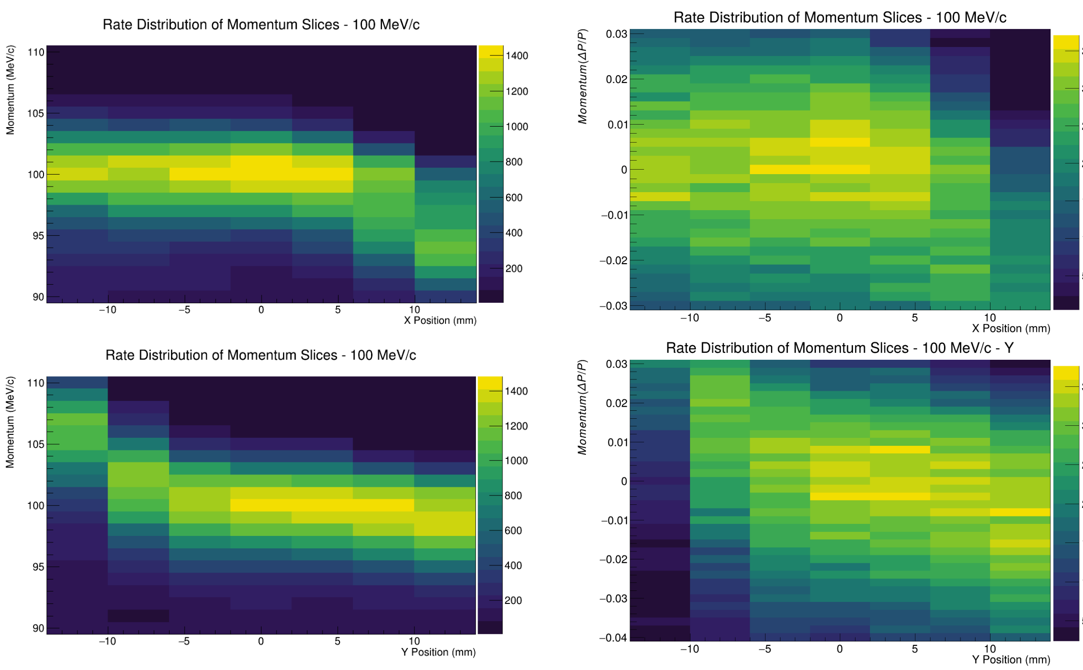

Figure 38: Position-momentum distribution for 100 MeV/c muon beam. Left plots show the full distribution and right shows the part of the full distribution used for dispersion calculation post cuts - horizontal (X) [TOP] and vertical (Y) [BOTTOM].

Hence, the final **6D phase space @SciFi** for the 100 MeV/c open slits setting takes the form (without the uncertainties due to formatting limitations):

$$\sigma^{(Open)}_{100\text{MeV/c}} = \begin{pmatrix} 12.55^2\ \text{mm}^2 & 69.74\ \text{mm.mrad} & 0 & 0 & \sigma_{xl} & -0.0574\ \text{mm} \\ & 74.10^2\ \text{mrad}^2 & 0 & 0 & \sigma_{\theta l} & \sigma_{\theta\delta} \\ & & 13.99^2\ \text{mm}^2 & 184.62\ \text{mm.mrad} & \sigma_{yl} & -0.0736\ \text{mm} \\ & & & 20.24^2\ \text{mrad}^2 & \sigma_{\phi l} & \sigma_{\phi\delta} \\ & & & & 3.194^2\ \text{ns}^2 & -0.044\ \text{ns} \\ & & & & & 3.15\% \end{pmatrix} \tag{55}$$

5.2.2 Both Slits at 5mm Square

All slabs of the two slit systems were set symmetrically to 2.5mm so as to form a $(5 \times 5)\text{mm}^2$ square for the beam to pass through. The 100 MeV/c and hence also the 125 MeV/c beamtunes were manually optimized in this setting, and phase space measurements were made before it was realized that the slits were in this closed configuration. Although recreating a phase space with a slit acceptance after the quadrupole used in the quadrupole scans (as in the case of FS00 positioned after QSK811) does not yield the most meaningful results as they would only yield the results for the conserved phase space that made it through the square slits, they have been included here nonetheless as it did provide some insights about the energy spread that was not accounted for during the beamtime as discussed in the previous subsection. It is to be noted that the energy dispersion measurement is the same for both the settings as the same beamtune was used. The beamspot at the SciFi is shown in Figure 39. The correlation between the 2 transverse axes that is closely related to the phase matrix element σ_{xy} (covariance) was not high enough to discard the null hypothesis of $[\sigma_{xy} = 0]$.

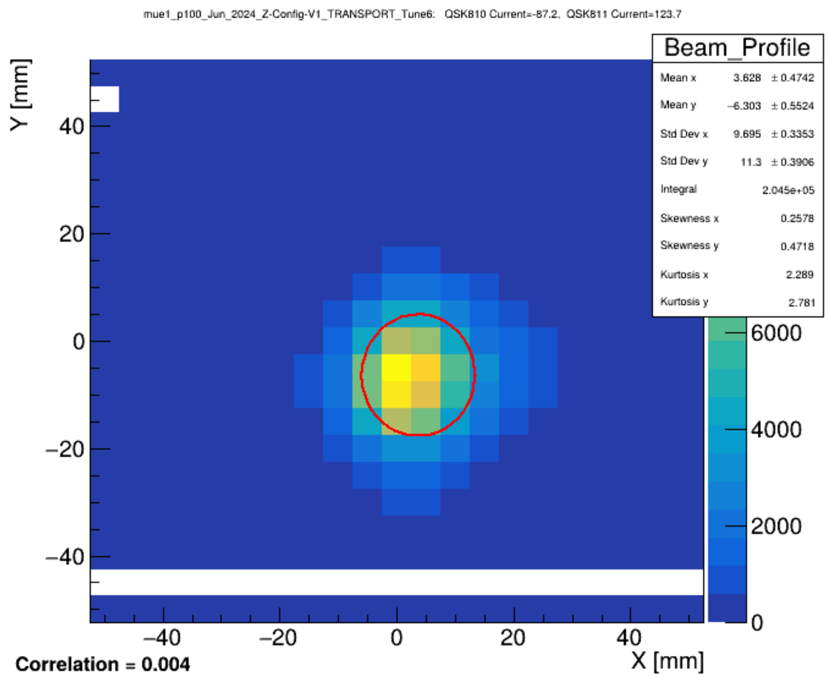

Figure 39: Beamspot of the 100 MeV/c beamtune with $(5 \times 5)\text{mm}^2$ slits. Correlation between X and Y (σ_{xy}) is not sufficiently high to disregard null hypothesis of $[\sigma_{xy} = 0]$. All kurtosis shown is excess kurtosis. Total rate of this beam setting is 11.381 MHz/mA.

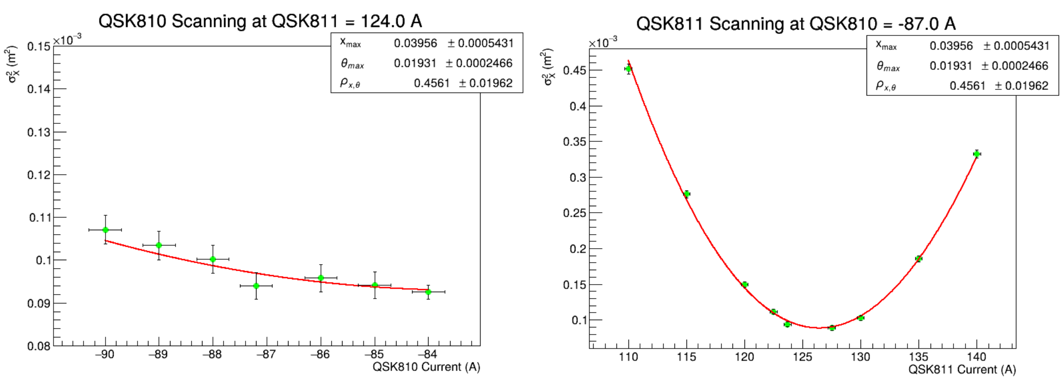

Figure 40: Horizontal (X) phase space simultaneous fits of the quadrupole scan data for the 100 MeV/c 5mm square slit setting.

The beamspot provides values of $\sqrt{\sigma_{xx}}$ and $\sqrt{\sigma_{yy}}$ in the form of the standard deviations. Further confirmation of these elements as well as the measurements of the remaining elements of the 4D phase space elements can be obtained from the quadrupole scan technique's results as seen in Figures 40, 41, and 42 with the **Twiss parameters at the SciFi** summarized in Table 6. The total rate of this beam setting is 11.381 MHz/mA. The 5th and 6th dimensions of this beam setting is the same the 100 MeV/c fully open slit settings (Equations (46), (47) and (50)) except for the energy spread, the details of which are expanded upon in Section 5.2.1.

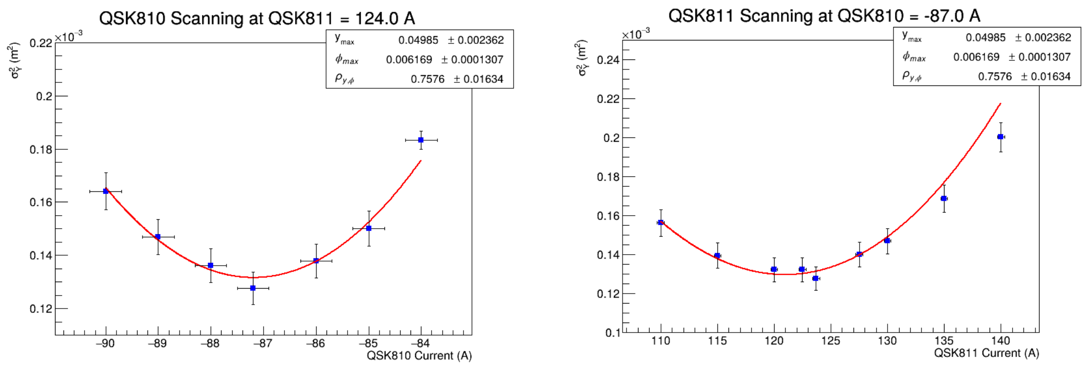

Figure 41: Vertical (Y) phase space simultaneous fits of the quadrupole scan data for the 100 MeV/c 5mm square slit setting.

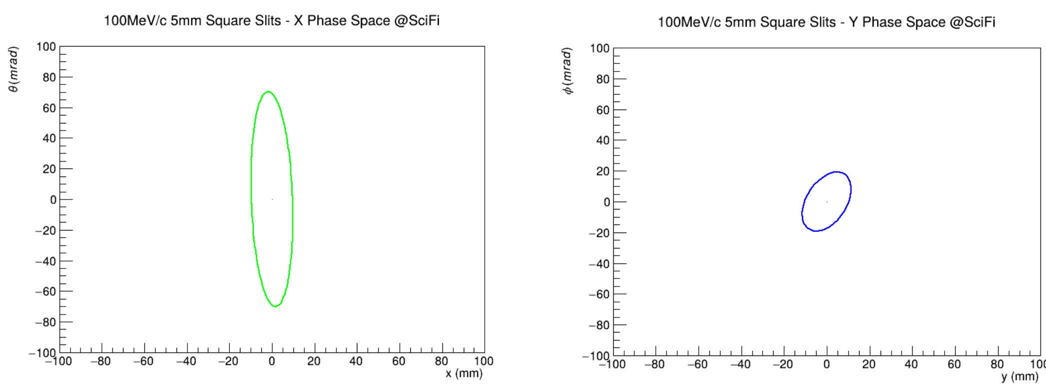

Figure 42: Transverse phase space ellipses of the 100 MeV/c 5mm square slit setting at the SciFi. X phase space is in green and Y phase space is in blue.

Parameter [units]	Horizontal (X)	Vertical (Y)
α []	0.1752 ± 0.0116	-0.4627 ± 0.0693
β [m/rad]	0.1420 ± 0.0142	0.6564 ± 0.1943
γ [rad/m]	7.2592 ± 0.5098	1.8498 ± 0.0251
ε [mm.mrad]	679.647 ± 35.107	200.716 ± 36.648

Table 6: Twiss parameters of the 100 MeV/c 5mm square slit setting at the SciFi. Note that the emittance (ε) here is the area of the ellipses.

Hence, the final **6D phase space @SciFi** for the 100 MeV/c 5mm square slit setting looks thus (without the uncertainties due to formatting limitations):

$$\sigma^{(5mm)}_{100\mathrm{MeV/c}} = \begin{pmatrix} 9.70^2\ \mathrm{mm}^2 & -119.07\ \mathrm{mm.mrad} & 0 & 0 & \sigma_{xl} & -0.0574\ \mathrm{mm} \\ & 70.24^2\ \mathrm{mrad}^2 & 0 & 0 & \sigma_{\theta l} & \sigma_{\theta\delta} \\ & & 11.30^2\ \mathrm{mm}^2 & 92.87\ \mathrm{mm.mrad} & \sigma_{yl} & -0.0736\ \mathrm{mm} \\ & & & 19.27^2\ \mathrm{mrad}^2 & \sigma_{\phi l} & \sigma_{\phi\delta} \\ & & & & 3.194^2\ \mathrm{ns}^2 & -0.035\ \mathrm{ns} \\ & & & & & 2.51\% \end{pmatrix} \quad (56)$$

5.3 125 MeV/c Backward Decay Muons - Phase Space

As mentioned earlier, two beamtunes of 125 MeV/c backward decay muon momentum were used to take phase space measurements - a self-optimized 'new' beamtune and the μSR beamtune used in μSR experiments at PSI. All slits were kept completely open for the 4D phase space measurements in both cases and closed to 5mm square slit setting for the energy measurement as in the case of the 100 MeV/c beamtune. Both beamtunes are described in this section.

5.3.1 New Beamtune

Beamtune: mue1_p125_Jun_2024_Z-Config-V1_Tune1.sp

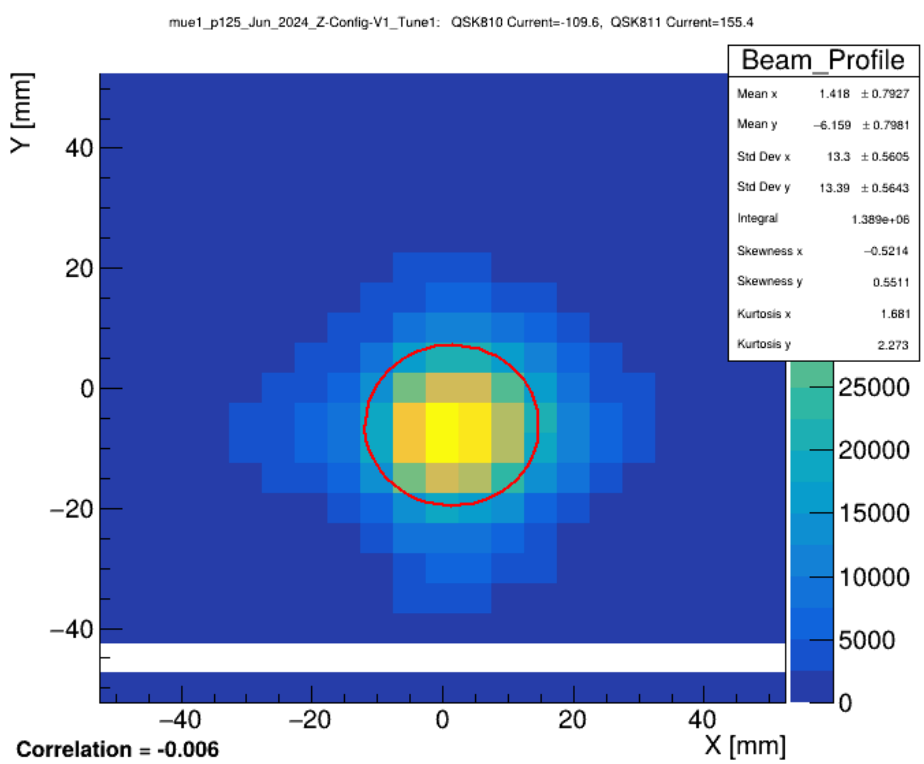

Figure 43: Beamspot of the 125 MeV/c new beamtune. Correlation between X and Y (σ_{xy}) is not sufficiently high to disregard null hypothesis of [$\sigma_{xy} = 0$]. All kurtosis shown is excess kurtosis. Total rate of this beam setting is 68.756 MHz/mA.

The currents of the 100 MeV/c beamtune were scaled by the momentum ratio of 1.25 and then another round of optimization was performed to obtain this beamtune. The transverse beamspot at the SciFi is shown in Figure 43. The correlation between the 2 transverse axes that is closely related to the phase matrix element σ_{xy} (covariance) was not high enough to discard the null hypothesis of $[\sigma_{xy} = 0]$. Like before, the beamspot provides values of $\sqrt{\sigma_{xx}}$ and $\sqrt{\sigma_{yy}}$ in the form of the standard deviations. Further confirmation of these elements as well as the measurements of the remaining elements of the 4D phase space elements can be obtained from the quadrupole scan technique's results as seen in Figures 44 and 45 with the **Twiss parameters at the SciFi** summarized in Table 7. The total rate of this beam setting is 68.756 MHz/mA.

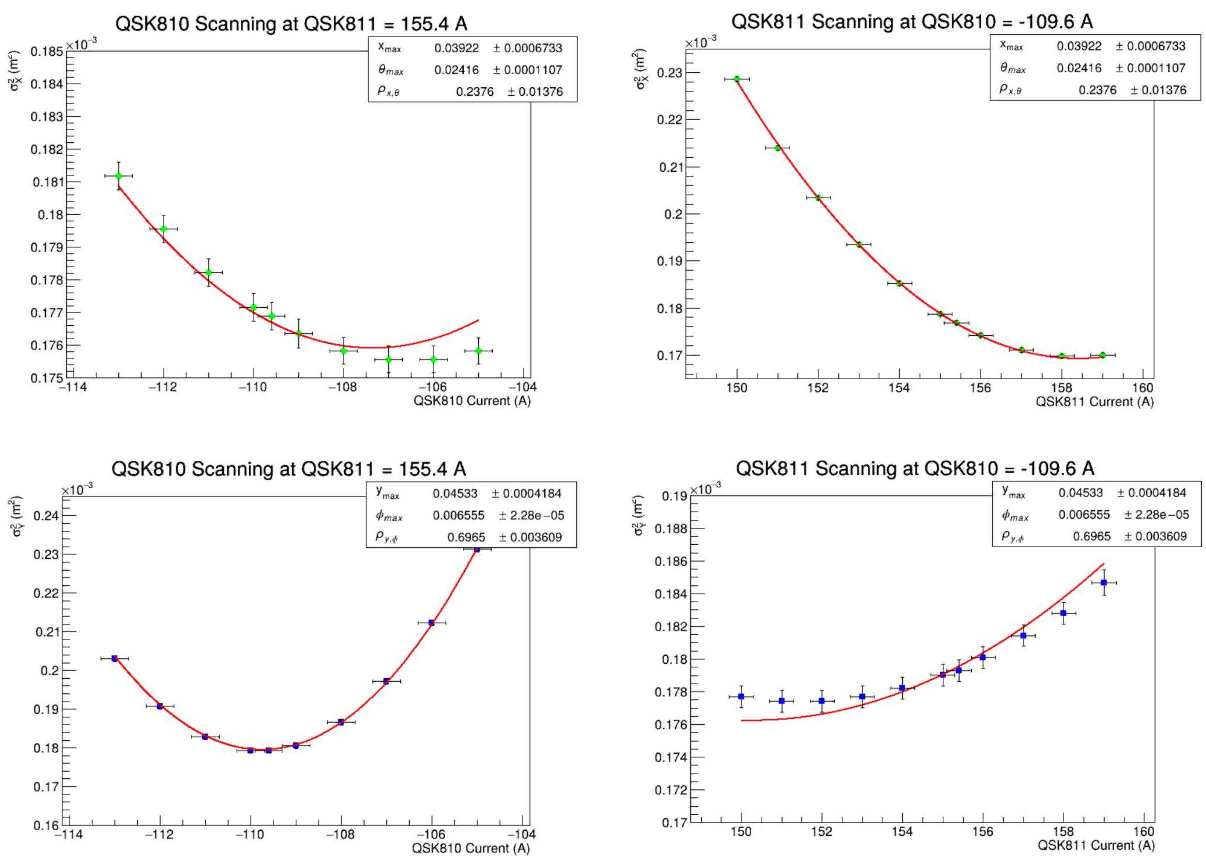

Figure 44: Phase space simultaneous fits of the quadrupole scan data for the 125 MeV/c new beamtune - horizontal (X) [TOP] and vertical (Y) [BOTTOM].

Parameter [units]	Horizontal (X)	Vertical (Y)
α []	0.0384 ± 0.0029	-0.6219 ± 0.0167
β [m/rad]	0.1920 ± 0.0189	0.8420 ± 0.0444
γ [rad/m]	5.2165 ± 0.0167	1.6470 ± 0.0040
ε [mm.mrad]	920.336 ± 45.405	213.236 ± 8.120

Table 7: Twiss parameters of the 125 MeV/c new beamtune at the SciFi. Note that the emittance (ε) here is the area of the ellipses.

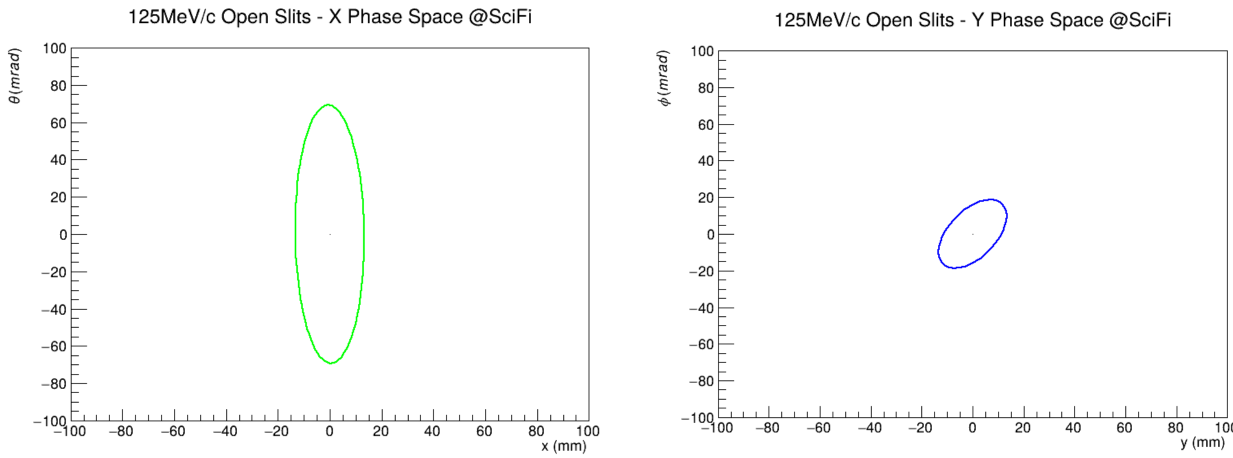

Figure 45: Transverse phase space ellipses of the 125 MeV/c new beamtune at the SciFi. X phase space is in green and Y phase space is in blue.

The ToF-energy distribution for the 125 MeV/c beamtune is shown in Figure 46 yielding values of σ_{ll} and $\sigma_{l\delta}$ given in Equations (57) and (58) respectively. The uncertainties of these values were obtained purely from statistics.

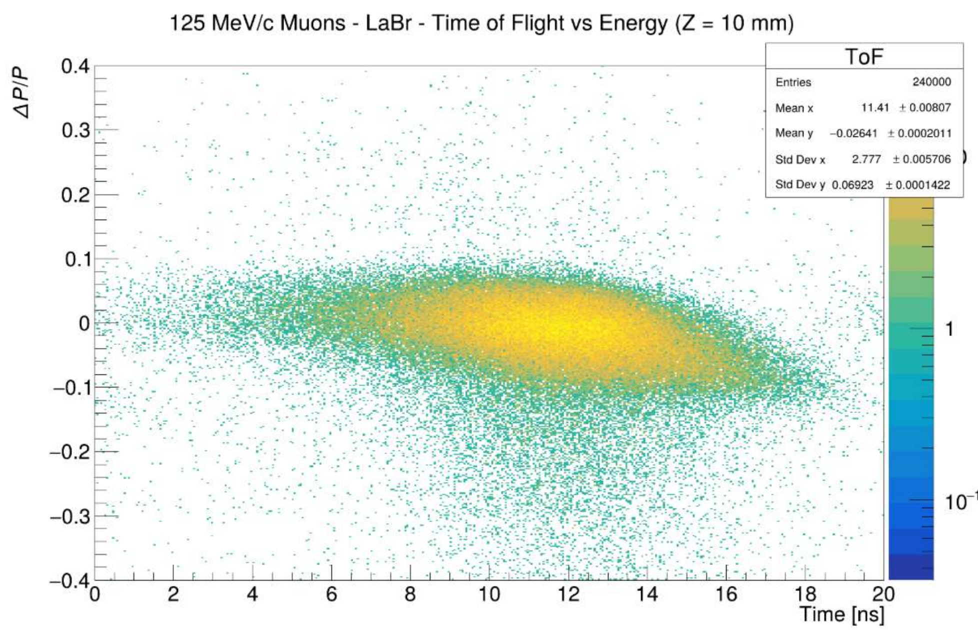

Figure 46: ToF-energy distribution for the 125 MeV/c beamtunes.

$$\sqrt{\sigma_{ll}} = (2.777 \pm 0.006) \text{ ns}, \tag{57}$$

$$\sigma_{l\delta} = (-0.048 \pm 0.003) \text{ ns}. \tag{58}$$

The momentum or energy spread ($\Delta P/P$) was found using the kinetic energy spread (Figure 47) after taking broadening effects according to Equation (44) into account. Using the same Geant4 energy loss simulation as described in Figure 25, it was found that the 125 MeV/c muons initially of kinetic energy $E_k = 58.0$ MeV lose about 6.3 MeV of kinetic energy before reaching the LaBr, making the corrected kinetic energy:

$$E'_k = 51.7 \text{ MeV}, \tag{59}$$

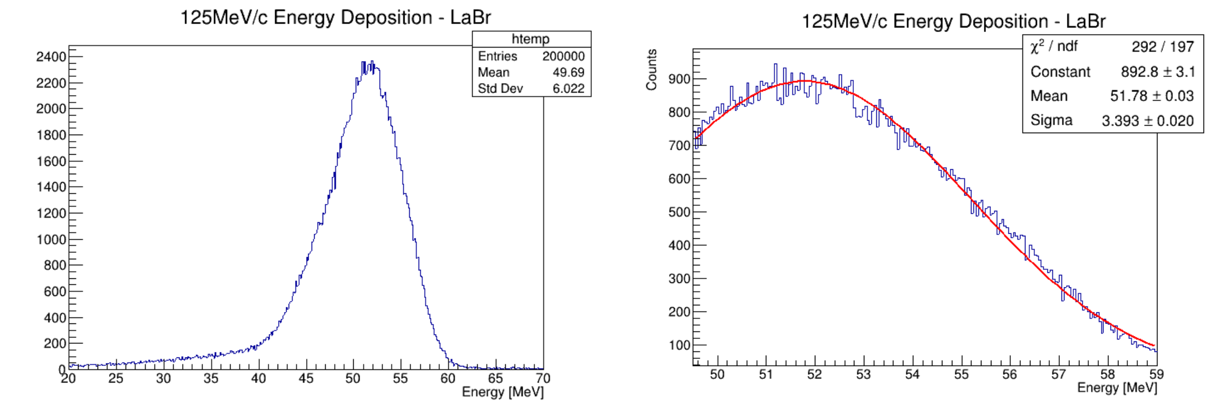

Figure 47: Post-energy loss kinetic energy (E'_k) spread of the 125 MeV/c beamtune used to calculate $\Delta P/P$.

$$\frac{\Delta P}{P}_{\text{125MeV/c}} = (3.41 \pm 0.20)\%. \tag{60}$$

This energy spread was also collected in the $(5{\times}5)\text{mm}^2$ square slit setting as all the energy measurements were made with this setting so as to avoid pile-up in the WaveDAQ used to collect data from the SciCross and LaBr, however no SciFi rates data was taken for the 5mm square slit setting for 125 MeV/c beamtunes, and hence a comparison similar to the 100 MeV/c rates comparison is difficult. The energy spread was found to be the same (within each other's uncertainty) for the new and μSR beamtunes, but the energy dispersion was different.

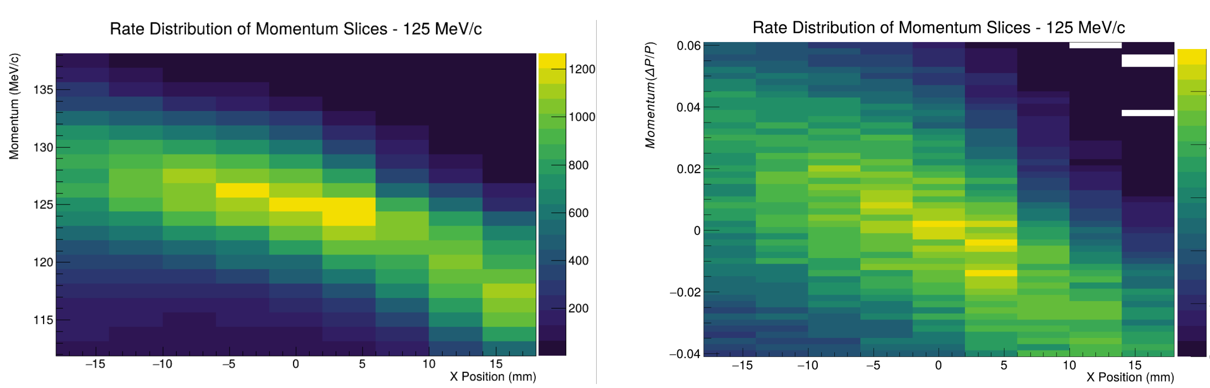

Figure 48: Position-momentum distribution for the 125 MeV/c new beamtune horizontal (X) direction - full distribution [LEFT] ; the part of the full distribution used for dispersion calculation post cuts [RIGHT].

The horizontal energy dispersion function ($D_x(\delta)$) was then calculated and is described in Figure 48. Since the SciCross-LaBr scans were only made in the horizontal (X) direction and NOT in the vertical (Y) direction, the **vertical energy dispersion ($\sigma_{y\delta}$) is not available for 125 MeV/c muon momentum**. The covariance ($\sigma_{x\delta}$) was calculated using the position-momentum slicing and so was the corresponding dispersion function using Equation (37) and are shown in Equations (61) and (62) respectively.

$$\sigma_{x\delta} = (-0.1758 \pm 0.0143)\ \text{mm}, \tag{61}$$

$$D_x(\delta) = (-151.18 \pm 12.30)\ \text{mm}. \tag{62}$$

Thus, the final **6D phase space @SciFi** for the 125 MeV/c new beamtune (without the uncertainties due to formatting limitations) is described in Equation (63):

$$\sigma^{(New)}_{125\text{MeV/c}} = \begin{pmatrix} 13.30^2\ \text{mm}^2 & -35.02\ \text{mm.mrad} & 0 & 0 & \sigma_{xl} & -0.1758\ \text{mm} \\ & 69.29^2\ \text{mrad}^2 & 0 & 0 & \sigma_{\theta l} & \sigma_{\theta\delta} \\ & & 13.39^2\ \text{mm}^2 & 132.49\ \text{mm.mrad} & \sigma_{yl} & \sigma_{y\delta} \\ & & & 18.74^2\ \text{mrad}^2 & \sigma_{\phi l} & \sigma_{\phi\delta} \\ & & & & 2.777^2\ \text{ns}^2 & -0.048\ \text{ns} \\ & & & & & 3.41\% \end{pmatrix} \tag{63}$$

5.3.2 μSR Beamtune

Beamtune: mue1_p125_Jun_2024_Z-Config-MUSR_TunePion_v3.sp

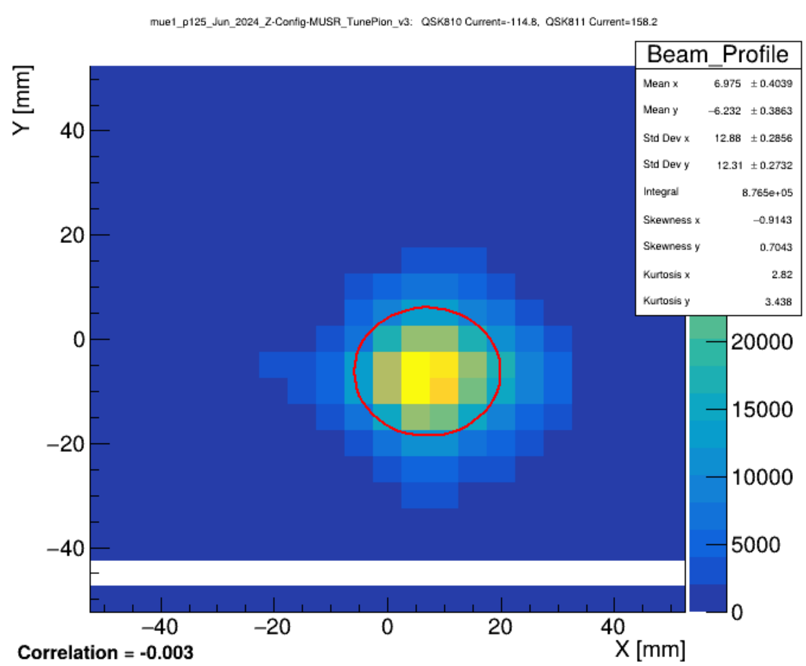

Figure 49: Beamspot of the 125 MeV/c μSR beamtune.σ_{xy} is 0, and all kurtosis shown is excess kurtosis. Total rate of this beam setting is 43.336 MHz/mA.

The beamtune used for the results in this subsection was obtained from the μSR group at PSI[42, 43] and then optimized once. The transverse beamspot at the SciFi is shown in Figure 49. Like the other beamtunes, the correlation between the two transverse axes that is closely related to the phase matrix element σ_{xy} (covariance) was not high enough to discard the null hypothesis of $[\sigma_{xy} = 0]$. The beamspot provides values of $\sqrt{\sigma_{xx}}$ and $\sqrt{\sigma_{yy}}$ in the form of the standard deviations, and the measurements of the remaining elements of the 4D phase space elements can be obtained from the quadrupole scan technique's results as seen in Figures 50 and 51 with the **Twiss parameters at the SciFi** summarized in Table 8. The total rate of this beam setting is 43.336 MHz/mA.

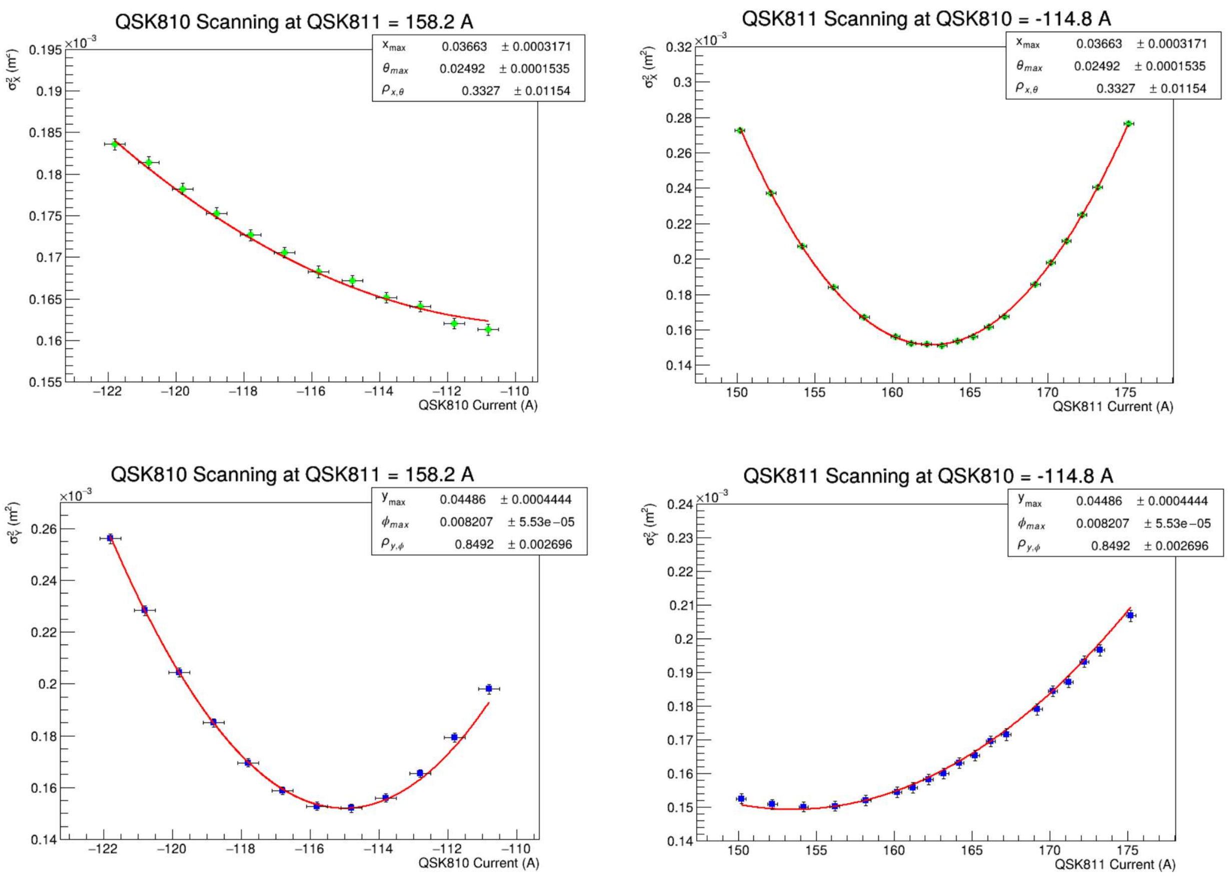

Figure 50: Phase space simultaneous fits of the quadrupole scan data for the 125 MeV/c μSR beamtune - horizontal (X) [TOP] and vertical (Y) [BOTTOM].

Parameter [units]	Horizontal (X)	Vertical (Y)
α []	0.1415 ± 0.0059	-0.5693 ± 0.0127
β [m/rad]	0.1933 ± 0.0091	0.7818 ± 0.0342
γ [rad/m]	5.2779 ± 0.0240	1.6937 ± 0.0103
ε [mm.mrad]	860.811 ± 20.670	194.441 ± 5.865

Table 8: Twiss parameters of the 125 MeV/c μSR beamtune at the SciFi. Note that the emittance (ε) here is the area of the ellipses.

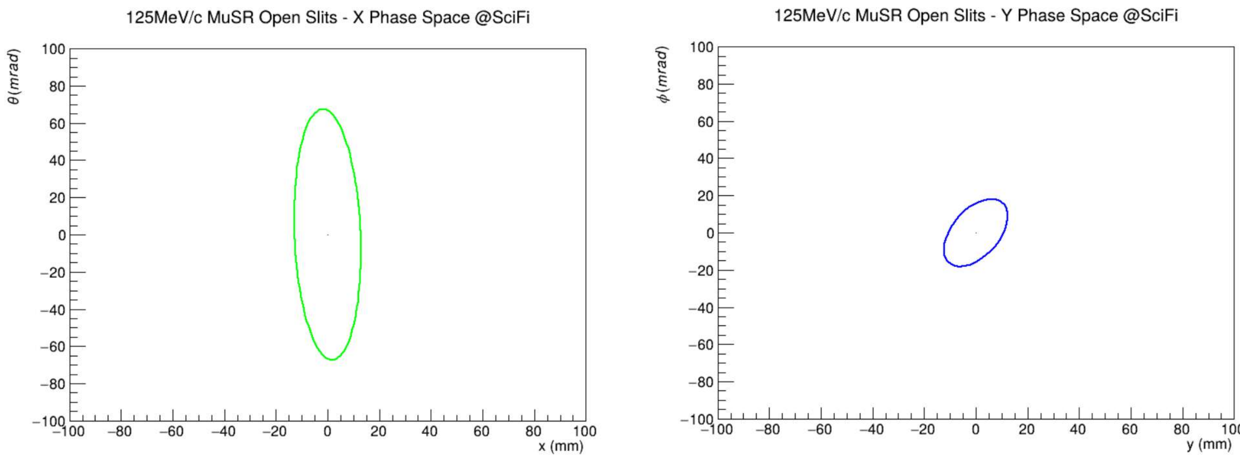

Figure 51: Transverse phase space ellipses of the 125 MeV/c μSR beamtune at the SciFi. X phase space is in green and Y phase space is in blue.

The ToF-energy distribution for the μSR beamtune is the same as that of the 125 MeV/c new beamtune, and is shown in Figure 46 yielding values of σ_{ll} and $\sigma_{l\delta}$ given in Equations (57) and (58) respectively. The energy spread ($\Delta P/P$) too is the same as that for the 125 MeV/c new beamtune and can be observed in Figure 47 with its value given in Equation (60), however the energy dispersion was found to differ.

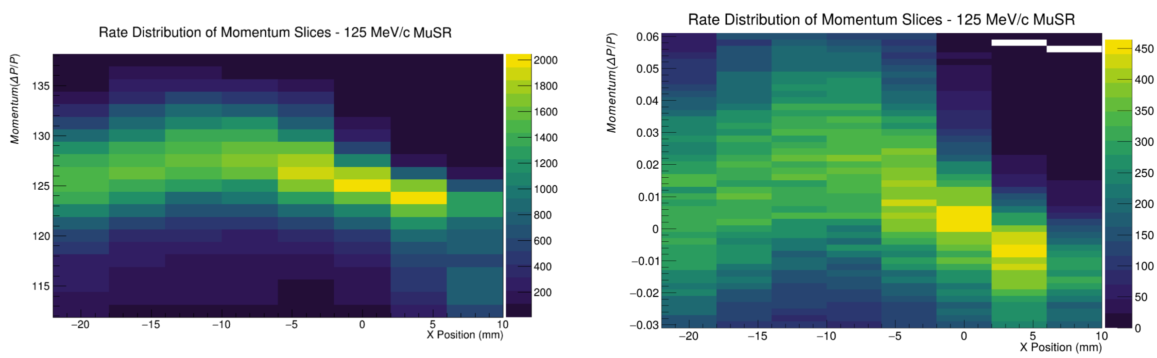

Figure 52: Position-momentum distribution for the 125 MeV/c μSR beamtune horizontal (X) direction - full distribution [LEFT] ; the part of the full distribution used for dispersion calculation post cuts [RIGHT].

The horizontal energy dispersion function ($D_x(\delta)$) was then calculated as before (see Figure 52). As stated earlier, the vertical energy dispersion ($\sigma_{y\delta}$) is not available for 125 MeV/c muon momentum. The covariance ($\sigma_{x\delta}$) was calculated using the position-momentum slicing and so was the corresponding dispersion function using Equation (37) and are shown in Equations (64) and (65) respectively.

$$\sigma_{x\delta} = (-0.1279 \pm 0.0090)\ \text{mm}, \tag{64}$$

$$D_x(\delta) = (-110.03 \pm 7.74)\ \text{mm}. \tag{65}$$

Thus, the final **6D phase space @SciFi** for the 125 MeV/c μSR beamtune (without the uncertainties due to formatting limitations) is described in Equation (66):

$$\sigma^{(\mu SR)}_{125\mathrm{MeV/c}} = \begin{pmatrix} 12.88^2\ \mathrm{mm}^2 & -121.54\ \mathrm{mm.mrad} & 0 & 0 & \sigma_{xl} & -0.1279\ \mathrm{mm} \\ & 67.40^2\ \mathrm{mrad}^2 & 0 & 0 & \sigma_{\theta l} & \sigma_{\theta\delta} \\ & & 12.31^2\ \mathrm{mm}^2 & 110.80\ \mathrm{mm.mrad} & \sigma_{yl} & \sigma_{y\delta} \\ & & & 18.15^2\ \mathrm{mrad}^2 & \sigma_{\phi l} & \sigma_{\phi\delta} \\ & & & & 2.777^2\ \mathrm{ns}^2 & -0.048\ \mathrm{ns} \\ & & & & & 3.41\% \end{pmatrix} \quad (66)$$

5.4 140 MeV/c Forward Decay Muons - Phase Space

Beamtune: mue1_pi127_mu140_Jun_2024_Z-Config-MUSR_Tune1.sp

The 140 MeV/c forward decay muon beamtune was manually optimized using the knowledge gained from the ToF studies of pions forward decaying to muons. This beamtune was primarily operated in four settings - fully open slits for beamspot data, $(20\times20)\mathrm{mm}^2$ square slits setting (both slits), transverse slits for Z scan transverse profiles data and with the upstream (FS81) slit closed to a 5mm square slit and the downstream slit (FS00) fully open (referred to henceforth as the 'asymmetric setting'). The transverse beamspot at the SciFi for the fully open slits setting is shown in Figure 53. Like the other beamtunes, σ_{xy} (covariance) was not high enough to discard the null hypothesis of $[\sigma_{xy} = 0]$. The total rate of all particles at the SciFi for the open slits configuration was 0.605 MHz/mA. The beamspots of the other settings were also obtained but have not been included here for brevity's sake but can be made available upon request, and have also been uploaded to the 'Analysis/muE1_Z_June2024' GitLab repository of the μEDM experiment.

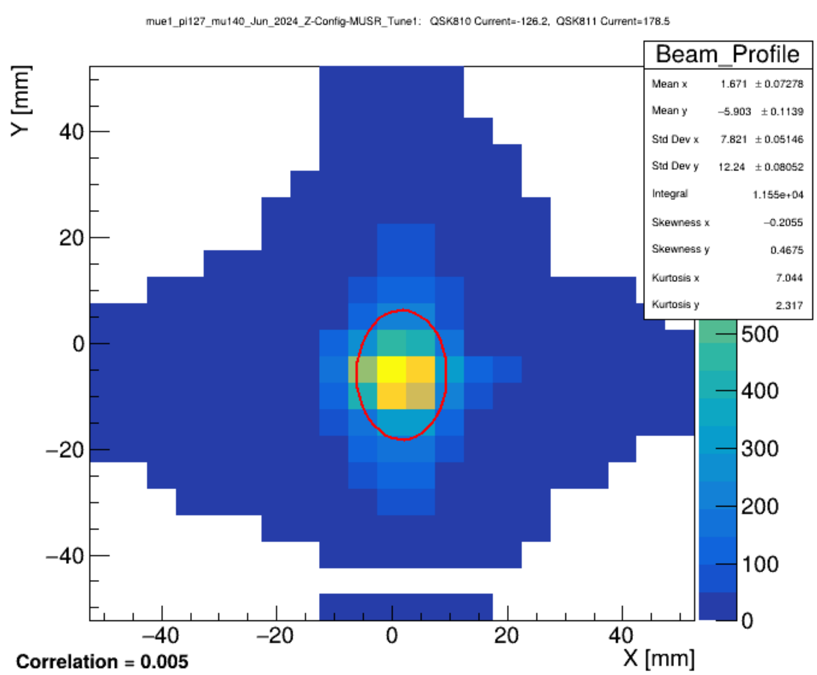

Figure 53: Beamspot of the fully open slits setting of the 140 MeV/c forward decay beamtune. σ_{xy} is 0, and all kurtosis shown is excess kurtosis. Total rate of this beam setting is 0.605 MHz/mA.

The Z scan technique was used instead of the quadrupole scan technique to gather the 4D phase space data in case of the 140 MeV/c beamtune. Data from the 20mm square slits setting was used for the 4D phase space measurement during the analysis as that data seemed to be the most coherent of all with the other data frequently being interrupted by beam interruptions or simply being incomplete or incompatible with the Z scan method. The Z scans used for the final 4D phase space measurement took transverse beam profile data of the rates at the SciCross detector only for 23 positions of X and Y each for 3 different Z positions - [Z = 10mm], [Z = 20mm] and [Z = 30mm]. The beam profiles obtained from these scans are shown in Figure 54, and the subsequent phase space ellipses obtained **(at the SciFi)** using the Z scan method are shown in Figure 55, while the Twiss parameters obtained for the 140 MeV/c forward decay beamtune are listed in Table 9.

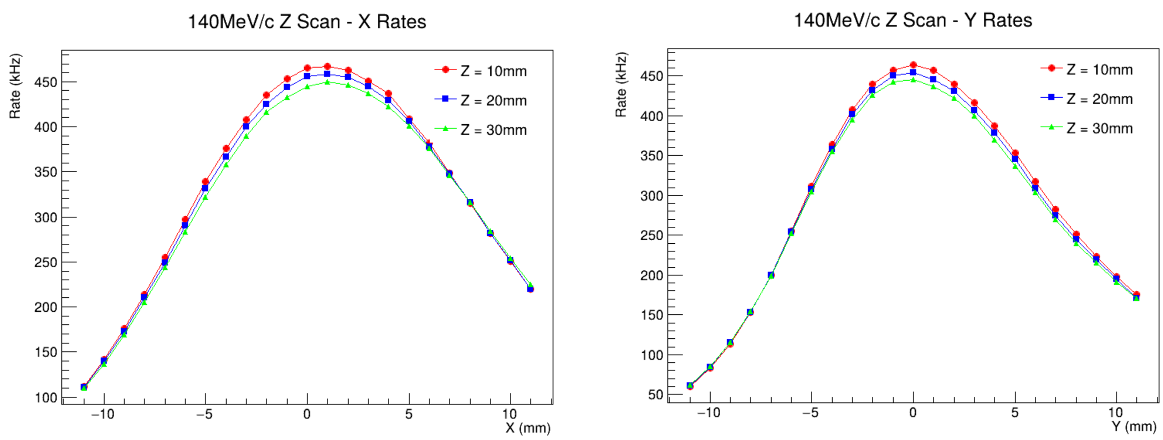

Figure 54: Transverse beam profiles obtained using the SciCross detector for the Z scan transverse phase space measurement - horizontal (X) [LEFT] and vertical (Y) [RIGHT].

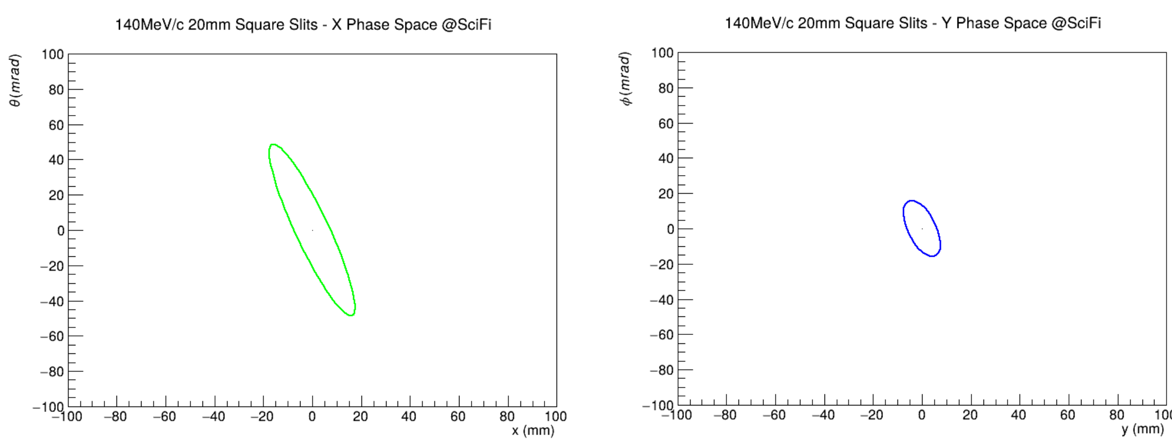

Figure 55: Transverse phase space ellipses of the 140 MeV/c beamtune at the SciFi obtained using the Z scan method. X phase space is in green and Y phase space is in blue.

One can notice that the uncertainties of the Twiss parameters for this beamtune has not been provided in the table. This is because the uncertainties of the Twiss parameters were estimated at a later point in the analysis than when the parameters themselves were extracted, and since it was determined by the time in question that the forward decay beamtunes would not be viable candidates for the μEDM experiment's phase 2 measurement for reasons that are discussed below, the

Parameter [units]	Horizontal (X)	Vertical (Y)
α []	2.1161	0.6746
β [m/rad]	0.8422	0.5773
γ [rad/m]	6.5043	2.5205
ε [mm.mrad]	365.057	99.079

Table 9: Twiss parameters of the 140 MeV/c forward decay beamtune **at the SciFi**.

error estimation (as well as further analysis) of the 140 MeV/c beamtune's data was not pursued in favour of focusing the limited time and effort available into the thorough analysis of the viable beamtunes (100 MeV/c, 125 MeV/c and 125 MeV/c μSR).

The ToF-energy distribution for the 140 MeV/c beamtune was taken for 2 different Z positions - [Z = 10mm] and [Z = 500mm] - to observe the change in the distribution. The SciCross and the LaBr ToF distributions for [Z = 10mm] is shown in Figure 56, and that for [Z = 500mm] is shown in Figure 57.

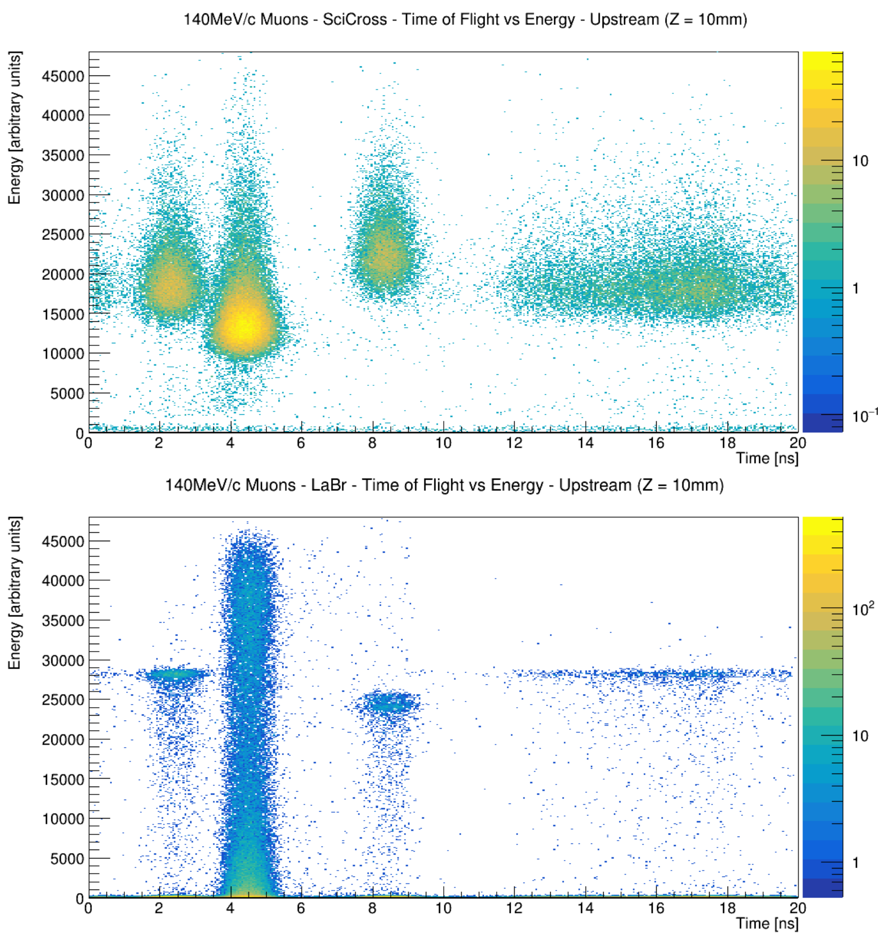

Figure 56: ToF distributions for 140 MeV/c (Z = 10mm) - SciCross [TOP] ; LaBr [BOTTOM].

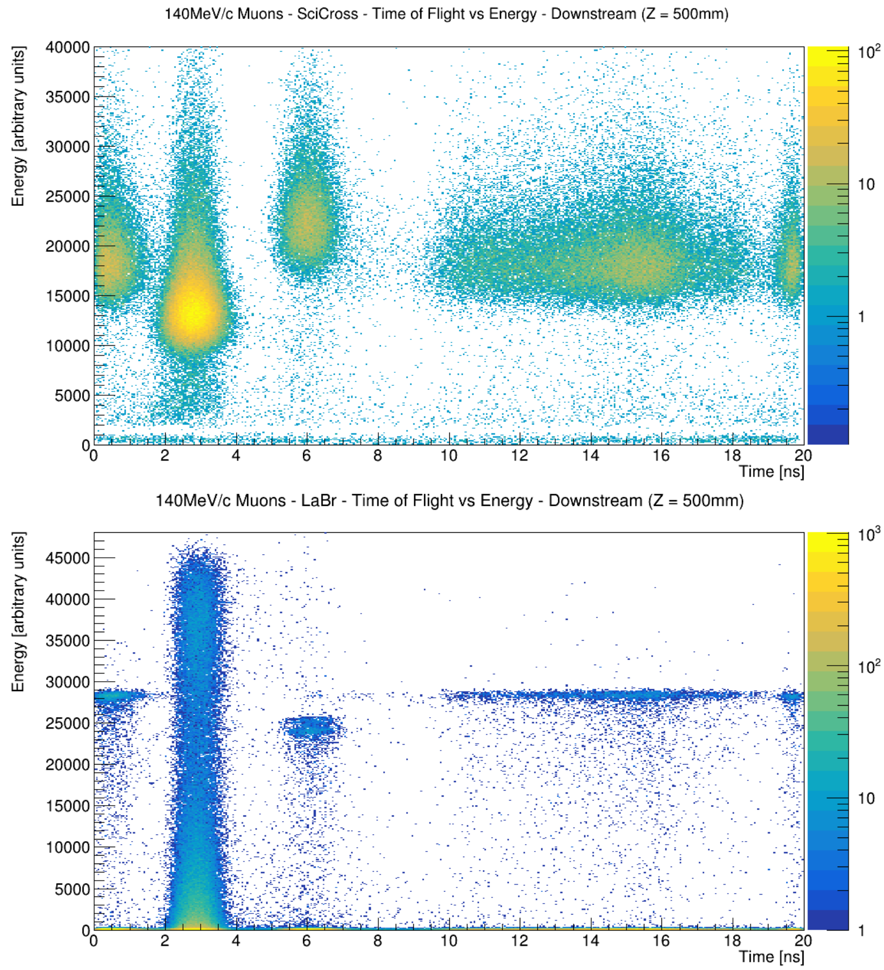

Figure 57: ToF distributions for 140 MeV/c (Z = 500mm) - SciCross [TOP] ; LaBr [BOTTOM]. Much greater energy smearing can be seen in these plots when compared to the 10mm case due to the particles losing energy to collisions with air particles.

In the ToF-energy distributions of the 140 MeV/c forward decay beamtune, 3 particle species can be identified using the principles of Bragg's energy deposition of particles in materials[44] from the 4 clusters. The cluster that starts at the lowest energy in the SciCross (and displays the delta-like function in the LaBr) are positrons that have propagated through the beamline directly from the proton on target (PoT) collision. The cluster that begins at the highest energy in the SciCross plots are the pions from the PoT collisions. Finally, the cluster that is to the left-end of the distributions are the muons produced directly from PoT collisions while the smeared cluster to the right-most are the muons that were produced from pion decays after the PoT produced pions decayed within the beamline. The last particle species, namely muons, are all that can be seen in the backward decay beamtunes and not the other particles as the former have been selected due to the different momentum acceptance of the beamline sections upstream and downstream of the decay channel. Since the SciCross is not a calorimeter, the particles are NOT stopped in the SciCross and thus the energies shown on the SciCross plots are NOT the total energies of the detected particles, while the energies on the LaBr plot are indeed the total energies as most of the particles stop completely in the LaBr. It is to be noted that since the SciCross and the LaBr were connected to different WaveDREAM boards which had different SiPMs with non-identical light yields, **the energy values are not necessarily to scale with each other**. The pions, being of the same momentum as the muons, possess less kinetic energy than muons as they have a higher mass. Since all kinetic energy (and not total energy) is deposited in a calorimeter, the pions deposit lesser energy compared to the muons in the LaBr.

The fractional rates of the particles were then calculated in order to estimate the muon rate of this forward decay beamtune. The fractional contributions to the total rate of each of the 3 particle species mentioned were:

$$f_\mu = 0.349, \quad (67)$$

$$f_e = 0.506, \quad (68)$$

$$f_\pi = 0.119. \quad (69)$$

This brings the total rate of muons (direct and decayed) for the 140 MeV/c forward decay beamtune to be:

$$R_\mu = (0.605 \times 0.349) = 0.211 \text{ MHz/mA}. \quad (70)$$

These rates turn out to be extremely low if the aimed sensitivity of μEDM phase 2 is to achieved, especially when compared to the 125 MeV/c new beamtune, as the sensitivity of the muon EDM measurement scales with the number of particles studied $\left(\sigma(d_\mu) \propto \frac{1}{\sqrt{N}} \text{ (13)}\right)$. This is besides the fact that the forward decay setting also includes other particle species of pions and positrons - unlike the backward decay beamtunes - which could introduce a very big systematic into the experiment which would need to be accounted for. For these reasons, it was concluded that the 140 MeV/c forward decay beamtune, and possibly forward decay beamtunes in general, would not be ideal for the μEDM experiment. Hence, further analysis of the phase space of this beamtune was not pursued in favour of dedicating greater time and effort into the backward decay beamtunes (100 MeV/c, 125 MeV/c and 125 MeV/c μSR) that seem much more promising. Hence, the full 6D phase space measurement was not extracted for the 140 MeV/c forward decay beamtune.

6 Beamline Modelling using Simulation Software

The results obtained from the June 2024 beamtime were reproduced in three different simulation software programs - Transport[26], G4Beamline[45] and Python's XSuite module[46] - in an attempt to model the μE1 beamline's phase space for future studies and optimizations. The 100 MeV/c new beamtune (Section 5.2), 125 MeV/c new beamtune (Section 5.3.1) and 125 MeV/c μSR beamtune (Section 5.3.2) were modelled using the aforementioned simulation software programs. The differences and similarities between the three software programs and their simulation methods are summarized in the table below:

	XSuite	**G4Beamline**	**Transport**
Method	Single-Particle Tracking	Monte Carlo Method	Transport Matrix Multiplication
Focus	Tracks individual particles' phase-space trajectories, including non-linear effects, using symplectic integration.	Simulates particle behaviour, including probabilistic interactions with materials and fields, using monte carlo integration.	Models beam dynamics using linear optics and matrix multiplication.
Physics	Beam dynamics, non-linear optics, chromaticity, resonance effects.	Scattering, energy loss, radiation, particle decay, and secondary particle generation.	First and sometimes second-order beamline optics (no non-linearities).
Randomness	No randomness unless explicitly added (e.g. scattering).	Inherently random, driven by stochastic processes.	None. Assumes ideal, deterministic conditions.
Accuracy	High precision. Includes non-linear effects and individual particle trajectories.	Realistic modelling of complex physical processes and stochastic effects.	Accurate only for linear systems or small deviations from linearity.
Input	Initial conditions (position, momentum, energy) for each particle.	Initial conditions (position, momentum, energy) for each particle.	Twiss parameters, transfer matrices, and beam optics parameters.
Output	Trajectories of individual particles in phase space.	Statistical distributions of particle properties, secondary particles, and energy deposition.	Final beam parameters (e.g. centroid, Twiss functions).

Table 10: Comparison of the 3 simulation software used - XSuite[46], G4Beamline[47] and Transport[26].

In the following subsections, the efforts to model the results using each of the 3 software programs are described. Propagating phase space obtained in the results backwards through the whole μE1 beamline, extracting the phase space at the start of the beamline and then simulating the whole beamline should yield the same results at the SciFi if modelled correctly. This idea was successfully implemented analytically for the last 2 quadrupoles in order to obtain the results in the previous section and has been reproduced using the 3 simulation frameworks in the following subsections. The time-reversed propagation of the phase space through the whole beamline has also been set-up in the aforementioned programs as a starting point for future work, with the modelling of the bending dipole magnets requiring further dedicated effort. The simulation input files have been uploaded to the μEDM GitLab repository (under 'Analysis/muE1_Z_June2024/Simulations') and the specific instructions for use have been included in the 'README.md' files of the respective directories.

6.1 Simulations using Transport

Transport is a beamline simulation software developed at CERN in the 1970s, and it uses matrix multiplication to propagate the phase space of a user-input beam through a customizable beamline[26]. Although the pre-beamtime Transport optimized beamtune did not work as expected - most likely due to an incorrect input phase space which was not known at the time - the backward decay beamtunes used in the June 2024 beamtime (100 MeV/c, 125 MeV/c new and 125 MeV/c μSR beamtunes) were modelled successfully using the Transport software for the last 2 quadrupoles (QSK810 and QSK811), with all simulated phase space output values at the position of the SciFi being within the uncertainties of the measured phase space values. The Transport simulations for the 3 backward decay beamtunes used are shown in Figure 58.

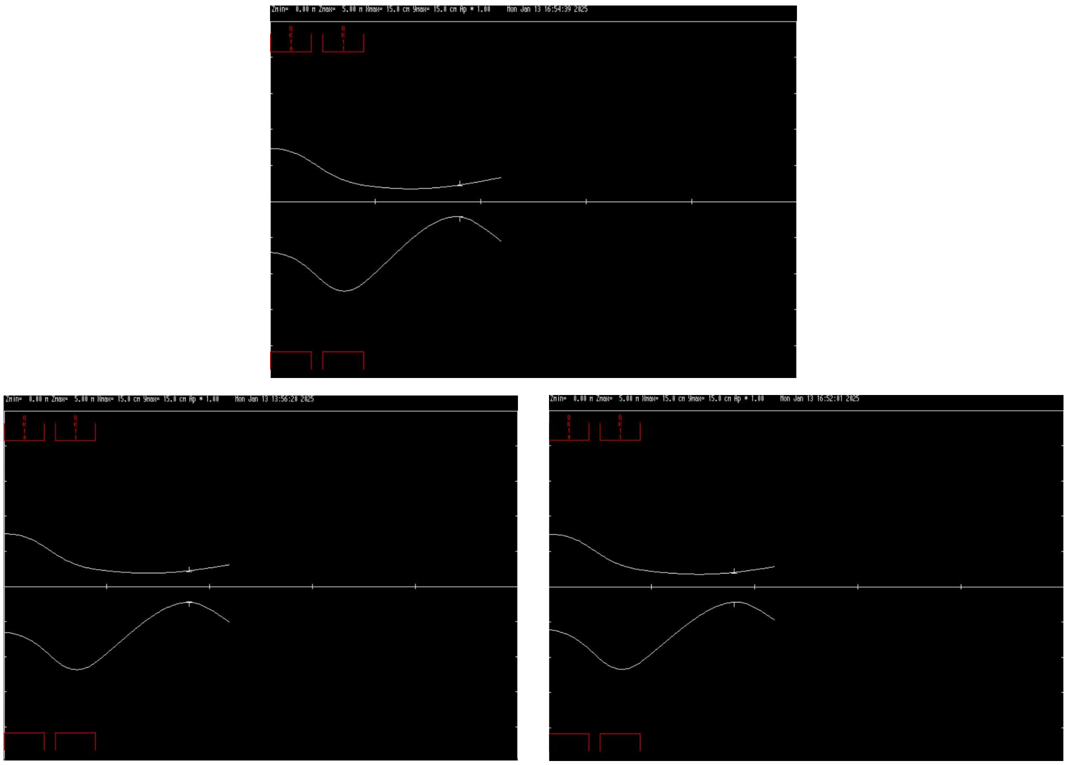

Figure 58: Transport simulations for beam propagation through QSK810 and QSK811 - 100 MeV/c beamtune [TOP] ; 125 MeV/c new beamtune [BOTTOM-LEFT] ; 125 MeV/c μSR beamtune [BOTTOM-RIGHT]. 'T' symbols demarcate the position of the SciFi.

In the Transport graphics shown in Figure 58 above, the red rectangles at the top and bottom represent quadrupoles (and blue rectangles usually represent dipoles, though none are included here), specifically QSK810 and QSK811 in this case. The central line represents the direction of propagation (Z), the white curve in the top half represents the 1σ spread of the beam in the vertical 'Y' direction ($\sqrt{\sigma_{yy}}$) and the white curve of the bottom half represents the 1σ spread of the beam in the horizontal 'X' direction ($\sqrt{\sigma_{xx}}$). A dotted white curve usually describes the horizontal energy dispersion along the beamline, however it isn't shown here as the dispersion before the 2 quadrupoles wasn't extracted in the analysis (but can be done so by simply back-propagating the 6D phase space at the SciFi through said quadrupoles). In this simulation, each gradation along the Y-axis of the plot represents 3cm of beam spread, and each gradation along the Z direction represents 1m.

The comparison between the output and measured values at the SciFi for the 100 MeV/c beamtune is displayed in Table 11, that for the 125 MeV/c new beamtune can be seen in Table 12 and a similar comparison for the 125 MeV/c μSR beamtune is shown in Table 13.

	Data	Transport	Error
$\sqrt{\sigma_{xx}}$	(12.55 ± 0.50) mm	12.80 mm	1.99%
$\sqrt{\sigma_{\theta\theta}}$	(74.10 ± 0.23) mrad	74.33 mrad	0.31%
$\rho_{x\theta}$	(0.075 ± 0.007)	0.092	0.85%
$\sqrt{\sigma_{yy}}$	(13.99 ± 1.61) mm	14.25 mm	1.86%
$\sqrt{\sigma_{\phi\phi}}$	(20.24 ± 2.11) mrad	20.42 mrad	0.89%
$\rho_{y\phi}$	(0.652 ± 0.086)	0.662	0.50%

Table 11: Comparison between the measured and Transport simulated 4D phase space parameters at the SciFi for the 100 MeV/c beamtune.

	Data	Transport	Error
$\sqrt{\sigma_{xx}}$	(13.30 ± 1.04) mm	13.68 mm	2.86%
$\sqrt{\sigma_{\theta\theta}}$	(69.29 ± 2.43) mrad	69.57 mrad	0.49%
$\rho_{x\theta}$	(-0.038 ± 0.008)	-0.014	1.20%
$\sqrt{\sigma_{yy}}$	(13.39 ± 0.62) mm	13.93 mm	4.03%
$\sqrt{\sigma_{\phi\phi}}$	(18.74 ± 0.51) mrad	19.01 mrad	1.44%
$\rho_{y\phi}$	(0.528 ± 0.024)	0.548	1.00%

Table 12: Comparison between the measured and Transport simulated 4D phase space parameters at the SciFi for the 125 MeV/c new beamtune.

	Data	Transport	Error
$\sqrt{\sigma_{xx}}$	(12.88 ± 0.48) mm	13.11 mm	1.79%
$\sqrt{\sigma_{\theta\theta}}$	(67.40 ± 1.17) mrad	69.64 mrad	3.32%
$\rho_{x\theta}$	(-0.140 ± 0.007)	-0.119	1.05%
$\sqrt{\sigma_{yy}}$	(12.31 ± 0.46) mm	12.72 mm	3.33%
$\sqrt{\sigma_{\phi\phi}}$	(18.15 ± 0.39) mrad	18.36 mrad	1.16%
$\rho_{y\phi}$	(0.496 ± 0.019)	0.513	0.85%

Table 13: Comparison between the measured and Transport simulated 4D phase space parameters at the SciFi for the 125 MeV/c μSR beamtune.

Here, the errors for the correlations (ρ) have been estimated by normalizing the relative differences between the simulation and data values to the range of correlations (2). As can be seen, nearly all simulated phase space values are within the uncertainties of the measured values with even the few exceptions being very close to the measurements with small % errors with most of said deviations being from correlations. Thus, one can conclude that the phase space measurement of the June 2024 beamtime has been successfully modelled using the Transport software for the 3 main backward decay muon beamtunes.

6.2 Simulations using Python XSuite

XSuite is a recently developed Python-based library designed for simulating and analysing the dynamics of charged particle beams in accelerators[46]. It provides a modular framework for modelling beam transport, tracking particles through various beamline elements, and studying beam dynamics under various conditions. Among its core submodules, XTrack is a robust single-particle tracking tool capable of high-precision simulations of particle trajectories through accelerator elements, including dipoles, quadrupoles, and higher-order multipoles. The ability of XTrack to handle both detailed element-by-element tracking and collective beam effects has seen it recently become one of the most favoured software for simulating beam dynamics. Exhaustive information on XTrack and all the other submodules of XSuite can be found in the XSuite documentation online (https://xsuite.readthedocs.io/en/latest/index.html).

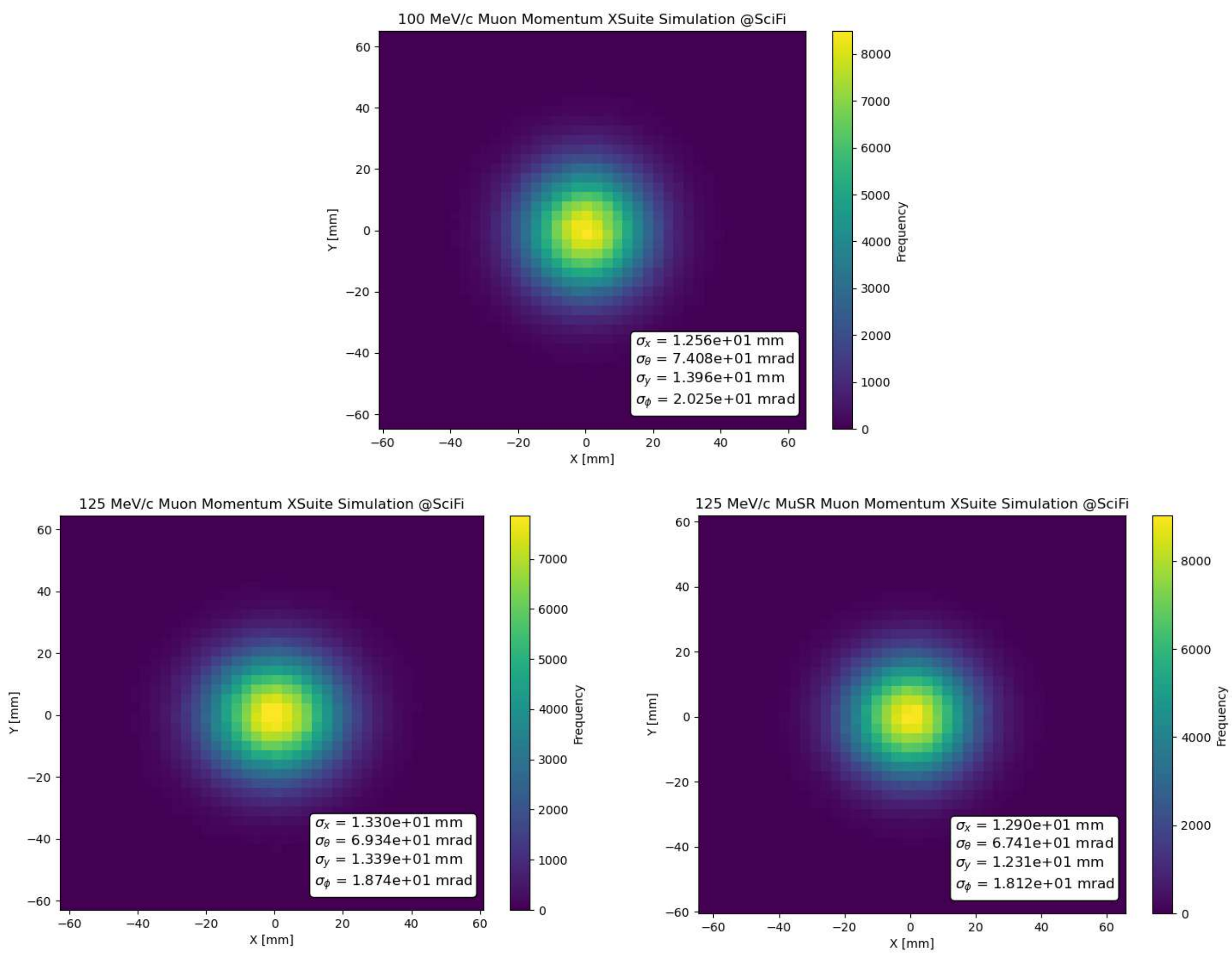

Figure 59: Xsuite simulations for beam propagation through QSK810 and QSK811 - 100 MeV/c beamtune [TOP] ; 125 MeV/c new beamtune [BOTTOM-LEFT] ; 125 MeV/c μSR beamtune [BOTTOM-RIGHT]. The 4D phase space parameters obtained at the SciFi are shown in the bottom right of the plots.

As mentioned earlier, XTrack has been employed to model the measured phase space of the μE1 beamline in the Z-configuration. Like in the case of the Transport modelling attempts, the backward decay beamtunes (100 MeV/c, 125 MeV/c new and 125 MeV/c μSR beamtunes) were modelled successfully using XTrack for the last 2 quadrupoles (QSK810 and QSK811), with all simulated phase space output values at the position of the SciFi being well within the uncertainties of the measured phase space values with many matching the measured values down to the last significant figure. The XSuite-XTrack simulations for the 3 backward decay beamtunes used are shown in Figure 59, and the comparisons between the output and measured values at the SciFi, like before, for the 100 MeV/c, 125 MeV/c new and 125 MeV/c μSR beamtunes are displayed in Tables 14, 15, and 16 respectively.

	Data	**XSuite**	**Error**
$\sqrt{\sigma_{xx}}$	(12.55 ± 0.50) mm	12.56 mm	0.08%
$\sqrt{\sigma_{\theta\theta}}$	(74.10 ± 0.23) mrad	74.08 mrad	0.03%
$\rho_{x\theta}$	(0.075 ± 0.007)	0.076	0.05%
$\sqrt{\sigma_{yy}}$	(13.99 ± 1.61) mm	13.96 mm	0.21%
$\sqrt{\sigma_{\phi\phi}}$	(20.24 ± 2.11) mrad	20.25 mrad	0.05%
$\rho_{y\phi}$	(0.652 ± 0.086)	0.654	0.10%

Table 14: Comparison between the measured and XSuite simulated 4D phase space parameters at the SciFi for the 100 MeV/c beamtune.

	Data	**XSuite**	**Error**
$\sqrt{\sigma_{xx}}$	(13.30 ± 1.04) mm	13.30 mm	0.00%
$\sqrt{\sigma_{\theta\theta}}$	(69.29 ± 2.43) mrad	69.34 mrad	0.07%
$\rho_{x\theta}$	(-0.038 ± 0.008)	-0.037	0.05%
$\sqrt{\sigma_{yy}}$	(13.39 ± 0.62) mm	13.39 mm	0.00%
$\sqrt{\sigma_{\phi\phi}}$	(18.74 ± 0.51) mrad	18.74 mrad	0.00%
$\rho_{y\phi}$	(0.528 ± 0.024)	0.529	0.05%

Table 15: Comparison between the measured and XSuite simulated 4D phase space parameters at the SciFi for the 125 MeV/c new beamtune.

	Data	**XSuite**	**Error**
$\sqrt{\sigma_{xx}}$	(12.88 ± 0.48) mm	12.90 mm	0.16%
$\sqrt{\sigma_{\theta\theta}}$	(67.40 ± 1.17) mrad	67.41 mrad	0.01%
$\rho_{x\theta}$	(-0.140 ± 0.007)	-0.141	0.05%
$\sqrt{\sigma_{yy}}$	(12.31 ± 0.46) mm	12.31 mm	0.00%
$\sqrt{\sigma_{\phi\phi}}$	(18.15 ± 0.39) mrad	18.12 mrad	0.17%
$\rho_{y\phi}$	(0.496 ± 0.019)	0.495	0.05%

Table 16: Comparison between the measured and XSuite simulated 4D phase space parameters at the SciFi for the 125 MeV/c μSR beamtune.

The input parameters for the simulation were the measured phase spaces of each of the beamtunes before the last 2 quadrupoles, the lengths of the quadrupoles and the drift spaces, the momenta of the muons and the currents of the ideal settings of the quadrupoles for each beamtune in the form of the quadrupole focussing strengths. The phase spaces, given the inputs, were simulated for 10^6 randomly generated particles and the output phase space at the SciFi were calculated from the statistics of the output particle trajectories. It is to be noted that XTrack **does not use matrix multiplication** as was the case for Transport and the method used to analyse the measured phase spaces of the beamtunes. Instead, XTrack works on single-particle tracking and uses symplectic integration. As can be seen, the simulated values match the measured values to a very high precision while using a different method to calculate the output. Thus, a very strong case can be made to use XTrack (or XSuite in general) to model the μE1 beamline in order to achieve high accuracy between simulation and experiment. The code used for the simulation and instructions to use it have been uploaded on the μEDM GitLab page under 'Analysis/muE1_Z_June2024/Simulations/XSuite'.

6.3 Simulations using G4BeamLine

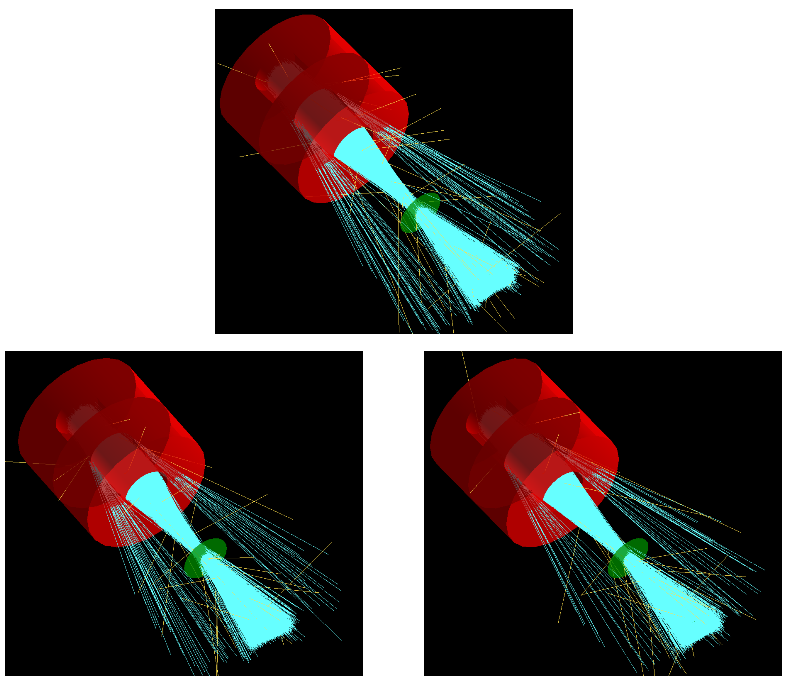

Figure 60: G4Beamline simulations for beam propagation through QSK810 and QSK811 - 100 MeV/c beamtune [TOP] ; 125 MeV/c new beamtune [BOTTOM-LEFT] ; 125 MeV/c μSR beamtune [BOTTOM-RIGHT]. Muons (μ^+) are displayed as light blue tracks, positrons (e^+) as yellow tracks and the quadrupoles are in red. The SciFi detector has been depicted as a green circle.

G4Beamline is a Geant4 based simulation software for simulating particle dynamics in matter-dominated particle beams[47]. For the modelling of the June 2024 beamtime's results, an NTuple of the 6D phase space of particles (along with other properties[45]) was generated using a ROOT code based on the measured phase space before the last 2 quadrupoles. This NTuple is then used as the beam input for the G4beamline simulation. The quadrupoles are implemented using the measured field map of the QSK magnets ('feldqsk.txt') with the currents used for each beamtunes scaled by $-(1/38.5)$. The output is then extracted as an NTuple at the SciFi. The input generator ROOT code, the field map and the G4beamline file (.g4bl) used to run the simulation have been uploaded to the muEDM GitLab page in the directory 'Analysis/muE1_Z_June2024/Simulations/G4beamline/'. The simulation outputs of the G4beamline visualizer for each of the 3 backward decay beamtunes used are shown in Figure 60, and the comparisons between the output and measured values at the SciFi, like before, for the 100 MeV/c, 125 MeV/c new and 125 MeV/c μSR beamtunes are displayed in Tables 17, 18 and 19 respectively.

	Data	**G4Beamline**	**Error**
$\sqrt{\sigma_{xx}}$	(12.55 ± 0.50) mm	13.75 mm	9.56%
$\sqrt{\sigma_{\theta\theta}}$	(74.10 ± 0.23) mrad	74.49 mrad	0.53%
$\sqrt{\sigma_{yy}}$	(13.99 ± 1.61) mm	16.87 mm	20.59%
$\sqrt{\sigma_{\phi\phi}}$	(20.24 ± 2.11) mrad	20.45 mrad	1.04%

Table 17: Comparison between the measured and G4Beamline simulated 4D phase space parameters at the SciFi for the 100 MeV/c beamtune.

	Data	**G4Beamline**	**Error**
$\sqrt{\sigma_{xx}}$	(13.30 ± 1.04) mm	13.97 mm	5.04%
$\sqrt{\sigma_{\theta\theta}}$	(69.29 ± 2.43) mrad	70.13 mrad	1.21%
$\sqrt{\sigma_{yy}}$	(13.39 ± 0.62) mm	16.71 mm	24.79%
$\sqrt{\sigma_{\phi\phi}}$	(18.74 ± 0.51) mrad	18.40 mrad	1.81%

Table 18: Comparison between the measured and G4Beamline simulated 4D phase space parameters at the SciFi for the 125 MeV/c new beamtune.

	Data	**G4Beamline**	**Error**
$\sqrt{\sigma_{xx}}$	(12.88 ± 0.48) mm	13.19 mm	2.41%
$\sqrt{\sigma_{\theta\theta}}$	(67.40 ± 1.17) mrad	68.63 mrad	1.82%
$\sqrt{\sigma_{yy}}$	(12.31 ± 0.46) mm	15.98 mm	29.81%
$\sqrt{\sigma_{\phi\phi}}$	(18.15 ± 0.39) mrad	17.84 mrad	1.71%

Table 19: Comparison between the measured and G4Beamline simulated 4D phase space parameters at the SciFi for the 125 MeV/c μSR beamtune.

As can be clearly seen, the G4beamline simulation does not match the results nearly as well as the Transport and especially XSuite simulations. This is because G4beamline is geared more towards modelling particle dynamics accurately with an inherent randomness imposed due to the stochastic nature of Geant4. A discrepancy of 10% or 20% as seen here is a well accepted tolerance of G4beamline when compared to experimentally measured value. Due to this fact, it can be concluded that the June 2024 measurements have been modelled successfully using G4beamline, although the XSuite simulation remains the most precise and accurate, and hence the latter is recommended over G4beamline or Transport for further modelling and optimization of the μE1 beamline in the Z-configuration.

7 Discussion

As discussed in the theory section, the sensitivity of the muon EDM measurement using the frozen spin technique is related to number of muons analysed $\left(\sigma(d_\mu) \propto \frac{1}{\sqrt{N}}\right)$ and also to the momentum of the muons analysed (13). Thus, an ideal muon beam for the EDM measurement would possess the highest possible rates and the highest possible muon momentum (within constraints). As can be inferred from Figure 31, the June 2024 backward decay 125 MeV/c new beamtune in the Z-configuration yields the highest rates even when compared to the U-configuration 2019 125 MeV/c beamtune. Given that at present 125 MeV/c is close to the highest backward decayed muon momentum that can be accommodated in the μE1 beamline[11], a strong initial case can be made for the use of the June 2024 beamtime 125 MeV/c new beamtune in phase 2 of the μEDM experiment scheduled for 2030s. However, the 'High-Intensity Muon Beam' (HIMB) project at PSI[48, 49] which aims to achieve order of magnitude $\sim$10 GHz muon rate at PSI is also worth looking into for μEDM phase 2 as it would provide about 100 times more muons than the current best beamtune on the μE1 beamline, thus potentially improving the final sensitivity of the muon EDM measurement. In addition to having higher rates compared to the U-configuration, both the 125 MeV/c Z-configuration beamtunes studied in June 2024 also possess lower emittances when compared to the U-configuration beamtunes used in 2019[14]. Lower emittances increase the acceptance of the muons from the beam in the final experiment ultimately leading to a larger number of muons being studied and thus, lower emittances are desirable. The comparison between these emittances is summarized in Table 20.

Beamtune		Emittance [mm.mrad]	
125 MeV/c Muon Momentum		Z	U
New Beamtune	Horizontal (X)	920.336 ± 45.405	946
	Vertical (Y)	213.236 ± 8.120	716
μSR Beamtune	Horizontal (X)	860.811 ± 20.670	995
	Vertical (Y)	194.441 ± 5.865	331

Table 20: Comparison of the emittances of the 125 MeV/c (new and μSR) beamtunes between Z and U-configurations. U-configuration values were obtained from [14].

As can be seen, except the horizontal emittance of the 125 MeV/c new beamtune in Z-configuration which is similar to that of its U-configuration counterpart, all the 125 MeV/c conserved emittances in the Z-configuration were found to be smaller than their respective U-configuration counterparts. This lends further credence to the case of the Z-configuration for use in the μEDM experiment, however further efforts need to be made in order to determine the ideal muon beamtune for μEDM phase 2, and using the simulations set up in this thesis, the muon beamtunes used can be further optimized offline in order to increase the rates and decrease the emittances in order to prepare the particle beam for the phase 2 measurement.

The use of beams that involve pions forward decaying to muons so as to receive muon momenta higher than 125 MeV/c (e.g. 140 MeV/c beamtune) seems limited owing to low muon rates and high contamination from other particle species. These low rates could be the result of the pion momentum, as the pions used for the 100 MeV/c and 125 MeV/c backward decay muon beamtunes were of 173 MeV/c and 216 MeV/c respectively, while those used for the 140 MeV/c forward decay muon momentum were of 127 MeV/c momentum. This positive correlation between the pion momentum and observed rates in the experimental area is due to the momentum of the protons which collide with the 'E' target during the PoT collisions to produce pions[50] (the pion part of the πE1 beamline at PSI mirrors that of the μE1 beamline as can be seen in Figure 2, and thus has a similar pion momentum distribution). This is because given a proton beam of a particular momentum, the momenta of the pions produced during the collision of that proton beam with a target follow a Gaussian distribution centred around a most-probable pion momentum. Hence, since the magnets of the μE1 beamline cannot at present focus the muons produced from the forward decay of pions of momenta greater than 200 MeV/c (as the currents of the magnets do not go that high as of the time of this thesis), the forward decay beamtunes remain unlikely candidates for phase 2.

It was observed during the energy dispersion measurement of the 100 MeV/c beamtune that the vertical (Y) spread of the beam had non-zero energy dispersion. This fact persists even though the beamline does not bend vertically at any point, and the most likely explanation remains that the vertical dispersion is an artifact of the pion decay solenoid which would lead to twisting of the whole particle beam in the transverse directions. However, the observed correlation between the vertical and horizontal axes in the experimental area remains zero, and thus it is likely that beamline elements after the 8 metre-long decay solenoid (starting from QSK81) bend and focus the beam such that the transverse correlation (σ_{xy}) is lost but the vertical energy dispersion ($\sigma_{y\delta}$) remains. This hypothesis requires testing which could not be done using the data acquired in the June 2024 beamtime, as it was assumed during data taking that the vertical dispersion would be zero. Hence, no vertical energy dispersion measurements were made, except for the 100 MeV/c beamtune which was made before the decision to desist was taken in the interest of time. Another possible explanation of this non-zero vertical dispersion could be that the observed departure might be due to partial energy deposition from the muons that do not stop in the calorimeter or from other particle species (namely pions and positrons), however this hypothesis is hard to justify given lack of supporting evidence for other species in the backward decay beamtunes and the 5-point coincidence used in the SciCross-LaBr compound detector for the energy measurements. The vertical energy dispersion of the μE1 beamline needs to be studied further in order to avoid unknown systematics in the final EDM measurement. Similarly, dipole scans also need to be performed at a later date if the $\sigma_{\theta\delta}$ and $\sigma_{\phi\delta}$ phase space parameters are to be estimated and understood for the final EDM measurement as discussed earlier in Section 4.1.6. Another potential source of systematic error is the hysteresis error of the beamline magnets which was not estimated during the analysis due to lack of data.

The time-reversed propagation of the phase space observed at the SciFi detector was performed analytically for the last 2 quadrupoles and subsequently reproduced in all 3 of the simulation software programs used. Using this result, the full μE1 beamline can be modelled and then used for time-reversed propagation of the phase space through the whole beamline in order to extract the input phase space. Once performed successfully, this input phase space along with the simulation of the full beamline can then be used to optimize the muon beam for phase 2 of the μEDM experiment. These full beamline simulations have already been set-up to a large degree and uploaded to the μEDM GitLab repository for future work with the modelling of the bending dipole magnets remaining as one of the major hurdles to overcome, especially so in the case of the ASK82 magnet which possesses a weak focussing fringe field component which needs to be modelled with care.

8 Conclusion and Outlook

This thesis successfully characterized the 6D phase-space of the μE1 beamline at PSI in its Z-configuration for 100 MeV/c and 125 MeV/c backward decay muon momenta in addition to the 4D phase-space measurement of the 140 MeV/c forward decay muon momentum. The backward decay beamtunes were modelled using 3 different simulation software programs (Transport, XSuite and G4Beamline) and it was found that the XSuite simulation agreed with the results from data analysis the closest.

Owing to high rates, high muon momentum and low emittances, the 125 MeV/c new beamtune presents itself to be the best candidate for the future μEDM phase 2 measurement. It had the highest muon rates compared to all the other beamtunes in the Z and U-configurations of the μE1 beamline, and the 125 MeV/c momentum muons are obtained from 216 MeV/c pions which is close to the highest possible pion momentum selectable by the μE1 beamline's magnets (220 MeV/c pion momentum being maximum). The beamtune can be optimized further using simulations set-up in this thesis (Section 6) as well, however further studies need to be conducted to conclude if it is indeed the best possible option. The use of the Z-configuration in general is supported by the fact that lower emittance values in both the horizontal and vertical directions were observed for all beamtunes when compared to the their U-configuration counterparts (Section 7).

It is important to note however that non-zero vertical energy dispersion was found in the 100 MeV/c beamtune studied in this thesis which was unfortunately the only beamtune for which the vertical energy dispersion's data was taken. It is favourable to minimize energy dispersion (which is the dependence of muon energy on the transverse axes) on both axes in order to attain higher acceptance, and thus better statistics, for μEDM experiment. The existence of a vertical dispersion in the data is probably owing to the decay of pions to the observed muons in the decay solenoid present upstream of the QSK81 quadrupole magnet in the μE1 beamline, however further studies need to be conducted in order to not only confirm or rule out this hypotheses, but more importantly to also get a better grasp on the vertical energy dispersion of the μE1 beamline in order to better estimate systematic errors for the final phase 2 muon EDM measurement.

In conclusion, the characterization of the μE1 beamline in the Z-configuration performed in this thesis will not only help the μEDM experiment plan and prepare for phase 2 of the experiment, but will also help any future experiments that seek to use the Z-configuration of the μE1 beamline. Going forth, the modelling of the entire μE1 beamline will be required, the bulk of which has already been set up in the 3 simulation software programs used and uploaded to the μEDM GitLab repository. The modelling of the two ASK bending magnets stands as the final hurdle to be overcome in the quest to fully characterize the μE1 beamline at PSI, and efforts to do the same are underway. The next steps of the μEDM experiment will be to carry out the testing of the various parts of the phase 1 apparatus of the experiment during a beamtime at the end of 2025, followed by the muon EDM measurement at an aimed sensitivity of $|d_\mu| < 3 \times 10^{-21} e.cm$ during phase 1 of the μEDM experiment, which will be commissioned in 2026. The precession signal from the muon g-2 is also aimed to be measured during the 2026 EDM measurement in order to tune the electric field central to implementing the frozen-spin technique. The results from this thesis are already informing the ongoing planning of phase 2 of the μEDM experiment which aims to measure the muon EDM at a sensitivity of $|d_\mu| < 6 \times 10^{-23} e.cm$ in the 2030s.

References

[1] Robert Oerter. *The theory of almost everything: The standard model, the unsung triumph of modern physics*. Penguin, 2006.

[2] Scott Dodelson and Fabian Schmidt. *Modern cosmology*. Academic press, 2020.

[3] Andrei D Sakharov. Violation of cp-invariance, c-asymmetry, and baryon asymmetry of the universe. In *In The Intermissions... Collected Works on Research into the Essentials of Theoretical Physics in Russian Federal Nuclear Center, Arzamas-16*, pages 84–87. World Scientific, 1998.

[4] Tareq Albahri, A Anastasi, A Anisenkov, K Badgley, S Baeßler, I Bailey, VA Baranov, E Barlas-Yucel, T Barrett, A Basti, et al. Measurement of the anomalous precession frequency of the muon in the fermilab muon g-2 experiment. *Physical Review D*, 103(7):072002, 2021.

[5] Kim Siang Khaw, Andreas Adelmann, Malte Backhaus, Niklaus Berger, Manfred Daum, Massimo Giovannozzi, KLAUS KIRCH, Andreas Knecht, Angela Papa, Claude Petitjean, Francesco Renga, Mikio Sakurai, and Philipp Schmidt-Wellenburg. Search for the muon electric dipole moment using frozen-spin technique at PSI. *PoS*, NuFact2021:136, 2022.

[6] James H Christenson, Jeremiah W Cronin, Val L Fitch, and René Turlay. Evidence for the 2 π decay of the k 2 0 meson. *Physical Review Letters*, 13(4):138, 1964.

[7] Gerhart Lüders. On the equivalence of invariance under time reversal and under particle-antiparticle conjugation for relativistic field theories. *Dan. Mat. Fys. Medd.*, 28:1–17, 1954.

[8] GW Bennett, B Bousquet, HN Brown, G Bunce, RM Carey, P Cushman, GT Danby, PT Debevec, M Deile, H Deng, et al. Improved limit on the muon electric dipole moment. *Physical Review D—Particles, Fields, Gravitation, and Cosmology*, 80(5):052008, 2009.

[9] Tanya S Roussy, Luke Caldwell, Trevor Wright, William B Cairncross, Yuval Shagam, Kia Boon Ng, Noah Schlossberger, Sun Yool Park, Anzhou Wang, Jun Ye, et al. An improved bound on the electron's electric dipole moment. *Science*, 381(6653):46–50, 2023.

[10] Yohei Ema, Ting Gao, and Maxim Pospelov. Improved indirect limits on muon electric dipole moment. *Phys. Rev. Lett.*, 128:131803, Apr 2022.

[11] Switzerland Paul Scherrer Institute, Villigen. μe1 beam line. https://www.psi.ch/en/smus/e1.

[12] Mike Seidel, S Adam, A Adelmann, C Baumgarten, YJ Bi, R Doelling, H Fitze, A Fuchs, M Humbel, J Grillenberger, et al. Production of a 1.3 mw proton beam at psi. *IPAC10*, page 1309, 2010.

[13] MK Craddock et al. Eighty years of cyclotrons. In *Proc. XIX Int. Conf. Cyclotron Appl*, pages 1–8, 2010.

[14] Mikio Sakurai. *Towards a Search for the Muon Electric Dipole Moment using the Frozen-spin Technique*. PhD thesis, ETH Zurich, 2023.

[15] Switzerland Paul Scherrer Institute, Villigen. Secondary beam lines (sbl), psi. https://www.psi.ch/en/sbl.

[16] Philipp Schmidt-Wellenburg, Ciro Calzolaio, Ritwika Chakraborty, Anastasia Doinaki, Chavdar Dutsov, Timothy Hume, Ljiljana Morvaj, Angela Papa, Mikio Sakurai, muEDM Collaboration, et al. Search for a muon edm at the paul scherrer institute. In *Proceedings of Science*, volume 452. Proceedings of Science, 2024.

[17] Timothy Hume, Ritwika Chakraborty, Anastasia Doinaki, Chavdar Dutsov, Massimo Giovannozzi, Katia Michielsen, Ljiljana Morvaj, Angela Papa, Philipp Schmidt-Wellenburg, David Stäger, et al. Implementation of the frozen-spin technique for the search for a muon electric dipole moment. *Journal of Instrumentation*, 19(01):P01021, 2024.

[18] A Adelmann, M Backhaus, C Chavez Barajas, N Berger, T Bowcock, C Calzolaio, G Cavoto, R Chislett, A Crivellin, M Daum, et al. Search for a muon edm using the frozen-spin technique. *arXiv preprint arXiv:2102.08838*, 2021.

[19] Helmut Wiedemann. *Particle accelerator physics*. Springer Nature, 2015.

[20] Martin Fertl. *A laser based mercury co-magnetometer for the neutron electric dipole moment search*. PhD thesis, ETH Zurich, 2013.

[21] Stuart Turner, Shin-ichi Kurokawa, Shyh-yuan Lee, and Eugene A Perevedentsev. *Beam Measurement-Proceedings Of The Joint Us-cern-japan-russia School On Particle Accelerators*. World Scientific, 1999.

[22] Moses Chung, Hong Qin, and Ronald C Davidson. Twiss parameters and beam matrix formulation of generalized courant–snyder theory for coupled transverse beam dynamics. *Physics of plasmas*, 17(8), 2010.

[23] Angela Papa, P-R Kettle, Emanuele Ripiccini, and Giada Rutar. Scintillating fibres coupled to silicon photomultiplier prototypes for fast beam monitoring and thin timing detectors. *Nuclear Instruments and Methods in Physics Research Section A: Accelerators, Spectrometers, Detectors and Associated Equipment*, 824:128–130, 2016.

[24] L Galli, AM Baldini, F Cei, M Chiappini, M Francesconi, M Grassi, U Hartmann, M Meucci, F Morsani, D Nicolò, et al. Wavedaq: An highly integrated trigger and data acquisition system. *Nuclear Instruments and Methods in Physics Research Section A: Accelerators, Spectrometers, Detectors and Associated Equipment*, 936:399–400, 2019.

[25] Hannes Friederich, Giovanna Davatz, Ulisse Gendotti, Hanspeter Meyer, and David Murer. Real-time data analysis using the wavedream data acquisition system. In *2012 18th IEEE-NPSS Real Time Conference*, pages 1–7. IEEE, 2012.

[26] Karl L Brown, Frank Rothacker, David C Carey, and Christoph Iselin. Transport-a computer program for designing charged particle beam transport systems. Technical report, European Organization for Nuclear Research, 1980.

[27] Massimo Mascotto and Senior Marketing Engineer. Silicon photomultiplier technology at stmicroelectronics. *CERN, Geneva, February 17th*, 2011.

[28] Elise Moss. *Getting started with onshape*. SDC Publications, 2021.

[29] Angela Papa and Patrick Schwendimann. A first large calorimeter prototype based on lanthanum bromide coupled to silicon photomultipliers: Status and prospects. *Nuclear Instruments and Methods in Physics Research Section A: Accelerators, Spectrometers, Detectors and Associated Equipment*, 936:130–132, 2019.

[30] A Kuhn, S Surti, JS Karp, PS Raby, KS Shah, AE Perkins, and G Muehllehner. Design of a lanthanum bromide detector for time-of-flight pet. *IEEE Transactions on Nuclear Science*, 51(5):2550–2557, 2004.

[31] Peter R Menge, G Gautier, A Iltis, C Rozsa, and V Solovyev. Performance of large lanthanum bromide scintillators. *Nuclear Instruments and Methods in Physics Research Section A: Accelerators, Spectrometers, Detectors and Associated Equipment*, 579(1):6–10, 2007.

[32] Patrick Schwendimann and Angela Papa. Study of 3d calorimetry based on lyso or labr3: Ce crystals for future high energy precision physics. *Journal of Instrumentation*, 15(06):C06018, 2020.

[33] Eduard Prat and Masamitsu Aiba. Four-dimensional transverse beam matrix measurement using the multiple-quadrupole scan technique. *Physical Review Special Topics-Accelerators and Beams*, 17(5):052801, 2014.

[34] U.S. Particle Accelerator School. Uspas emmittance. https://uspas.fnal.gov/materials/09UNM/Emittance.pdf.

[35] Gianluigi Arduini, Massimo Giovannozzi, K Hanke, Django Manglunki, and M Martini. New methods to derive the optical and beam parameters in transport channels. *Nuclear Instruments and Methods in Physics Research Section A: Accelerators, Spectrometers, Detectors and Associated Equipment*, 459(1-2):16–28, 2001.

[36] Brandon Lee Cathey. *First Full Six-Dimensional Phase Space Measurement of a Hadron Beam*. PhD thesis, University of Tennessee, 2018.

[37] Dan Green. *The physics of particle detectors*, volume 12. Cambridge University Press, 2000.

[38] Andrzej Wolski. Alternative approach to general coupled linear optics. *Physical Review Special Topics—Accelerators and Beams*, 9(2):024001, 2006.

[39] Sea Agostinelli, John Allison, K al Amako, John Apostolakis, Henrique Araujo, Pedro Arce, Makoto Asai, D Axen, Swagato Banerjee, GJNI Barrand, et al. Geant4—a simulation toolkit. *Nuclear instruments and methods in physics research section A: Accelerators, Spectrometers, Detectors and Associated Equipment*, 506(3):250–303, 2003.

[40] M Moszyński, A Syntfeld-Każuch, L Swiderski, M Grodzicka, J Iwanowska, P Sibczyński, and T Szcześniak. Energy resolution of scintillation detectors. *Nuclear Instruments and Methods in Physics Research Section A: Accelerators, Spectrometers, Detectors and Associated Equipment*, 805:25–35, 2016.

[41] Cong Chen. Peronal Communication, January 2025.

[42] Switzerland Paul Scherrer Institute, Villigen. μsr group @psi. https://www.psi.ch/en/bulk-musr.

[43] Adrian D Hillier, Stephen J Blundell, Iain McKenzie, Izumi Umegaki, Lei Shu, Joseph A Wright, Thomas Prokscha, Fabrice Bert, Koichiro Shimomura, Adam Berlie, et al. Muon spin spectroscopy. *Nature Reviews Methods Primers*, 2(1):4, 2022.

[44] William Henry Bragg and Richard Kleeman. Xxxix. on the α particles of radium, and their loss of range in passing through various atoms and molecules. *The London, Edinburgh, and Dublin Philosophical Magazine and Journal of Science*, 10(57):318–340, 1905.

[45] Tom Roberts. G4beamline user's guide. *Muons, Inc*, pages 3468–3470, 2013.

[46] G Iadarola, R De Maria, S Lopaciuk, A Abramov, X Buffat, D Demetriadou, L Deniau, P Hermes, P Kicsiny, P Kruyt, et al. Xsuite: An integrated beam physics simulation framework. *arXiv preprint arXiv:2310.00317*, 2023.

[47] Thomas J Roberts and Daniel M Kaplan. G4beamline simulation program for matter-dominated beamlines. In *2007 IEEE Particle Accelerator Conference (PAC)*, pages 3468–3470. IEEE, 2007.

[48] M Aiba, A Amato, A Antognini, S Ban, N Berger, L Caminada, R Chislett, P Crivelli, A Crivellin, G Dal Maso, et al. Science case for the new high-intensity muon beams himb at psi. *arXiv preprint arXiv:2111.05788*, 2021.

[49] Giovanni Dal Maso. *Optimization of the High-Intensity Muon Beamlines for MEG II, Mu3e and HIMB*. PhD thesis, ETH Zurich, 2024.

[50] Switzerland Paul Scherrer Institute, Villigen. πe1 beam line. https://www.psi.ch/en/sbl/pie1-beamline.